THESIS FOR THE DEGREE OF LICENTIATE OF ENGINEERING

Charge and Energy Noise from On-demand Electron Sources

NASTARAN DASHTI

Department of Microtechnology and Nanoscience (MC2)
Applied Quantum Physics Laboratory
CHALMERS UNIVERSITY OF TECHNOLOGY

Göteborg, Sweden 2018

Charge and Energy Noise from On-demand Electron Sources
NASTARAN DASHTI

© NASTARAN DASHTI, 2018

Thesis for the degree of Licentiate of Engineering
ISSN 1652-0769
Technical Report MC2-376

Applied Quantum Physics Laboratory
Department of Microtechnology and Nanoscience (MC2)
Chalmers University of Technology
SE-412 96 Göteborg
Sweden
Telephone: +46 (0)31-772 1000

Cover
Schematic of our proposed noise detection system, with injector and detector part

Printed by Chalmers Reproservice
Göteborg, Sweden 2018

Charge and Energy Noise from On-demand Electron Sources
Thesis for the degree of Licentiate of Engineering

NASTARAN DASHTI

Department of Microtechnology and Nanoscience (MC2)
Applied Quantum Physics Laboratory
Chalmers University of Technology

Abstract

On-demand single electron sources (SES) are of key importance for future electronic applications such as metrology or quantum optics with electron. They allow for achieving a controlled, low-fluctuations flow of particles in a coherent mesoscopic conductor. One way to characterize the precision and spectrum of the injected single-particle state from these sources is to study correlations of charge- and energy currents.

We analyze a prominent example for such single-electron sources which is the emission of single electrons from a driven mesoscopic capacitor in the quantum-Hall regime. By employing the Floquet scattering approach, we study the features of this source in charge- and energy-current noise. Whereas the charge-current noise is proportional to the number of emitted particles, the energy-current noise is sensitive to properties of the driving potential. When the mesoscopic capacitor is driven slowly, we compare its features with the application of a Lorentzian-shaped, time-dependent potential to a coherent conductor. Both sources emit exactly the same pulse but with different type and number of particles.

In contrast to charge currents, energy currents and their fluctuations are more difficult to access experimentally. We theoretically propose a setup for the detection of fluctuating charge and energy currents, as well as their correlations, generated by an arbitrary time-dependently driven electronic source. Employing the Boltzmann-Langevin approach, we show that these fluctuations are detectable through a read-out of frequency-dependent temperature and electrochemical-potential fluctuations. We discuss the feasibility of our detection scheme for a concrete example of the mesoscopic capacitor setup in the quantum Hall regime. Finally, we review different, experimental-related aspects that should be taken into account when optimizing the proposed detection scheme.

Keywords: single-electron source; time-dependently driven mesoscopic capacitor; Floquet scattering theory; charge current; energy and heat currents; fluctuations and noise; Boltzmann-Langevin approach.

Acknowledgements

Firstly, I would like to state my profound appreciation to my supervisor Janine Splettstoesser for her continuous and daily support during my PhD study. I would like to also thank her for giving me the opportunity to research in her group. My sincere gratitudes go to Maciej Misiorny, my co-supervisor who has spent countless amount of time in helping me to resolve my scientific problems, and thanks for being such a nice person.

Besides my main advisors in Chalmers University of Technology, I would like to especially thank Peter Samuelsson for his hospitality and productive discussions during my visit at Lund University.

In addition, I thank all my friends in both Chalmers and Lund Universities, my past and present office mates and everyone who tried to make such a friendly and excellent environment at work.

Finally, many thanks to my family for their ever existed support and encouragement.

Contents

Abstract iii

Acknowledgements v

Contents ix

1 Introduction 1
- 1.1 On-demand single-electron sources . . . 2
  - 1.1.1 Time-dependently driven mesoscopic capacitor . . . 2
  - 1.1.2 Lorentzian bias voltage . . . 3
- 1.2 Thesis outline . . . 4

2 Theoretical description of time-dependent transport phenomena in mesoscopic systems 5
- 2.1 Setup . . . 5
- 2.2 Floquet scattering matrix . . . 6
  - 2.2.1 Second quantization . . . 8
- 2.3 Time representation of the scattering matrix . . . 9
- 2.4 Charge current . . . 10
- 2.5 Energy current . . . 11
- 2.6 Current noise . . . 13
  - 2.6.1 Zero-frequency noise . . . 14
- 2.7 Adiabatic approximation . . . 15
  - 2.7.1 First-order approximation . . . 16

3 Characterization of on-demand electron sources 17
- 3.1 Emission schemes . . . 17
  - 3.1.1 Time-dependently driven mesoscopic capacitor . . . 17
  - 3.1.2 Lorentzian bias voltage . . . 21
- 3.2 Comparison of two different on-demand single electron sources . . . 23
  - 3.2.1 Charge and energy currents . . . 23
  - 3.2.2 Charge- and energy-current noises . . . 26
  - 3.2.3 Transport quantities at zero temperature . . . 31

4 Analysis of single electron pulses: beyond the adiabatic-response regime 33
- 4.1 Emission scheme beyond the adiabatic-response regime . . . 33
  - 4.1.1 First-order approximation of the scattering matrix . . . 34
- 4.2 Charge current . . . 36

4.2.1 Spectral current . . . 38
4.2.2 Energy current . . . 39
4.2.3 Current noise . . . 42

5 Detection of noise in the mesoscopic capacitor through probe fluctuations 45
5.1 Setup . . . 45
5.1.1 Probe properties . . . 46
5.2 Boltzmann-Langevin approach . . . 47
5.2.1 Correlation of electrochemical-potential fluctuations . . . 48
5.2.2 Correlation of temperature fluctuation . . . 49
5.3 Extraction of information about the source from the probe . . . 50
5.3.1 Correlator decomposition . . . 51
5.4 Discussion . . . 52

6 Summary 53

Appendices 55

A Current operator 57

B Energy current density 59

C Scattering matrix of the mesoscopic capacitor 61
C.1 Scattering matrix in slow driving regime . . . 62

D Currents with the mixed-representation scattering matrix 65
D.1 Time-dependent charge current . . . 65
D.1.1 Adiabatic-response regime . . . 66
D.1.2 Correction to the adiabatic-response regime . . . 66
D.2 Time-dependent energy current . . . 67
D.2.1 Adiabatic-response regime . . . 67
D.2.2 Correction to the adiabatic-response regime . . . 68

E Average energy current for the mesoscopic capacitor setup 69

F Interference part of the energy-current noise 71

References 73

1 Introduction

Miniaturization of electronic devices to the mesoscopic and nanoscale regime, over the last 30 years, has enabled one to address charge transport on the same scale. On-demand single electron sources, which are one kind of mesoscopic devices, are of key importance for future electronic applications. In fact, driven single electron sources allow for a controlled and noiseless injection of particles into a coherent mesoscopic conductor, which is of interest for both experimental and theoretical research. For instance, in metrological applications [1], one aims to redefine the standard unit of Ampere with an accurate source emitting one discrete electron-charge e per period at frequency in the GHz regime. Other novel applications are related to quantum information processing [2] and quantum optics with electrons [3, 4] in the quantum Hall regime. In the latter case, the possibility of achieving a tunable synchronization of electrons emitted from such sources was essential for implementation of fermionic interferometers (such as, Mach-Zender interferometer [5] and Hanburry-Brown-Twiss interferometer [6]), in analogy to their photonic counterparts.

For all of these applications, one needs an accurate on-demand single electron source with low fluctuations. Such a source can be characterized by studying transport quantities, and in particular, noise. Importantly, the precision of sources that inject single electrons into a mesoscopic conductor cannot be accessed by studying only the average charge current, as it contains no information on the statistics of particles. Therefore, one has to resort to the second moment of the statistics, which corresponds to the low-frequency charge-current noise [4, 7–9], and it provides information on the number of injected particles, including the neutral electron-hole pair excitations. The particles injected from the source carry energy [10–13] in addition to their charge. In recent years, this has motivated theoretical research on the fluctuations of energy currents, and also mixed correlations of charge and energy currents as a spectroscopic tool for both static [14–19] and driven systems [20–24]. Understanding these, are of essential importance for efficient application of on-demand sources, because we get information about energy properties and quality of the emitted pulses. Finally the question arises how charge current, heat current and their corresponding noises are experimentally accessible in order to characterize single electron emitters.

The detection of charge-current fluctuations has extensively been studied for different kind of sources in Refs. [4, 9, 25, 26]. However, in contrast to charge currents, energy currents –both their average and their fluctuations– are difficult

to access experimentally. For instance, Battista et al. [22] suggested to measure power fluctuations in order to detect heat-current noise in the situation when the single electron source realized by employing a time-dependent bias voltage. In this thesis, we propose another feasible way to access energy- and charge-current fluctuations caused by time-dependently driven single-electron sources. Our suggestion is to measure temperature and electrochemical-potential fluctuations [27–29] in a probe contact.

1.1 On-demand single-electron sources

This thesis analyzes two different ways of how to create single electrons: First, in the quantum-confinement regime with a time-dependently driven mesoscopic capacitor [6], single electrons are pumped from a time-dependent QD to a quantum Hall edge state through a quantum point contact (QPC). This source is of key importance for fermionic quantum optics. Second, without dealing with quantum confinement, single electrons can be emitted by applying a time-periodic bias voltage across a junction thereby minimizing additional excitations of electron-hole pairs. In this thesis, we consider the ideal case, namely, when a Lorentzian-shaped time-dependent potential is applied to a coherent conductor [4, 30–32].

There are also many other feasible approaches, for instance: (i) by using surface acoustic waves, see Refs. [33–35], single electrons from a quantum dot (QD) move from one side to the other of a conductor created by a two-dimensional electron-gas (2DEG) with the velocity of the surface acoustic wave; (ii) in superconducting turnstiles [36], by connecting a superconductor island to two normal leads. Single electrons can tunnel from normal lead to the superconductor if the charging energy, which is created due to the energy gap, can be provided by applying a gate or bias voltage.

1.1.1 Time-dependently driven mesoscopic capacitor

The first realization of a mesoscopic capacitor working as an accurate single-electron source has been demonstrated by Fève et al. [6]. This experiment employs quantum-Hall edge state created in 2DEG by a application of a large perpendicular magnetic field. A QD with discrete energy spectrum and level spacing Δ is coupled to an edge state at one side of a coherent conductor. The connection is made through a QPC which works as a beam splitter with transparency D_{s} and it is controlled by a gate voltage, see in Fig. 1.1(a). After injection from a mesoscopic capacitor, particles propagate ballistically along the edge state in a coherent way.

By applying a time-periodic voltage to the QD, one of the energy levels can be moved above the Fermi level, so that an electron is emitted. When the energy level is brought back to its initial value, one hole leaves the dot, or in other words, the level become again occupied by an electron, Fig. 1.1(b). Then, the electron

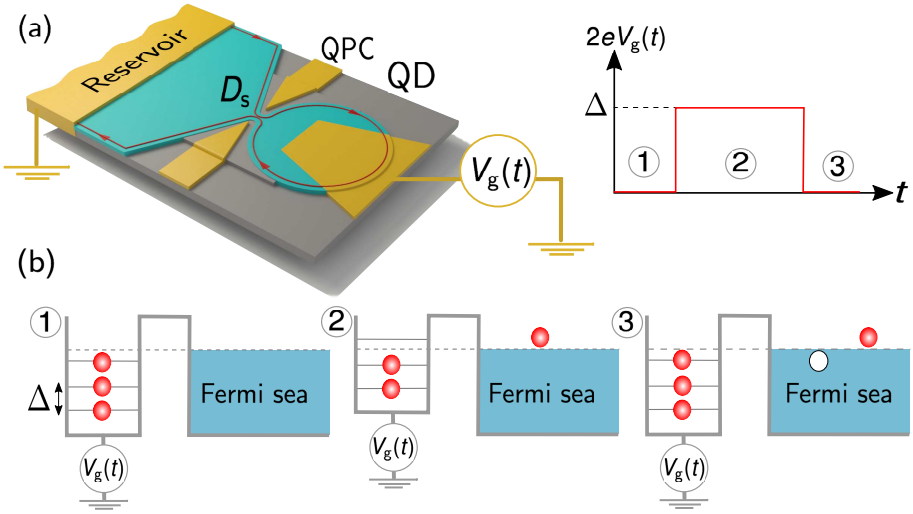

Figure 1.1: *(a) Scheme of the mesoscopic capacitor. It contains a quantum dot (QD), coupled to a two-dimensional electron gas (2DEG) through a quantum point contact (QPC) with transparency D_s. (b) A sketch of the single particle emission, with the application of a time-dependent gate voltage: (1) The QD is initially in equilibrium. (2) By increasing the potential, one occupied level of the QD can be brought above the Fermi sea, so that one electron is emitted. (3) Then, the energy level of the QD is brought back to its initial value and one electron can enter the QD, which corresponding to the emission of a hole [6].*

and the hole propagate along the 1D edge state in the 2DEG. The direction of such a propagation id indicated in Fig. 1.1(a) by the red arrows. More details of the working principle of this setup is explained in Chap. 3. The mesoscopic capacitor is also called *single-electron gun*, since it injects exactly one electron and one hole, one after the other.

1.1.2 Lorentzian bias voltage

Creating single particles without quantum confinement has been studied theoretically by Levitov et al. [30–32], and experimentally confirmed in by Dubois et al. [4]. It is known fact that by applying a regular periodic voltage, for instance, a sinusoidal voltage on a conductor, a bunch of electron-hole pairs is excited, shown in Fig. 1.2(a). However, by applying a particular shape of the voltage, pulse of a quantized single-electron charge can be generated onto the surface of the Fermi sea without extra electron-hole pairs. This is achieved by a voltage pulse that changes periodically in time like a Lorentzian function,

$$V_b(t) = \frac{h}{e\pi} \sum_{n=-\infty}^{\infty} \frac{W}{(t - n\mathcal{T})^2 + W^2}. \tag{1.1}$$

By applying this voltage, the excitation of an electron-like particle is created, which propagates coherently through the conductor. This single-electron excita-

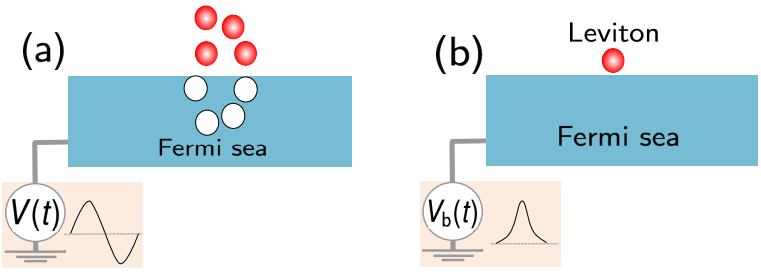

Figure 1.2: *(a) By applying a sinusoidal pulse, many electron-hole excitations are created out of the Fermi sea. (b) By applying Lorentzian pulses, a single Leviton is created.*

tion has recently been called a Leviton [4], see Fig. 1.2(b).

1.2 Thesis outline

The topic of this work is a theoretical study of on-demand single electron sources. We start by introducing Floquet scattering theory in Chap. 2, to study transport quantities in a time-dependent mesoscopic system. It is followed by Chap. 3 where we describe the emission of injected particles from two different sources: First, the adiabatic-response of a slowly driven mesoscopic capacitor in a chiral system, and second, a Lorentzian-shaped bias voltage applied to a coherent conductor. We study precision and spectral properties of these systems through charge current, energy current and their fluctuations with the help of Floquet scattering theory.

In Chap. 4, we focus on the mesoscopic capacitor source. We show how slightly increasing the driving frequency of the potential (requiring a treatment, which includes one order higher in an expansion in the driving frequency) leads to a modification of the temporal pulse, the energy properties without modifying the number of emitted particles.

In Chap. 5 we briefly overview the appended paper. We propose there a experimental method allowing for the extraction of transport properties which are studied in previous chapters through reading out macroscopic fluctuations. Specifically, we theoretically derive the relation between the charge current, energy current, and their fluctuations with electrochemical potential and temperature fluctuations in a probe contact. Moreover, we discuss experimental issues in detecting of these quantities in the time-dependently driven mesoscopic capacitor. We give an overview of different, experiment-related aspects that should be taken into account when optimizing the proposed detection scheme. Finally, all results of the work are summarized and presented in Chap. 6.

2 Theoretical description of time-dependent transport phenomena in mesoscopic systems

Over the past two decades, a scattering matrix approach, also referred to as the Landauer-Buttiker approach [37, 38], has proven to be an invaluable tool to study both equilibrium and non-equilibrium transport phenomena in non-interacting mesoscopic systems. In particular, the time-dependent (Floquet) scattering theory [39, 40] is used to describe a periodically driven mesoscopic system.

In this chapter, we present a review of the basics of Floquet scattering theory. Within this framework we derive transport quantities, such as charge current, energy current and their fluctuations, to characterize the system.

2.1 Setup

Our aim is to investigate transport properties in a periodically driven mesoscopic system. For this purpose, we introduce here a generic setup that captures main features of systems of interest in this thesis. In particular, it consists of a coherent mesoscopic conductor referred to as a scatterer connected to two contacts via

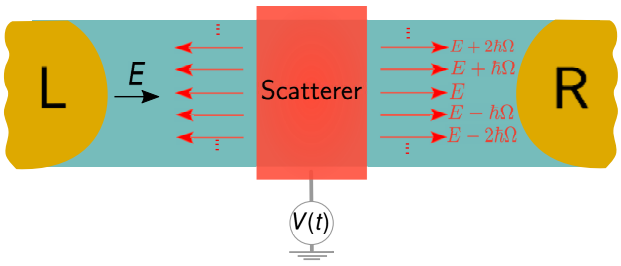

Figure 2.1: *Schematic representation of the system under consideration: A scattering region (red area) is periodically driven with frequency Ω (red area) connected to two electronic reservoirs (yellow area) via leads (green area). Particles with energy E emitted from the L(eft) reservoir can be reflected or transmitted by the scatterer while absorbing or emitting n Floquet quanta of energy (red arrows).*

ideal ballistic leads, as illustrated in Fig. 2.1. The system can be brought out of equilibrium with a periodically time-dependent potential energy. For example, this can be achieved either by applying a gate voltage to the scattering region or by applying a bias voltage to the contacts, see Chap. 1 for the two example systems treated here. Both left ($\alpha = L$) and right ($\alpha = R$) contacts act as an reservoirs of non-interacting electrons with well-defined temperature T_α and electrochemical potential μ_α. Furthermore, it is assumed that the temperature and electrochemical potential are not affected by the flow of particles into and out of the reservoir[1]. The scatterer and the reservoirs are connected to each other through ballistic leads. Each lead can support N transport channels which basically work as waveguides for electrons, however, for simplicity we consider here only one channel per lead. Electrons injected from reservoirs propagate coherently in the leads and can either be reflected or transmitted through the scatterer periodically driven with a frequency of $\Omega = 2\pi/\mathcal{T}$, where $\mathcal{T}$ is the period of the driving. In the next section we study this scatterer through Floquet scattering matrix.

2.2 Floquet scattering matrix

According to the Floquet scattering theory [40–42], electrons can absorb or emit n energy quanta $\hbar\Omega$ (Floquet quanta) when scattering at a time-dependent potential energy, as schematically indicated with the red arrows in Fig. 2.1. In the following, we derive a relation between the incoming and outgoing wave functions by introducing the Floquet scattering matrix.

The time-dependent Schrödinger equation for an electron in the scattering region, characterized by the wave function ψ and mass m, is given by

$$\frac{\partial\psi(t,\vec{r})}{\partial t} = [H(\vec{r}) + U(t)]\,\psi(t,\vec{r}), \tag{2.1}$$

with the potential energy $U(t)$ being periodic in time, $U(t+\mathcal{T}) = U(t)$. The Floquet function method [43, 44] assumes that if $\psi(t,\vec{r})$ is a solution to Eq. (2.1), then so is $\psi(t+\mathcal{T},\vec{r})$. This result is known as the Floquet theorem. Consequently, in analogy with the Bloch theorem, the wave function can be written as

$$\psi(t,\vec{r}) = e^{-i\frac{Et}{\hbar}} \sum_{q=-\infty}^{\infty} e^{-iq\Omega t}\psi_q(\vec{r}). \tag{2.2}$$

This so-called Floquet wave function is a superposition of an infinite number of sidebands corresponding to different energies. Note that in the stationary case, that is, when driving in the scattering region is switched off, only the term with $q = 0$ survives. The energy E is not uniquely defined, which means that if E

[1]Note that, this is only the case until Chap. 5

changes by an arbitrary number $p \in \mathbb{Z}$ of energy quanta to $E + p\hbar\Omega$, the wave function remains unaffected. Thus, it is convenient to choose the energy E to be the Floquet energy, since it is defined up to the energy quantum $\hbar\Omega$.

The wave function in the leads (outside of the scatterer), which is a superposition of impinging wave functions and outgoing wave functions from the scatterer, is described also by Eq. (2.2) [45]. Note that impinging wave functions are described by Eq. (2.2) with $q = 0$. We add index $\alpha = \mathrm{R}$ (L) to the wave function $\psi_{\alpha q}(\vec{r})$ which refers to the wave function associated with the right (left) side of the conductor with respect to the scattering region. The unknown wave function $\psi_{\alpha q}(\vec{r})$ is derived by solving the time-independent Schrödinger equation for a stationary Hamiltonian in the leads,

$$H_\alpha(\vec{r}) = \frac{P_{\alpha x}^2}{2m} + \frac{P_{\alpha\perp}^2}{2m}. \tag{2.3}$$

Eigenstates $\psi_{\alpha,q}(\vec{r})$ of $H_\alpha(\vec{r})$ can be expanded in orthogonal basis states

$$\psi_{\alpha q} \propto \chi_\alpha(\vec{r}_\perp) e^{ik_{\alpha q}x}. \tag{2.4}$$

Here, $k_{\alpha q} = \sqrt{2m(E_q - E_\alpha)/\hbar}$ is the wave vector of an electron moving freely in the longitudinal direction (x-axis) and $\chi_\alpha(\vec{r}_\perp)$ is the standing wave which describes the transverse component of the wave function. The wave function $\psi_{\alpha q}(\vec{r})$ is the superposition of incoming and outgoing basis states in lead α. The basis states which enter the scatterer are described by Eq. (2.4) with $k > 0$, while these exiting the scatterer are given by Eq. (2.4) with $k < 0$. The full state in the lead α reads as

$$\psi_\alpha(t, \vec{r}) = \int \mathrm{d}E\, \chi_\alpha(\vec{r}_\perp) \sum_q \left[\frac{a_\alpha(E_q)}{\sqrt{\hbar v_\alpha(E_q)}} e^{ik_{\alpha q}x} + \frac{b_\alpha(E_q)}{\sqrt{\hbar v_\alpha(E_q)}} e^{-ik_{\alpha q}x} \right] e^{-i\frac{E_q t}{\hbar}}, \tag{2.5}$$

where $v_\alpha(E_q)$ is the velocity of each state. Here, $a_\alpha(E_q)/\sqrt{\hbar v_\alpha(E_q)}$ is the probability amplitude of the current carrying states into the scatterer at the energy E_q [1], and $b_\alpha(E_q)/\sqrt{\hbar \nu_\alpha(E_q)}$ is the probability amplitude of the current carrying states from the scatterer at the energy E_q.

If we assume that the incoming coefficients $a_\alpha(E_q)$ are known, the outgoing coefficients $b_\alpha(E_q)$ are found from

$$b_\alpha(E_q) = \sum_{\beta=\mathrm{L,R}} \sum_{m=-\infty}^{\infty} S_{\mathrm{F},\alpha\beta}(E_q, E_m) a_\beta(E_m), \tag{2.6}$$

[1] Note that E_q is equal to $E + q\hbar\Omega$. Since the Floquet energy E is defined up to $\hbar\Omega$ and q can take negative numbers, also E_q can be negative. As a result, $E_q - E_\alpha$ can become negative, leading in turn to imaginary $k_{\alpha q} = \sqrt{2m(E_q - E_\alpha)/\hbar}$, which corresponds to a bound state that does not contribute to transport.

where $S_{\mathrm{F},,\alpha\beta}(E_q, E_m)$ is the Floquet scattering matrix. All information about transport properties are encoded in this matrix. The amplitudes of this matrix depend on two energies: First, the incident energy $E + m\hbar\Omega$ from the lead β, and second, the scattered energy $E + q\hbar\Omega$ to the lead α. The number $q - m$ is the amount of absorbed or emitted energy quanta, which means that energy is not conserved during a scattering process. However, in the stationary case (when the driving is off), these amplitudes are entirely determined by the incoming energy [46]. Therefore, the relation between the incident and the scattered amplitude reduces to $b_\alpha(E) = \sum_{\beta=\mathrm{L,R}} S_{\alpha\beta}(E) a_\beta(E)$, meaning that energy is conserved.

Conservation of the number of particles during the scattering process leads to unitarity of the Floquet scattering matrix,

$$\sum_n \sum_\alpha S^*_{\mathrm{F},,\alpha\beta}(E_n, E_m) S_{\mathrm{F},,\alpha\gamma}(E_n, E) = \delta_{m0}\delta_{\beta\gamma}. \tag{2.7}$$

2.2.1 Second quantization

In order to calculate the transport quantities, it is convenient to use the second quantization representation. To use this formalism, the amplitudes are replaced by annihilation [creation] operators $\hat{a}_\alpha(E)$ $[\hat{a}^\dagger_\alpha(E)]$ corresponding to an incoming electron from a reservoir α at energy E. Likewise, $\hat{b}_\alpha(E)$ $[\hat{b}^\dagger_\alpha(E)]$ refers to an annihilation [creation] operator corresponding to an outgoing electron to a reservoir α at energy E. The field operator is determined after replacing $a_\alpha(E)$ and $b_\alpha(E)$ in Eq. (2.5) with $\hat{a}_\alpha(E)$ and $\hat{b}_\alpha(E)$, respectively. This yields

$$\hat{\psi}_\alpha(t, \vec{r}) = \int \mathrm{d}E \sum_q \frac{\chi_\alpha(\vec{r}_\perp)}{\sqrt{h\nu_\alpha(E_q)}} \left[\hat{a}_\alpha(E_q) e^{ik_{\alpha q}x} + \hat{b}_\alpha(E_q) e^{-ik_{\alpha q}x}\right] e^{-i\frac{E_q}{\hbar}t}, \tag{2.8}$$

$$\hat{\psi}^\dagger_\alpha(t, \vec{r}) = \int \mathrm{d}E \sum_q \frac{\chi^*_\alpha(\vec{r}_\perp)}{\sqrt{h\nu_\alpha(E_q)}} \left[\hat{a}^\dagger_\alpha(E_q) e^{-ik_{\alpha q}x} + \hat{b}^\dagger_\alpha(E_q) e^{ik_{\alpha q}x}\right] e^{i\frac{E_q}{\hbar}t}. \tag{2.9}$$

Using these field operators, we can define current operator in terms of the incoming and outgoing operators. If we assume that the incoming operators are known, the outgoing operators are defined by

$$\hat{b}_\alpha(E_q) = \sum_{\beta=\mathrm{L,R}} \sum_{m=-\infty}^{\infty} S_{\mathrm{F},\alpha\beta}(E_q, E_m) \hat{a}_\beta(E_m), \tag{2.10}$$

$$\hat{b}^\dagger_\alpha(E_q) = \sum_{\beta=\mathrm{L,R}} \sum_{m=-\infty}^{\infty} S^*_{\mathrm{F},\alpha\beta}(E_q, E_m) \hat{a}^\dagger_\beta(E_m). \tag{2.11}$$

The operators $\hat{a}_\beta(E)$ and $\hat{b}_\alpha(E)$ are fermionic operators, reflecting the fact that we are dealing with electrons. Therefore, they obeys anti-commutation rules, $\left\{\hat{a}^\dagger_\alpha(E), \hat{a}_\beta(E')\right\} = \delta_{\alpha\beta}\delta(E - E')$, and the same holds for $\hat{b}_\beta(E)$.

As it will be seen in Sec. 2.4, to derive currents and their fluctuations, we need to evaluate the quantum-statistical average of products of pair operators,

$\langle \hat{a}^\dagger_\alpha(E)\hat{a}_\beta(E')\rangle$ and $\langle \hat{b}^\dagger_\alpha(E)\hat{b}_\beta(E')\rangle$. Assuming that the reservoirs are in an equilibrium state, the statistics of the incoming operators can be determined by the equilibrium statistical properties of the reservoirs. These properties are characterized by the Fermi-Dirac distribution function of the reservoir, $f_\alpha(E) = 1/[1 + e^{(E-\mu_\alpha)/k_\mathrm{B}T_\alpha}]$, with temperature T_α, Boltzmann constant k_B and electrochemical potential μ_α. Consequently, the expression describing the distribution function for the incoming particles is

$$\langle \hat{a}^\dagger_\alpha(E)\hat{a}_\beta(E')\rangle = \delta_{\alpha\beta}\delta(E - E')f_\alpha(E). \tag{2.12}$$

The statistics of the outgoing operators derived using Eq. (2.10) and Eq. (2.11),are given by

$$\langle \hat{b}^\dagger_\alpha(E)\hat{b}_\beta(E')\rangle = \sum_{\alpha',\beta'}\sum_{n,m=-\infty}^{\infty} S_{\mathrm{F},\alpha\alpha'}(E, E_n)S_{\mathrm{F},\beta\beta'}(E', E'_m)\langle \hat{a}^\dagger_{\alpha'}(E_n)\hat{a}_{\beta'}(E'_m)\rangle.$$

For the stationary case, the relation above reduces with the help of Eq. (2.12) to $\langle \hat{b}^\dagger_\alpha(E)\hat{b}_\alpha(E')\rangle = \sum_\beta |S_{\alpha\beta}(E)|^2 f_\beta(E)$.

2.3 Time representation of the scattering matrix

We have introduced above the scattering matrix in the energy representation. However, in next chapter where we describe the mesoscopic capacitor, another representation of the scattering matrix will be more convenient to use. By means of a Fourier transform, the scattering matrix can be expressed in time space, $\hat{S}(t, t')$, in which the incident particle at time t can be detected at t'. For our purposes, a more useful representation is actually the mixed time-energy form. Performing a partial Fourier transform it can be written in the form

$$\hat{S}(t, E) = \sum_{n=-\infty}^{\infty} \mathrm{e}^{-in\Omega t}\, \hat{S}(E_n, E), \tag{2.13}$$

and

$$\hat{S}(E_n, E) = \int_0^{\mathcal{T}} \frac{\mathrm{d}t}{\mathcal{T}} \mathrm{e}^{in\Omega t}\, \hat{S}(t, E). \tag{2.14}$$

The scattering amplitude $S(t, E)$ is determined by the energy of the incident particle E and the time t when the particle leaves the scatterer. This representation is consistent with the Heisenberg uncertainty principle: When the time of departure from the scatterer is well defined, see Eq. (2.13), then the energy of the particle is not defined and its energy can be one of $E_n = E + n\hbar\Omega$.

Inserting the definition of $S(t, E)$ into Eq. (2.7), and making the inverse transformation, the unitarity condition is expressed as follows:

$$\int_0^{\mathcal{T}} \frac{\mathrm{d}t}{\mathcal{T}} \mathrm{e}^{in\Omega t}\, \hat{S}(t, E_n)\, \hat{S}(t, E) = \delta_{n0}\hat{I}. \tag{2.15}$$

This property will prove especially useful for reducing the number of scattering amplitudes that contribute in the transport quantities, when calculating current noises in Sec. 2.6.

2.4 Charge current

The charge current operator can be derived by using the continuity equation together with the Schrödinger equation. Let us begin with the continuity equation for particles, which can be written as

$$\frac{\partial \rho_\alpha}{\partial t} = -\vec{\nabla} j_\alpha(\vec{r}, t), \tag{2.16}$$

where j_α is the particle-current density, and $\rho_\alpha = |\psi_\alpha|^2$ is the particle density. Note that below for the sake of compact notation, we use $\psi_\alpha(t, \vec{r}) \equiv \psi_\alpha$. From the Schrödinger equation we have $i\hbar\partial_t\psi_\alpha = H\psi_\alpha$ and $-i\hbar\partial_t\psi_\alpha^* = H\psi_\alpha^*$, where $H(\vec{r}) = -\vec{\nabla}^2\hbar^2/2m + U(t)$. Therefore, the left side of the equation above can be calculated as follows,

$$\begin{aligned}\frac{\mathrm{d}}{\mathrm{d}t}\left[\psi_\alpha^*\psi_\alpha\right] &= \frac{\mathrm{d}\psi_\alpha^*}{\mathrm{d}t}\,\psi_\alpha + \psi_\alpha^*\,\frac{\mathrm{d}\psi_\alpha}{\mathrm{d}t} \\ &= \frac{\hbar}{2im}\vec{\nabla}\left[\vec{\nabla}\psi_\alpha^*\,\psi_\alpha - \psi_\alpha^*\,\vec{\nabla}\psi_\alpha\right].\end{aligned} \tag{2.17}$$

By comparing above equation with Eq. (2.16), we can extract the particle-current density. By substituting wave functions with field operators, we can define the particle-current density operator as

$$\hat{j}_\alpha(\vec{r}, t) = \frac{\hbar}{2mi}\left[\hat{\psi}_\alpha^\dagger(t, \vec{r})\frac{\partial\hat{\psi}_\alpha(t, \vec{r})}{\partial x} - \frac{\partial\hat{\psi}_\alpha^\dagger(t, \vec{r})}{\partial x}\hat{\psi}_\alpha(t, \vec{r})\right]. \tag{2.18}$$

Our aim is to calculate the charge current operator which is defined as $\hat{I}_\alpha(x, t) = -e\int d\vec{r}_\perp\hat{j}_\alpha(\vec{r}, t)$, where $d\vec{r}_\perp$ indicates the integral over the cross section of the lead α and the electron charge is $-e$ while $e > 0$. Now, we express the current operator in terms of the incoming and outgoing operators, Eq. (2.8) and Eq. (2.9), and we obtain (further details can be found in App. A)

$$\hat{I}_\alpha(t) = -\frac{e}{h}\iint \mathrm{d}E\mathrm{d}E' e^{i(E-E')t/\hbar}\left\{\hat{b}_\alpha^\dagger(E)\hat{b}_\alpha(E') - \hat{a}_\alpha^\dagger(E)\hat{a}_\alpha(E')\right\}. \tag{2.19}$$

The time-dependent charge current is obtained by evaluating the quantum average of Eq. (2.19), where the quantum averages $\langle\hat{a}_\alpha^\dagger(E)\hat{a}_\alpha(E')\rangle$ and $\langle\hat{b}_\alpha^\dagger(E)\hat{b}_\alpha(E')\rangle$ are given by Eq. (2.12) and Eq. (2.13):

$$\begin{aligned}I_\alpha(t) &= \langle\hat{I}_\alpha(t)\rangle \\ &= -\frac{e}{h}\sum_\beta\sum_{n,l}\int \mathrm{d}E e^{-il\Omega t}S_{\alpha\beta}^*(E, E_n)S_{\alpha\beta}(E_l, E_n)\{f_\beta(E_n) - f_\alpha(E)\}.\end{aligned} \tag{2.20}$$

Moreover, the time-averaged charge current, $\bar{I}_\alpha = (1/\mathcal{T})\int_0^{\mathcal{T}} \mathrm{d}t\langle\hat{I}_\alpha(t)\rangle$, is given by

$$\bar{I}_\alpha = -\frac{e}{h}\sum_\beta \sum_{m=-\infty}^{\infty} \int \mathrm{d}E\, |S_{\alpha\beta}(E, E_n)|^2 \{f_\beta(E_n) - f_\alpha(E)\}. \tag{2.21}$$

Note that the charge current in the stationary case (time-dependent potential is switched off) is obtained by substituting $S_{\alpha\beta}(E, E_n)$ with $S_{\alpha\beta}(E)\delta_{n0}$ in the above equations.

2.5 Energy current

Particles carry energy independent of their charge. Thus, by studying energy current, we can get information about the energy properties of the injected particle. The starting point is now the continuity equation for energy,

$$\frac{\partial \rho^E}{\partial t} = -\vec{\nabla} j^E + \rho_{\mathrm{S}}^E, \tag{2.22}$$

where j^E is the energy-current density and $\rho^E = \langle H\rangle$ is the energy density. Notice that since the time-dependent potential pumps here energy into the system, we have to add a source term ρ_{S}^E to the continuity equation. This term, ρ_{S}^E, is called energy density of a source. Following the same line as for the charge current, we consider first, the left hand side of this equation. Therefore, we look at the energy density separately, and start to calculate the expectation value for the energy of an electron with Hamiltonian $\mathcal{H}(t, \vec{r}) = -\vec{\nabla}^2\hbar^2/2m + V(t)$,

$$\begin{aligned}\langle H\rangle = \langle\psi|H|\psi\rangle =& \int \mathrm{d}\vec{r}\int \mathrm{d}\vec{r'}\langle\psi|\vec{r}\rangle\langle\vec{r}|H|\vec{r'}\rangle\langle\vec{r'}|\psi\rangle \\ =& \frac{1}{2}\int \mathrm{d}\vec{r}\left[\langle\psi|\vec{r}\rangle\langle\vec{r}|H|\psi\rangle + \langle\psi|H|\vec{r}\rangle\langle\vec{r}|\psi\rangle\right],\end{aligned} \tag{2.23}$$

and for its time derivative,

$$\partial_t \rho^E = \frac{1}{2}\int \mathrm{d}\vec{r}\,\partial_t\left[\langle\psi|\vec{r}\rangle\langle\vec{r}|H|\psi\rangle + \langle\psi|H|\vec{r}\rangle\langle\vec{r}|\psi\rangle\right]. \tag{2.24}$$

Then, the integrand is transformed with the help of the Schrödinger equation,

$$\begin{aligned}&\partial_t\left[\langle\psi|\vec{r}\rangle\langle\vec{r}|H|\psi\rangle + \langle\psi|H|\vec{r}\rangle\langle\vec{r}|\psi\rangle\right] \\ &= 2\frac{\partial V(t)}{\partial t}\psi^*\psi - \frac{\hbar^2}{2m}\left(\partial_t\psi^*\vec{\nabla}^2\psi + \psi^*\vec{\nabla}^2\partial_t\psi + \partial_t\psi\vec{\nabla}^2\psi^* + \psi\vec{\nabla}^2\partial_t\psi\right).\end{aligned} \tag{2.25}$$

After doing some straightforward algebra, given in App. B, the Eq. (2.24) can be reformulated as

$$\partial_t \rho^E = \frac{\partial V(t)}{\partial t}\rho - \frac{\hbar^2}{4m}\nabla\left[\psi^*\vec{\nabla}\partial_t\psi - \partial_t\psi^*\vec{\nabla}\psi + \psi\vec{\nabla}\partial_t\psi^* - \partial_t\psi\vec{\nabla}\psi^* - \frac{4m}{\hbar^2}V(t)j(\vec{r})\right]. \tag{2.26}$$

If we now compare the equation above and Eq. (2.22), we will find out that the first term in Eq. (2.26), due to the power provided by the time-dependent driving, acts as a source term, meaning that

$$\rho_{\mathrm{S}}^E = \frac{\partial V(t)}{\partial t}\rho, \tag{2.27}$$

and from the second term of Eq. (2.26), the energy-current density is found to be

$$j_\alpha^E(\vec{r},t) = -\frac{\hbar^2}{4m}\nabla\left[\psi^*\vec{\nabla}\partial_t\psi - \partial_t\psi^*\vec{\nabla}\psi + \psi\vec{\nabla}\partial_t\psi^* - \partial_t\psi\vec{\nabla}\psi^* - \frac{4m}{\hbar^2}V(t)j(\vec{r})\right]. \tag{2.28}$$

The energy-current density operator $\hat{j}^E$ is determined by replacing the wave functions with the field operators in the equation above. In the following, when considering the mesoscopic capacitor, we take $V(t) = 0$ in all reservoirs. Therefore, the total energy current operator, $\hat{I}_\alpha^E(x,t) = \int d\vec{r}_\perp \hat{j}_\alpha^E(\vec{r},t)$, is defined by

$$\hat{I}_\alpha^E(t) = \frac{1}{h}\iint \mathrm{d}E\mathrm{d}E' \frac{E+E'}{2} e^{i(E-E')t/\hbar}\left\{\hat{b}_\alpha^\dagger(E)\hat{b}_\alpha(E') - \hat{a}_\alpha^\dagger(E)\hat{a}_\alpha(E')\right\}. \tag{2.29}$$

Taking the quantum average of the energy-current operator, we obtain the time-dependent energy current,

$$I_\alpha^E(t) = \frac{1}{h}\sum_\beta\sum_{n,l}\int \mathrm{d}E\left(E + \frac{l\hbar\Omega}{2}\right)e^{-il\Omega t}S_{\alpha\beta}^*(E,E_n)S_{\alpha\beta}(E_l,E_n) \times \{f_\beta(E_n) - f_\alpha(E)\}. \tag{2.30}$$

In analogy to the charge current, we also obtain the average energy current by integrating the time-dependent energy current over one period of the driving, $\bar{I}_\alpha^E = (1/\mathcal{T})\int_0^{\mathcal{T}} \mathrm{d}t I_\alpha^E(t)$ and we get

$$\bar{I}_\alpha^E = \frac{1}{h}\sum_\beta\sum_{n=-\infty}^{\infty}\int \mathrm{d}E\, E\,|S_{\alpha\beta}(E,E_n)|^2\{f_\beta(E_n) - f_\alpha(E)\}. \tag{2.31}$$

Note that in the context of transport, the relevant physical quantity is the heat current. This quantity corresponds to the energy carried by particles, and

measured with respect to the electrochemical potential of the relevant contact when $V(t) = 0$,

$$J_\alpha(t) = I^E_\alpha(t) + \frac{\mu_\alpha}{e} I_\alpha(t). \tag{2.32}$$

The time-average heat current is then achieved by taking the average of the energy and the charge current.

2.6 Current noise

So far, we have focused on the expectation value of the charge, the energy and the heat current. However, these currents can also fluctuate. We analyze these fluctuations through their noise spectra in order to get additional information about the transport properties in mesoscopic conductors.

We follow Ref. [46] to explain the origin of noise in a mesoscopic coherent conductor. In general, the two main sources of noise in these type of systems are thermal fluctuations (thermal noise), and fluctuations due to random emission of particles (shot noise). At finite temperatures, thermal noise leads to fluctuations of the occupation of states in a conductors, which is charactrized by the occupation number n that can equal either zero or one for each fermionic state. The statistical average of the occupation number is given by the Fermi distribution function $\langle n \rangle = f$. At equilibrium (i.e., without applying any external voltage) fluctuations of the occupation number away from its statistical average are given by

$$\langle (n - \langle n \rangle)^2 \rangle = f(1 - f). \tag{2.33}$$

When the system is driven out of equilibrium (with a bias voltage or a time-dependent gate voltage) into a transport regime, one can observe shot noise, even at zero temperature. Shot noise in an electrical conductor is a consequence of charge quantization and provides information which cannot be obtained from a conductance measurement alone. To demonstrate the origin of shot noise, we consider the same system as in Fig. 2.1 where the scattering region is a barrier (stationary case) with energy-independent probability for transmission D and reflection $R = 1 - D$. Then, a stream of particles is sent towards the barrier.

Let us indicate the occupation number of the incident state by $n_{\rm inc}$. This state is occupied with probability 1 and on the average $\langle n_{\rm inc} \rangle = 1$, thereby the fluctuation $\Delta n_{\rm inc} = n_{\rm inc} - \langle n_{\rm inc} \rangle = 0$. Consider now the transmitted state and the reflected state characterized by the occupation numbers n_D and n_{1-D}, respectively. Since, due to scattering, a particle is either transmitted or reflected, we have $\langle n_D n_R \rangle = 0$. The average occupation numbers are $\langle n_D \rangle = D$ and $\langle n_R \rangle = 1 - D$, and owing to the fermionic nature of electrons the average of squares occupation numbers are $\langle (n_D)^2 \rangle = D$ and $\langle (n_R)^2 \rangle = 1 - D$. Using this, the mean squares of the transmitted and reflected beams as well as and their correlations are given by

$$\langle (\Delta n_R)^2 \rangle = \langle (\Delta n_D)^2 \rangle = -\langle \Delta n_D \Delta n_R \rangle = D(1 - D). \tag{2.34}$$

Such fluctuations are called *partition noise* because the scatterer divides the incident stream of particles into two streams of integer particles. The partition noise vanishes both in the limit of a transmission probability of unity and for vanishing D.

Let us provide a more formal derivation of Eqs. (2.33) and (2.34) by employing currents operator instead of occupation numbers. By calculating the quantum statistical expectation value of the correlator between the current fluctuations, we can determine the low frequency spectral density of the current noise $\mathcal{P}^{XY}_{\alpha\beta}(\omega)$. Using the Landauer-Buttiker formalism [38, 46], we have

$$2\pi\delta(\omega+\omega')\mathcal{P}^{XY}_{\alpha\beta}(\omega) = \frac{1}{2}\langle\{\delta\hat{X}_\alpha(\omega), \delta\hat{Y}_\beta(\omega')\}\rangle, \tag{2.35}$$

where $\Delta\hat{X} = \hat{X} - \langle\hat{X}\rangle$ is the current fluctuation. The charge-current noise $\mathcal{P}^{II}_{\alpha\beta}$ is obtained by replacing operators X and Y with the charge current operator, Eq. (2.19). Importantly, by substituting X and Y with I^E, energy-current noise $\mathcal{P}^{EE}_{\alpha\beta}$ is defined. This quantity is of the central interest in this thesis, as it allows for obtaining information about energy properties of the scattering regime. The mixed-current noise which stems from the fact that emitted particles carry both charge and energy, is described with the correlation between the charge-current operator $\hat{X} = \hat{I}$ and the energy-current operator $\hat{Y} = \hat{I}^E$ and shows different features from those of the charge- and energy-current noises. The current noise can be detected in the reservoirs $\alpha, \beta = \mathrm{L}, \mathrm{R}$. The case of $\alpha = \beta$ is referred to as the auto-correlation noise while the case of $\alpha \neq \beta$ is known as the cross-correlation noise.

2.6.1 Zero-frequency noise

The current noise $\mathcal{P}^{XY}_{\alpha\beta}(\omega)$ at zero-frequency can be written as

$$\mathcal{P}^{XY}_{\alpha\beta}(\omega=0) = \int_0^{\mathcal{T}} \frac{\mathrm{d}t}{\mathcal{T}} \int_{-\infty}^{\infty} \mathrm{d}t' \langle \Delta X_\alpha(t')\, \Delta Y_\beta(t+t')\rangle. \tag{2.36}$$

By employing the Floquet scattering theory [47], the zero-frequency noise is identified to have two different physical contributions. The first one stems from correlations due to the particle exchange between two different reservoirs, therefore, and we will refer to it as the *transport* part of the noise. It is given by

$$\begin{aligned}\mathcal{P}^{XY}_{\mathrm{tr}(\alpha\beta)} =& \frac{1}{h}\sum_{\gamma\neq\eta}\sum_{n,m,q}\int \mathrm{d}E\; x y_q\, f_\gamma(E_n)\; [1 - f_\eta(E_m)] \\ & \times S^*_{\alpha\gamma}(E,E_n) S_{\beta\gamma}(E_q,E_n) S_{\alpha\eta}(E,E_m) S^*_{\beta\eta}(E_q,E_m).\end{aligned} \tag{2.37}$$

On the other hand, the second contribution originates from correlations due to the exchange of particles between states with different energies in the same reservoir,

and thus, it is called the *interference* part of the noise,

$$\begin{aligned}\mathcal{P}^{XY}_{\mathrm{int}(\alpha\beta)} =& \frac{1}{h}\sum_{\gamma}\sum_{n,m,q}\int \mathrm{d}E\; x y_q\; f_\gamma(E_n)\;[1-f_\gamma(E_m)] \\ & \times S^*_{\alpha\gamma}(E,E_n)S_{\beta\gamma}(E_q,E_n)S_{\alpha\gamma}(E,E_m)S^*_{\beta\gamma}(E_q,E_m) \\ & -\frac{1}{h}\sum_{q}\int \mathrm{d}E\; x y_q\,|S_{\alpha\beta}(E,E_q)|^2 f_\beta(E_q)\;[1-f_\beta(E_q)] \\ & -\frac{1}{h}\sum_{q}\int \mathrm{d}E\; x_q y\;\left[|S_{\beta\alpha}(E,E_q)|^2-\delta_{\alpha\beta}\delta_{q,0}\right] f_\alpha(E_n)\;[1-f_\alpha(E_n)]\,.\end{aligned} \tag{2.38}$$

Here, the expression for the charge-current noise $\mathcal{P}^{II}$ is obtained when $x=y=-e$ and $x_q=y_q=-e$. The energy-current noise $\mathcal{P}^{EE}$ is acquire by replacing $x,y=E$ and $x_q=y_q=E+q\hbar\Omega$. The mixed-current noise $\mathcal{P}^{IE}$, is given when $x=E$ and $x_q=E+q\hbar\Omega$ and $y_q=y=-e$.

So far, we have formulated the transport quantities in the presence of the time-dependent potential energy, using the Floquet scattering matrix. However, calculating these quantities is a complicated task, in general. In the following, we are concerned with finding a regime in which, the calculation of these quantities is analytically possible.

2.7 Adiabatic approximation

To calculate the currents and their corresponding noises in terms of the Floquet scattering matrix, we need to solve the full time-dependent scattering problem which can only be done numerically. However, when the dynamical properties of the scattering region vary slowly, compared to the time a particle spends in the scatterer, an adiabatic approximation can be used instead. Such an approximation remains valid as long as the following condition is satisfied,

$$\frac{\hbar\Omega}{\delta E}\ll 1. \tag{2.39}$$

Here, δE is the interval energy over which the scattering matrix changes significantly, and Ω denotes the driving frequency with which the scatterer is modulated in time. In this limit, the Floquet scattering matrix can be expressed in terms of the frozen scattering matrix [40]. The frozen scattering matrix is not a real time dependent matrix, it rather corresponds to a stationary scattering matrix parametrized by time i.e., $S(\mathbf{x}(t),E)$ where $\mathbf{x}(t)=\left\{x_1(t),x_2(t),...,x_{N_\mathrm{p}}(t)\right\}$. Therefore, the adiabatic Floquet scattering matrix can be written as $S^{(0)}(t,E)=S(\mathbf{x}(t),E)$, where $\mathbf{x}(t)$ is a set of parameters changing slowly and periodically in time $\mathbf{x}(t)=\mathbf{x}(t+2\pi/\Omega)$.

The Floquet scattering matrix in the zeroth-order approximation is given by the Fourier transform of the frozen scattering matrix,

$$\hat{S}(t,E) \approx \hat{S}^{(0)}(t,E) = \sum_{n=-\infty}^{\infty} \mathrm{e}^{-in\Omega t}\, \hat{S}_n(E). \tag{2.40}$$

The elements $\hat{S}_n(E)$ are the Fourier coefficients of the frozen scattering matrix determined by the incident energy E and the transfered energy $n\hbar\Omega$,

$$\hat{S}_{\mathrm{ad}}(E,E_n) \equiv \hat{S}_n(E). \tag{2.41}$$

By inserting this equation in Eq. (2.7), we can see that this approximation still satisfies the unitarity condition up to the lowest order.

2.7.1 First-order approximation

In Ref. [47], the next leading (first) order in Ω of scattering matrix can be expanded through the frozen scattering matrix at the average of the initial and the final energy, $S_n\big([E_n+E]/2\big)$. One can then expand the frozen scattering matrix up to the first order in Ω and we end up with

$$\hat{S}(E,E_n) = \hat{S}_n(E) + \frac{n\hbar\Omega}{2}\,\frac{\partial \hat{S}_n(E)}{\partial E} + \hbar\Omega A_n(E). \tag{2.42}$$

Here, $A_n(E)$ is introduced for the unitarity condition Eq. (2.7) be to satisfied [1]. In Chap. 4 we derive the first-order correction of the scattering matrix to study transport quantities in the time-dependently driven mesoscopic capacitor beyond the adiabatic-response regime. We do this by explicitly expanding the time-evolution in the scattering matrix due to the periodically driven gate potential applied to the capacitor and find a result that exactly coincides with Eq. (2.42).

[1] Note that in this thesis because of our specific setup, $A_n(E)$ is zero. However, one would need to include this term, in systems with backscattering.

3 Characterization of on-demand electron sources

In this chapter, we investigate two different types of single-electron emission processes: First, from a driven mesoscopic capacitor [6], and second, from a time-dependent Lorentzian-shaped bias voltage [4, 30]. By employing time-dependent scattering theory we study transport phenomena, such as charge current, heat current and their corresponding noises as a spectroscopy tool to compare single particle pulses emitted from the two sources.

We start by describing the Floquet scattering matrix for two different setups: (i) a chiral setup including a slowly driven mesoscopic capacitor, and (ii) a non-chiral setup including a time-dependent, Lorentzian-shaped bias voltage. The main objective of this chapter is to compare these two types of setups analytically by studying transport quantities with the help of a Floquet scattering matrix approach.

We find that the two setups emit particles with equivalent energy spectra, however, they differ from each other in the number of emitted particles and design of the systems.

3.1 Emission schemes

Here, we describe the two different types of sources which were introduced in more details in Chap. 1. In both systems, there are two electronic reservoirs, which are kept at the same temperature, $k_{\mathrm{B}}T$. They are connected to each other *via* a mesoscopic conductor that includes a central scatterer, a QPC of energy-independent transparency D. Single electrons are injected from the left side and impinge on the central QPC from which they are scattered into either reservoir L or R. In this section, we describe the scatterer by the Floquet scattering matrix, which is comprised of two parts: first, the central QPC, and second, the single electron emitter.

3.1.1 Time-dependently driven mesoscopic capacitor

As Fig. 3.1(a) shows, the main ingredient of setup $\mathcal{A}$ is a chiral mesoscopic conductor. In the quantum Hall regime, single-channel edge states [red lines in

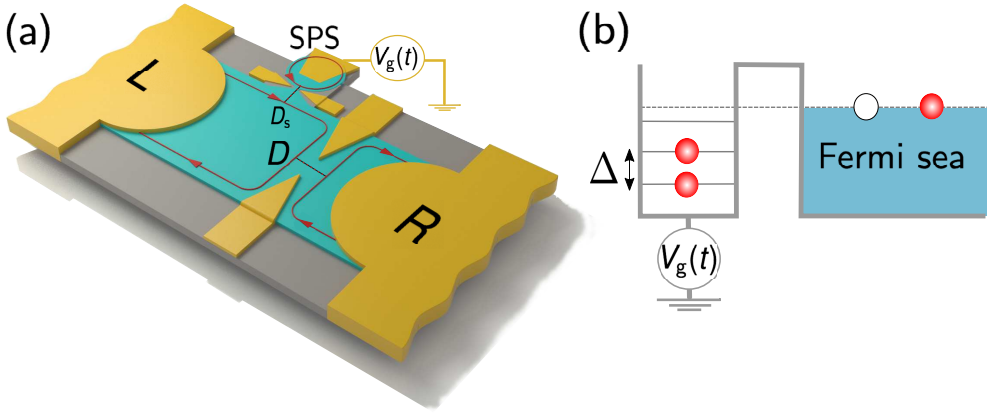

Figure 3.1: *(a) Sketch of the setup $\mathcal{A}$, the single particle source (SPS) consists of a mesoscopic capacitor with a time-dependently driven voltage $V_g(t)$. The capacitor is coupled to the edge state of a 2DEG (the green area) through the QPC with transparency D_s. Injected single particles from the capacitor propagate along an edge state (red lines with arrows) in the 2DEG. These particles can be reflected or transmitted by the central QPC with transparency D. (b) Principle of the single electron emission by the mesoscopic capacitor, it emits one electron/hole separately when an energy level of the QD resonates with the Fermi level of the reservoir. The level spacing of the capacitor is $\Delta = h/\tau$.*

Fig. 3.1(a)] arise due to the application of a high magnetic field perpendicular to a two-dimensional electron gas (2DEG).

It is assumed that only one edge state contributes to the transport, and acts as an electron waveguide. The core of setup $\mathcal{A}$ is a mesoscopic capacitor. It is coupled to the left-top edge state *via* a QPC with transparency D_s, demonstrated as modeled experimentally by Fève et al. [6]. Electrons propagating from reservoir L along the edge state, can be reflected with amplitude $\sqrt{1-D_\mathrm{s}}$ at the QPC, and continue their propagation along the edge state or, be transmitted into the capacitor region with amplitude $\sqrt{D_\mathrm{s}}$. Electrons which are transmitted into the capacitor acquire a time- and energy-dependent phase due to the time-dependently driven top-gate voltage and the discrete level spectrum of the confined region, respectively. It is convenient to construct the scattering matrix for this region semiclassically (using the analogy to a Fabry-Perot type scattering process [48]),

$$S_\mathrm{cap}(t,E) = -\sqrt{1-D_\mathrm{s}} + D_\mathrm{s}\sum_{q=1}^{\infty}\left(\sqrt{1-D_\mathrm{s}}\right)^{q-1} e^{iqkL - i\phi_q(t)}, \tag{3.1}$$

with the dynamical phase $\phi_q(t)$ that is given by

$$\phi_q(t) = \frac{1}{\hbar}\int_{t-q\tau}^{t} dt' U_\mathrm{g}(t'). \tag{3.2}$$

The scattering amplitude $S_\mathrm{cap}(t,E)$ depends on the energy of the incoming electron, E, and the time, t, at which the electron leaves the capacitor. The periodic

time-dependent potential energy of the electron is $U_{\rm g}(t) = \overline{U}_{\rm g} + \delta U_{\rm g}(t)$, where $\delta U_{\rm g}(\mathcal{T} + t') = \delta U_{\rm g}(t')$. Owing to the presence of this potential energy, electrons acquire a time-dependent phase $\phi_q(t)$, during such a propagation. The electron leaves the capacitor at time t after traveling q times around it, where the time for a single turn around the capacitor of length L is given by $\tau = m_e L/(\hbar k)$. The scattering amplitude can equivalently be written in terms of the incoming and outgoing energy, by taking a Fourier transform

$$S_{\rm cap}(E_n, E) = \int_0^{\mathcal{T}} \frac{dt}{\mathcal{T}} S_{\rm cap}(t, E) e^{in\Omega t}. \tag{3.3}$$

As shown in Fig. 3.1, electrons propagate along the edge state after being emitted from the capacitor, and they impinge on the central QPC with transparency D. These electrons can be reflected back to reservoir L with the probability amplitude $\sqrt{1-D}$ through the central QPC, or can be transmitted to reservoir R with the probability amplitude $\sqrt{D}$. The total scattering matrix, due to the central QPC and the mesoscopic capacitor, can be written as

$$S^{\mathcal{A}}(E_n, E) = \begin{pmatrix} \sqrt{1-D}\; S_{\rm cap}(E_n, E) & \sqrt{D}\; \delta_{n0} \\ \sqrt{D}\; S_{\rm cap}(E_n, E) & -\sqrt{1-D}\; \delta_{n0} \end{pmatrix}. \tag{3.4}$$

The obtained scattering matrix is energy-dependent. This makes the analytical derivation of transport quantities impossible. To this end, in the following, we describe the scattering matrix in the adiabatic-response regime, as explained in the Sec. 2.7.

Slowly driven mesoscopic capacitor: Adiabatic-response regime

In the adiabatic-response regime, Sec. 2.7, the scattering matrix of the mesoscopic capacitor can be described in terms of the frozen scattering matrix. Here, since the potential changes slowly with respect to the average time that an electron spends in the capacitor, one can only keep the first term in the expansion of the potential energy $U_{\rm g}(t')$ around time t in Eq. (3.2),

$$\int_{t-q\tau}^{t} dt' U_{\rm g}(t') = \int_{t-q\tau}^{t} dt' \left(U_{\rm g}(t) + (t'-t)\frac{\partial U_{\rm g}(t')}{\partial t'} + ... \right) = U_{\rm g}(t)\; q\tau. \tag{3.5}$$

This adiabatic expansion is valid only if the terms higher than the first order in $(q\Omega\tau)$ are negligible. This assumption can be made if the relevant adiabaticity parameter $\Omega\tau/D_{\rm s}$ is sufficiently small

$$\frac{\Omega\tau}{D_{\rm s}} \ll 1. \tag{3.6}$$

Note that the transparency D_s determines here the number of circulations of an electron around the capacitor after which the electron leaves it. In other words, the smaller the value of D_s is, the larger the number of circulations q will be and vice versa, i.e., $q \propto (1/D_\mathrm{s})$.

In the limit stated by Eq. (3.6), the scattering matrix, as formulated in Eq. (3.1), is given by the *frozen* scattering matrix

$$S^{(0)}_\mathrm{cap}(t,E) = \frac{\sqrt{1-D_\mathrm{s}} - e^{i\phi(t,E)}}{1-\sqrt{1-D_\mathrm{s}}e^{i\phi(t,E)}}. \tag{3.7}$$

Importantly, the time enters here only parametrically. Hence, the time- and energy-dependent phase acquired by an electron in the capacitor is

$$\phi(t,E) = k_\mu L + 2\pi\Delta^{-1}(E-\mu-\overline{U}_\mathrm{g}) - 2\pi\Delta^{-1}\delta U_\mathrm{g}(t). \tag{3.8}$$

In the above equation, we have linearized the energy spectrum around the Fermi level, $k(E) \sim k_\mu + (E-\mu)/(\hbar\nu)$, where k_μ is the wave number of an electron at the Fermi energy μ. Recall that $U_\mathrm{g}(t) = \overline{U}_\mathrm{g} + \delta U_\mathrm{g}(t)$, and notice also that we neglect the effect of screening, leading to a difference between the applied gate voltage $V_\mathrm{g}(t)$ and the induced potential [49–51]. Therefore, the potential energy is simply found to be proportional to the gate voltage through a negative charge $U_\mathrm{g}(t) = -eV_\mathrm{g}(t)$.

Here, we are interested in an ideal source that emits well-separated pulses which do not overlap with each other. First, we introduce the level width of the QD, that is $\delta = D_\mathrm{s}\Delta/(4\pi)$. This level width is defined by the coupling between the QD and the 2DEG. To have well-separated pulses, δ should be much smaller than the level spacing, $\delta \ll \Delta$, and for this reason, a weak coupling is required. This means that the transparency of the QPC has to be extremely small $D_\mathrm{s} \ll 1$. Consequently, as it is derived explicitly in App. C.1, the scattering matrix in the slow-driving regime gets the form [47, 52]

$$S^{(0)}_\mathrm{cap}(t,E) = \begin{cases} \dfrac{t-t^h_\mathrm{cap}-i\sigma_\mathrm{cap}}{t-t^h_\mathrm{cap}+i\sigma_\mathrm{cap}}, & 0 \le t < \mathcal{T}/2 \\ \dfrac{t-t^e_\mathrm{cap}+i\sigma_\mathrm{cap}}{t-t^e_\mathrm{cap}-i\sigma_\mathrm{cap}}, & \mathcal{T}/2 \le t < \mathcal{T}, \end{cases} \tag{3.9}$$

where 2σ is the width of the pulse in time, with σ given by

$$\sigma = \frac{D_\mathrm{s}}{2|\mathrm{d}\phi(t,E)/\mathrm{d}t|_{t^{h/e}_\mathrm{cap}}}. \tag{3.10}$$

Here, we assume that only one level of the QD contributes to the emission process. Therefore, the emission time of the electron, t^e_cap, is defined as the time at which the level of the QD crosses the Fermi level, while the potential energy is increased.

The time interval between electron t^e_{cap} and hole t^h_{cap} emission is long enough, so that the particles are definitely emitted before the next level crosses. This translates as

$$|t^e_{\mathrm{cap}} - t^h_{\mathrm{cap}}| \gg \sigma. \tag{3.11}$$

Now, using Eq. (3.3), the scattering matrix in the energy domain can be found to be

$$S_{n,\mathrm{cap}}(E) = \begin{cases} -2\Omega\sigma e^{-n\Omega\sigma_{\mathrm{cap}}} \mathrm{e}^{in\Omega t^e_{\mathrm{cap}}}, & n > 0, \\ -2\Omega\sigma e^{n\Omega\sigma_{\mathrm{cap}}} \mathrm{e}^{in\Omega t^h_{\mathrm{cap}}}, & n < 0, \\ \delta_{n,o}, & n = 0. \end{cases} \tag{3.12}$$

Where the parameters σ_{cap} and $t^{e/h}_{\mathrm{cap}}$ are, in principle, energy-dependent. However, the scattering matrix can be treated as energy-independent, when the thermal energy and the energy quanta of the driving frequency are much smaller than the energy scale for which the scattering matrix changes appreciably. In other words, this occurs when

$$\hbar\Omega, k_{\mathrm{B}}T \ll \hbar/\sigma. \tag{3.13}$$

In such a case, σ and $t^{h/e}_{\mathrm{cap}}$ are energy-independent and taken at the Fermi energy. The scattering matrix reads then as $S^{(0)}_{\mathrm{cap}}(t,\mu) = S_{\mathrm{cap}}(t)$. In consequence, the energy domain scattering matrix depends only on the energy difference, i.e., $S_{n,\mathrm{cap}}(\mu) = S_{n,\mathrm{cap}}$. Note that $S_{n,\mathrm{cap}}$ has to be unitary and fulfill $\sum_n |S_{n,\mathrm{cap}}|^2 = 1$. This is only necessary up to the first order in $\Omega\sigma$.

3.1.2 Lorentzian bias voltage

Now, we turn to describe the second example of on-demand single electron sources. Figure 3.2(a) shows a system consisting of a coherent conductor connected to reservoirs L and R. By applying a Lorentzian-shaped, time-dependent bias voltage, $V_{\mathrm{b}}(t)$, to reservoir L, single-particle pulses can be created. Due to the periodic nature of the driving potential, an electron can absorb or emit n energy quanta $\hbar\Omega$ with a probability amplitude [22]

$$c_n = \int_0^{\mathcal{T}} \frac{dt}{\mathcal{T}} c(t) \quad \text{with} \quad c(t) = e^{i\frac{e}{\hbar}\int_0^t dt' \left(V_{\mathrm{b}}(t') - \overline{V}_{\mathrm{b}}\right)}. \tag{3.14}$$

Here, $V_{\mathrm{b}}(t)$ is the periodically repeated Lorentzian-shaped, time-dependent voltage and is given by [30–32]

$$V_{\mathrm{b}}(t) = \frac{V_0\mathcal{T}}{\pi} \sum_{j=-\infty}^{\infty} \frac{\sigma_{\mathrm{lev}}}{\left(t - t^e_{\mathrm{lev}} - j\mathcal{T}\right)^2 + \sigma^2_{\mathrm{lev}}}. \tag{3.15}$$

Notice that the coefficient c_n depends only on the ac-component of the bias voltage, $V_{\mathrm{b}}(t) - \overline{V}_{\mathrm{b}}$, where $\overline{V}_{\mathrm{b}}$ is the dc-component of the voltage. Furthermore, $\mathcal{T}$ is

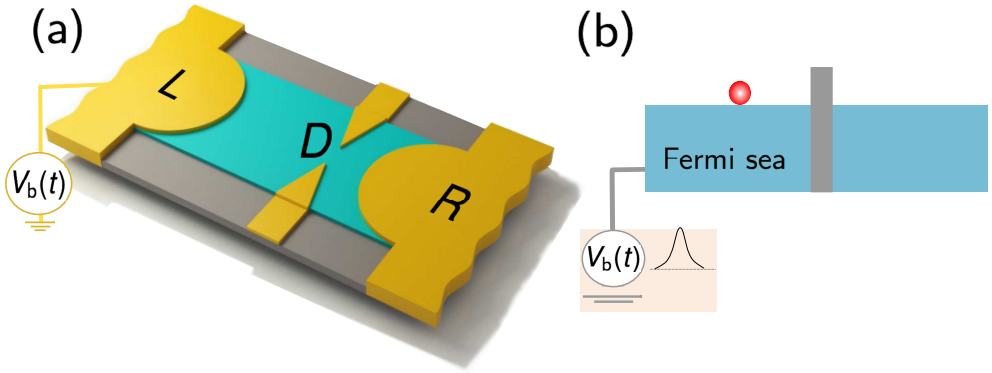

Figure 3.2: *(a) Sketch of setup $\mathcal{B}$, by applying the Lorentzian-shaped, time-dependent bias voltage $V_b(t)$ to reservoir L, single electrons propagate along a coherent conductor. These electrons can be reflected or transmitted by a central QPC with a transparency D. (b) Creation of a Leviton on the Fermi sea without any trace of a hole.*

the period of the bias voltage. An electron is emitted at time $t^e_{\rm lev}$ in every period and the width of the emitted pulse is equal to $2\sigma_{\rm lev}$. Integrating the voltage bias with respect to time over one period, $(e/h)\int_0^{\mathcal{T}} {\rm d}tV_{\rm b}(t)$, gives the integer number n of injected particles. Here, we assume that exactly one Leviton in every period is emitted. Thus, $n = 1$, if V_0 is given by $\hbar\Omega/e$,

$$\frac{e}{h}\int_0^{\mathcal{T}} {\rm d}tV_{\rm b}(t) = \frac{eV_0}{h/\mathcal{T}} = 1 \;\Rightarrow\; V_0 = \frac{h}{\mathcal{T}e}. \tag{3.16}$$

In the presence of $V_{\rm b}(t)$, the incoming operators $\hat{a}_{\rm L}$, which contribute in the current and noise operators, are not directly related to the operators $\hat{a}'_{\rm L}$ injected by the reservoir with equilibrium statistical properties. However, they are connected to each other through the relation

$$\hat{a}_{\rm L}(E) = \sum_{k=-\infty}^{+\infty} c_k \hat{a}'_{\rm L}(E_k). \tag{3.17}$$

The statistics of the operators $\hat{a}'$ and $\hat{a}'^{\dagger}$ are described by

$$\langle \hat{a}'^{\dagger}_{\rm L}(E)\hat{a}'_{\rm L}(E')\rangle = \sum_{k,l=-\infty}^{+\infty} f_\alpha(E_k)\delta(E_l - E'). \tag{3.18}$$

Notice that due to the absence of the time-dependent potential in reservoir R, $\hat{a}_{\rm R}(E) = \hat{a}'_{\rm R}(E)$. The particles impinging on the central QPC, can be reflected to the original reservoir or transmitted into the other one. The operators $\hat{b}_\alpha(E)$ of these scattered particles can also be related to the operators $\hat{a}'_\alpha(E)$, through the Floquet scattering matrix which reads

$$S^{\mathcal{B}}(E_n, E) = \begin{pmatrix} \sqrt{1-D}\;\delta_{n0} & \sqrt{D}\;c_n \\ \sqrt{D}\;c_n & -\sqrt{1-D}\;\delta_{n0} \end{pmatrix}. \tag{3.19}$$

Here, we have used $S(E_n, E)$ to keep the notation consistent. It is, however, important that the scattering matrix of setup $\mathcal{B}$ depends only on the transferred energy, $n\hbar\Omega$, and is independent of the incoming energy, E.

So far, we have described the scattering matrix of each setup, separately. They give the relation between the impinging and scattered operators contributing to the derivation of transport quantities. Next, we calculate these transport quantities to compare the emission scheme of the presented setups.

3.2 Comparison of two different on-demand single electron sources

In what follows, we compare two setups with different single electron sources that have been explained in the previous section, the mesoscopic capacitor in the slow-driving regime ($\mathcal{A}$) and the Lorentzian bias voltage ($\mathcal{B}$). We derive charge current, energy current and the corresponding noises in setup $\mathcal{A}$ to find its similarities and differences with setup $\mathcal{B}$ which has been studied in Refs. [10, 20, 21, 52].

It is important to keep in mind that the scattering amplitudes describing the slowly driven mesoscopic capacitor, Eq. (3.12), and the setup with the Lorentzian bias voltage, Eq. (3.14), depend only on the transferred energy. However, the former case is valid only at low temperatures and small frequencies, $\hbar\Omega, k_{\mathrm{B}}T \ll \hbar/\sigma$, while the latter one is held at any temperature and frequency ranges. In the next chapter, we study the mesoscopic capacitor when such a condition is relaxed.

3.2.1 Charge and energy currents

We start by calculating the time-dependent charge and energy currents of setup $\mathcal{A}$ and compare them with those of the setup $\mathcal{B}$ which have been studied in Ref. [10]. The time-dependent charge current in reservoir R for setup $\mathcal{A}$ with the slowly driven mesoscopic capacitor, see App. D.1 for more details, is found to be

$$I_{\mathrm{R}}^{\mathcal{A}}(t) = -\frac{e}{i2\pi} D \frac{\partial S_{\mathrm{cap}}^{*}(t)}{\partial t} S_{\mathrm{cap}}(t), \tag{3.20}$$

where we assumed $\mu_{\mathrm{L}} - \mu_{\mathrm{R}} = 0$. Here, $S_{\mathrm{cap}}(t)$ is the frozen scattering matrix of the mesoscopic capacitor in the slow-driving regime which is given in Eq. (3.9). By replacing Eq. (3.9) into the charge current, Eq. (3.20) becomes

$$I_{\mathrm{R}}^{\mathcal{A}}(t) = -\frac{e}{\pi} D \left[\frac{\sigma}{(t-t^{e})^2 + \sigma^2} - \frac{\sigma}{(t-t^{h})^2 + \sigma^2} \right]. \tag{3.21}$$

Likewise, for setup $\mathcal{B}$, one obtains

$$I_{\mathrm{R}}^{\mathcal{B}}(t) = -\frac{e}{\pi} D \frac{\sigma}{(t-t^{e})^2 + \sigma^2}. \tag{3.22}$$

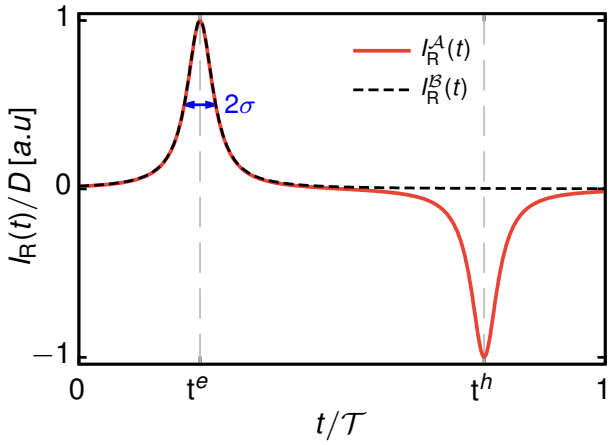

Figure 3.3: *Time-dependent charge current of setup $\mathcal{A}$ with the red solid line and setup $\mathcal{B}$ with the black dashed line in arbitrary units. The slowly driven mesoscopic capacitor emits one electron pulse at time t^e and one hole pulse at time t^h, while the Lorentzian-shaped bias voltage emits only one electron pulse at time t^e.*

In order to simplify the notation we henceforth indicate the pulse width by $\sigma_{\mathrm{cap}} = \sigma_{\mathrm{lev}} \equiv \sigma$. Analogously, we write the emission times of the capacitor as $t^e_{\mathrm{cap}} \equiv t^e$ and $t^h_{\mathrm{cap}} \equiv t^h$, and the emission time of the Leviton as $t^e_{\mathrm{lev}} \equiv t^e$.

Equation 3.21 is plotted in Fig. 3.3 with the red solid line. In setup $\mathcal{A}$, the electron-current pulse is emitted at time t^e with width 2σ, and the hole-current pulse is emitted at time t^h with the same width. Integrating each pulse with respect to time gives exactly one electric charge, e. This means that due to the emission of a hole and an electron pulse in each period, the average current is zero. In setup $\mathcal{B}$, the shape of the current pulse is the same. The only exception is that the hole-current pulse does not exist, as it is shown in Fig. 3.3 with the black dashed line.

Another difference can be found when studying the charge current in reservoir L for two different setups. In setup $\mathcal{A}$, the time-dependent charge current at reservoir L is obtained by substituting D with $1-D$ in Eq. (3.21). Therefore, we have

$$\frac{I^{\mathcal{A}}_{\mathrm{R}}(t)}{D} = \frac{I^{\mathcal{A}}_{\mathrm{L}}(t)}{1-D}. \tag{3.23}$$

The time-dependent charge current is not conserved unless we take into account the charging and discharging of the mesoscopic capacitor, which become clear from

$$I^{\mathcal{A}}_{\mathrm{R}}(t) + I^{\mathcal{A}}_{\mathrm{L}}(t) = e^2 \nu \frac{\partial U(t)}{\partial t}. \tag{3.24}$$

Here, ν is the instantaneous density of states in the capacitor and reads

$$\nu = \frac{1}{2\pi i} \frac{\partial S^*(t,E)}{\partial E}\bigg|_{E=\mu} S(t,\mu). \tag{3.25}$$

On the contrary, in setup $\mathcal{B}$, the time-dependent charge current is conserved at every instant

$$I_{\mathrm{R}}^{\mathcal{B}}(t) = -I_{\mathrm{L}}^{\mathcal{B}}(t). \tag{3.26}$$

This difference in conservation of the charge current in two setups $\mathcal{A}$ and $\mathcal{B}$, comes from the chirality of the conductor and also from the emission scheme. Unlike setup $\mathcal{B}$, particles in setup $\mathcal{A}$ are injected to the chiral edge state in the conductor from the *outside*. This leads to a contrast between Eqs. (3.23) and (3.26).

Beside charge, particles also carry energy. Thereby, it is useful to study the energy current to extract information on the energy properties of the emitted pulses. Importantly, the energy carried by the emitted particles does not depend on their charge. In analogy to the charge current, the time-dependent energy current in setup $\mathcal{A}$ is obtained by

$$I_{\mathrm{R}}^{E,\mathcal{A}}(t) = \frac{\hbar}{4\pi} D \, \frac{\partial S_{\mathrm{cap}}^{*}(t)}{\partial t} \, \frac{\partial S_{\mathrm{cap}}(t)}{\partial t}, \tag{3.27}$$

see App. D.2 for more details. By replacing $S_{\mathrm{cap}}(t)$ into Eq. (3.9), energy current is written as

$$I_{\mathrm{R}}^{E,\mathcal{A}}(t) = \frac{\hbar D}{2\pi\,\sigma^2} \left\{ \frac{\sigma^2}{\left[(t-t^e)^2+\sigma^2\right]^2} + \frac{\sigma^2}{\left[(t-t^h)^2+\sigma^2\right]^2} \right\}. \tag{3.28}$$

It can be clearly seen from the above equation that the energy-current pulse for both electron and hole have the same shape and sign. Integrating Eq. (3.28) over one period, time-averaged energy current is obtained as

$$\bar{I}_{\mathrm{R}}^{E,\mathcal{A}} = 2D\frac{\mathcal{E}}{\mathcal{T}}, \tag{3.29}$$

see App. E for more details. Here, we have introduced $\mathcal{E} = \hbar\Omega/(2\sigma)$, which corresponds to the average energy of the emitted pulse. Therefore, the average energy current of setup $\mathcal{A}$ is defined by the average energy that an electron pulse carries together with a hole pulse during one period.

The time-dependent energy current for setup $\mathcal{B}$ is the same as the one found for setup $\mathcal{A}$. The only difference comes from the fact that the Lorentzian-shaped bias voltage emits only one electron within a period. Therefore, the average current is derived to be

$$\bar{I}_{\mathrm{R}}^{E,\mathcal{B}} = D\frac{\mathcal{E}}{\mathcal{T}}, \tag{3.30}$$

and it differs from the result for setup $\mathcal{A}$ only by a factor 2.

In the same line as with the charge current, now, we inspect the conservation of the energy current in setup $\mathcal{A}$. First, we obtain the time-dependent energy current in reservoir L by substituting D with $1-D$ in Eq. (3.27). Then, the relation between the left and the right reservoir is found to be

$$\frac{I_{\mathrm{R}}^{E,\mathcal{A}}(t)}{D} = \frac{I_{\mathrm{L}}^{E,\mathcal{A}}(t)}{1-D}. \tag{3.31}$$

The energy current conservation is satisfied by considering the energy which is stored in the mesoscopic capacitor, given by

$$I_{\mathrm{R}}^{E,\mathcal{A}}(t) + I_{\mathrm{L}}^{E,\mathcal{A}}(t) = \frac{h}{2}\left(e\nu\,\frac{\partial U}{\partial t}\right)^2. \tag{3.32}$$

This is the continuity equation for energy, where the right hand side is related to the source energy and work performance of the system. However, in setup $\mathcal{B}$, the energy current is conserved at every instant,

$$I_{\mathrm{R}}^{E,\mathcal{B}}(t) = -I_{\mathrm{L}}^{E,\mathcal{B}}(t). \tag{3.33}$$

This difference comes from following an analogous argument as for the charge current, and ascribes to the chirality and emission scheme.

The obtained results suggest that, in general, there are two main, conceptual differences between the charge current and the energy current in these two different setups. The first difference is due to the number of emitted particles, while the second one stems from the system design. In setup $\mathcal{A}$, pumping from outside leads to an apparent violation of charge and energy-current conservation. Nevertheless, the current conservation is now restored when the charge and the energy stored in the mesoscopic capacitor is taken into account.

We emphasize again that this comparison is valid as long as the condition $\hbar\Omega, k_{\mathrm{B}}T \ll \hbar/\sigma$ is satisfied for the mesoscopic capacitor, while the Lorentzian bias voltage is applied at arbitrary temperature and driving frequency.

Finally, it is worth mentioning that the general properties of charge and energy currents for the two different sources discussed in this section, have previously been studied in Refs. [10, 20, 21, 52], independently.

3.2.2 Charge- and energy-current noises

The next transport quantities that we consider are the charge-current noise and the energy-current noise. To derive the current correlations in setup $\mathcal{A}$, we insert the scattering amplitudes from Eq. (3.4) in Eqs. (2.37) and (2.38). Then, by making use of the unitarity condition given by Eq. (2.7), the current noise in terms of the scattering amplitudes of the slowly driven mesoscopic capacitor S_{cap}, at the right reservoir with $\alpha, \beta = \mathrm{R}$, is derived to be

$$\mathcal{P}_{\mathrm{tr,R}}^{XY,\mathcal{A}} = \frac{D(1-D)}{h}\sum_n |S_{n,\mathrm{cap}}|^2 \int \mathrm{d}E xy \times \Big\{ f_{\mathrm{L}}(E_n)\left[1 - f_{\mathrm{R}}(E)\right] + f_{\mathrm{R}}(E)\left[1 - f_{\mathrm{L}}(E_n)\right] \Big\}, \tag{3.34}$$

and

$$\mathcal{P}^{XY,\mathcal{A}}_{\mathrm{int,R}} = \frac{D^2}{h}\sum_{nkq} S^*_{-q,\mathrm{cap}}\, S_{n-q,\mathrm{cap}}\, S_{-k,\mathrm{cap}}\, S^*_{n-k,\mathrm{cap}} \int \mathrm{d}E \times \left\{ \frac{xy_n + x_n y}{2} f_{\mathrm{L}}(E_q)\left[1 - f_{\mathrm{L}}(E_k)\right] + xy f_{\mathrm{R}}(E)\left[1 - f_{\mathrm{R}}(E)\right] \right\}, \quad (3.35)$$

where $X, Y = I, I^E$. In the case of the Lorentzian bias voltage in setup $\mathcal{B}$, the current correlations $\mathcal{P}^{XY,\mathcal{B}}_{\mathrm{tr,R}}$ and $\mathcal{P}^{XY,\mathcal{B}}_{\mathrm{int,R}}$ are obtained by substituting $S_{\mathrm{n,cap}}$ with c_n in Eqs. (3.34) and (3.35).

Charge-current noise

Having found the energy-current noise, we will now move on to calculate the charge-current noise for setup $\mathcal{A}$, and then discuss the similarities and differences with setup $\mathcal{B}$, which has been investigated previously in Ref. [22]. Using unitarity of the scattering amplitudes for the transport term in Eq. (3.34), we can write

$$\mathcal{P}^{II,\mathcal{A}}_{\mathrm{tr,R}} = D(1-D)\frac{e^2}{h}\sum_n |S_{n,\mathrm{cap}}|^2 \int \mathrm{d}E \times \left\{ f_{\mathrm{L}}(E_n)\left[1 - f_{\mathrm{R}}(E)\right] + f_{\mathrm{R}}(E)\left[1 - f_{\mathrm{L}}(E_n)\right] \right\}. \quad (3.36)$$

Performing the integral with respect to energy, we obtain

$$\mathcal{P}^{II,\mathcal{A}}_{\mathrm{tr,R}} = \frac{2e^2}{h} D(1-D) \sum_{n>0} |S_n|^2 (n\hbar\Omega)\, \coth\left(\frac{n\hbar\Omega}{2k_{\mathrm{B}}T}\right). \quad (3.37)$$

Additionally, inserting the expression for S_n Eq. (3.12), we end up with

$$\mathcal{P}^{II,\mathcal{A}}_{\mathrm{tr,R}} = \frac{2e^2}{h} D(1-D)(2\Omega\sigma)^2 \sum_{n>0} e^{-2n\Omega\sigma} (n\hbar\Omega)\, \coth\left(\frac{n\hbar\Omega}{2k_{\mathrm{B}}T}\right). \quad (3.38)$$

Recalling the assumption $k_{\mathrm{B}}T \ll \hbar/\sigma$, one quickly realizes that by increasing the summation index n, the term $\coth[n\hbar\Omega/(2k_{\mathrm{B}}T)] \approx 1$ well before the term $e^{-2n\sigma\Omega}$ deviates appreciably from unity. Thereby, we can write

$$\begin{aligned}\mathcal{P}^{II,\mathcal{A}}_{\mathrm{tr,R}} &= \frac{2e^2}{h} D(1-D)(2\Omega\sigma)^2 \sum_{n>0} e^{-2n\Omega\sigma} (n\hbar\Omega) \\ &= \frac{2e^2}{h} D(1-D)(2\Omega\sigma)^2 (\hbar\Omega)\, \frac{e^{2\sigma\Omega}}{(e^{2\sigma\Omega}-1)^2}. \end{aligned} \quad (3.39)$$

Finally, we expand the above equation to the leading order in $\sigma\Omega \ll 1$, and it is found to be

$$\mathcal{P}^{II,\mathcal{A}}_{\mathrm{tr,R}} = D(1-D)2\frac{e^2}{\mathcal{T}}. \quad (3.40)$$

The factor 2 in the transport part of the charge-current noise denotes the fact that exactly two particles are emitted from the source during one period.

The transport part of the charge noise for setup $\mathcal{B}$, from Ref. [22], is given by

$$\mathcal{P}^{II,\mathcal{B}}_{\mathrm{tr,R}} = D(1-D)\frac{e^2}{h}\sum_{n=-\infty}^{\infty}|c_n|^2(n\hbar\Omega)\,\coth\left(\frac{n\hbar\Omega - e\overline{V}_{\mathrm{b}}}{2k_{\mathrm{B}}T}\right). \tag{3.41}$$

A comparison between this and the obtained result for setup $\mathcal{A}$, Eq. (3.37), reveals that the only difference comes from the probability $|c_n|^2$, which in setup $\mathcal{A}$ is $|S_{n,\mathrm{cap}}|^2$.

Here, the interference part of the charge noise, Eq. (3.34), using the unitarity of the scattering matrix, is written as

$$\mathcal{P}^{II,\mathcal{A}}_{\mathrm{int,R}} = D^2\frac{e^2}{h}\int \mathrm{d}E\Big\{f_{\mathrm{L}}(E)[1-f_{\mathrm{L}}(E)] + f_{\mathrm{R}}(E)[1-f_{\mathrm{R}}(E)]\Big\}, \tag{3.42}$$

Being independent of $S_{n,\mathrm{cap}}$, this immediately gives

$$\mathcal{P}^{II,\mathcal{A}}_{\mathrm{int,R}} = D^2\frac{e^2}{h}2k_{\mathrm{B}}T_0. \tag{3.43}$$

The interference contribution to the charge noise stems only from the temperature fluctuations in the reservoirs and has nothing to do with the source of the single particle emitter. For the same reason, this term is exactly identical for setup $\mathcal{B}$ [22], $\mathcal{P}^{II,\mathcal{B}}_{\mathrm{int,R}} = \mathcal{P}^{II,\mathcal{A}}_{\mathrm{int,R}}$.

Energy-current noise

Along the same lines as for the charge-current noise, we start with deriving the energy-current noise by the expressions following from Eqs. (3.34) and (3.35) for setup $\mathcal{A}$, and then, we compare our results with those for setup $\mathcal{B}$, which have been studied previously in Refs. [20–22].

For the transport part, using the unitarity of $S_{n,\mathrm{cap}}$, after rearranging the terms, we can write,

$$\mathcal{P}^{EE,\mathcal{A}}_{\mathrm{tr,R}} = \frac{D(1-D)}{h}\sum_n |S_{n,\mathrm{cap}}|^2\int \mathrm{d}E E^2 \times\Big\{f_{\mathrm{R}}(E_n)[1-f_{\mathrm{L}}(E)] + f_{\mathrm{L}}(E)[1-f_{\mathrm{R}}(E_n)]\Big\}. \tag{3.44}$$

Then, following the integration with respect to energy, and using the energy-symmetry properties of the different terms, $|S_n|^2 = |S_{-n}|^2$, we have

$$\mathcal{P}^{EE,\mathcal{A}}_{\mathrm{tr,R}} = 2\frac{D(1-D)}{3h}\sum_{n>0}|S_{n,\mathrm{cap}}|^2\Big\{n\hbar\Omega(\pi k_{\mathrm{B}}T)^2 + (n\hbar\Omega)^3\Big\}\coth\left(\frac{n\hbar\Omega}{2k_{\mathrm{B}}T}\right). \tag{3.45}$$

Again, having in mind the limit $k_{\rm B}T \ll \hbar/\sigma$, in the same manner as for the charge noise, we replace the $S_{n,\rm cap}$ with the expression given in Eq. (3.12) to simplify Eq. (3.45) and get

$$\mathcal{P}^{EE,\mathcal{A}}_{\rm tr,R} = 2\frac{D(1-D)}{h}(2\Omega\sigma)^2 \sum_{n>0} e^{-2n\Omega\sigma}\,(n\hbar\Omega)^3. \tag{3.46}$$

The resulting adiabatic-response limit for the transport term becomes

$$\mathcal{P}^{EE,\mathcal{A}}_{\rm tr,R} = D(1-D)\,4\frac{\mathcal{E}^2}{\mathcal{T}}. \tag{3.47}$$

The equation above tells us that the transport part of the energy-current noise is proportional to the square of the average emitted energy, $\mathcal{E} = \hbar\Omega/(2\sigma)$. On the other hand, the average energy of the emitted particles $\mathcal{E}$ is inversely proportional to the temporal width of the pulse σ. Hence, the transport part of the energy-current noise is connected to the pulse shape.

The transport part of the energy noise in setup $\mathcal{B}$ has been derived in Refs. [20–22], and it is given by

$$\mathcal{P}^{EE,\mathcal{B}}_{\rm tr,R} = \frac{D(1-D)}{3h}\sum_{n=-\infty}^{\infty}|c_n|^2\Big\{n\hbar\Omega(\pi k_{\rm B}T - e\overline{V}_{\rm b})^2 + (n\hbar\Omega)^3\Big\} \times \coth\left(\frac{n\hbar\Omega - e\overline{V}_{\rm b}}{2k_{\rm B}T}\right). \tag{3.48}$$

As discussed earlier for the transport part of the charge-current noise, the only difference between Eq. (3.45) and Eq. (3.48) is in the different probability amplitudes which is $|c_n|^2$ in $\mathcal{B}$ and $|S_{n,\rm cap}|^2$ in $\mathcal{A}$.

To complete the discussion of the energy-current noise, we need to derive the interference part from Eq. (3.35). To begin with, one can write

$$\mathcal{P}^{EE,\mathcal{A}}_{\rm int,R} = \frac{D^2}{h}\sum_{k,q,n} S_{q-n}S^*_{k-n}S_kS^*_q\int {\rm d}E\; E_qE_k \times\Big\{f_{\rm L}(E_n)[1-f_{\rm L}(E)] + f_{\rm R}(E)[1-f_{\rm R}(E)]\Big\}. \tag{3.49}$$

In the equation above, we have dropped the subscript 'cap', for simplicity, in the notation for the scattering amplitudes. Integrating with respect to energy, as derived in App. F, we end up with

$$\mathcal{P}^{EE,\mathcal{A}}_{\rm int,R} = \frac{D^2}{h}(\hbar\Omega)^2\sum_{n>0}\left|\sum_q qS_{q-n}S^*_q\right|^2 (n\hbar\Omega)\coth\left(\frac{n\hbar\Omega}{2k_{\rm B}T}\right) + \frac{D^2}{h}\frac{2\pi^2}{3}(k_{\rm B}T)^3. \tag{3.50}$$

Implementing the adiabatic condition, $\sigma\Omega \ll 1$, we can expand the summation to the leading order in $\sigma\Omega$, as

$$\sum_q q S_{q-n} S_q^* = e^{-|n|\sigma\Omega} \left(e^{i|n|t^e\Omega} - e^{i|n|t^h\Omega} \right). \tag{3.51}$$

Moreover, using the limit $k_\mathrm{B}T \gg \hbar/\sigma$ in Eq. (3.50), this equation can be written as

$$\mathcal{P}_{\mathrm{int,R}}^{EE,\mathcal{A}} = \frac{D^2}{h}(\hbar\Omega)^2\, 2\sum_{n>0} e^{-2n\Omega\sigma}[1-\cos(nz_\mathrm{eh})](n\hbar\Omega) + \frac{D^2}{h}\frac{2\pi^2}{3}(k_\mathrm{B}T)^3, \tag{3.52}$$

where, for the sake of brevity, we have introduced the auxiliary notation $z_\mathrm{eh} = \Omega[t^e - t^h]$. The first term in the above equation, again using $\sigma\Omega \ll 1$, can be expressed as

$$(2\Omega\sigma)^2 \sum_{n>0} e^{-2n\Omega\sigma} n[1-\cos(nz_\mathrm{eh})] = 1 - \frac{(\sigma\Omega)^2[(\sigma\Omega)^2\cos^2(z_\mathrm{eh}/2) - \sin^2(z_\mathrm{eh}/2)]}{\left[(\sigma\Omega)^2\cos^2(z_\mathrm{eh}/2) + \sin^2(z_\mathrm{eh}/2)\right]^2}. \tag{3.53}$$

From this expression it is clear that for electron and hole emissions well inside each half-period, i.e. $|t^e - t^h| \gg \sigma$ (or equivalently $z_\mathrm{eh} \gg \sigma\Omega$), the sum in Eq. (3.53) approaches unity and hence, the correlator does not depend on the electron and hole emission times $t^{e(h)}$. Performing the summation in Eq. (3.52), we find

$$\mathcal{P}_{\mathrm{int,R}}^{EE,\mathcal{A}} = D^2\, 2\frac{\varepsilon^2}{\mathcal{T}} + \frac{D^2}{h}\frac{2\pi^2}{3}(k_\mathrm{B}T)^3. \tag{3.54}$$

In the equation above, the first term is proportional to the energy of the emitted particle and the second term, likewise the one which is derived for the interference part of the charge noise Eq. (3.43), is associated with the thermal fluctuations. The interference part of the energy noise for setup $\mathcal{B}$ is obtained by substituting S_n with c_n in Eq. (3.49),

$$\mathcal{P}_{\mathrm{int,R}}^{EE,\mathcal{B}} = \frac{D^2}{2h}\sum_{n=-\infty}^{\infty} |eV_n|^2 (n\hbar\Omega)\coth\left(\frac{n\hbar\Omega - e\overline{V}_\mathrm{b}}{2k_\mathrm{B}T}\right) + \frac{D^2}{h}\frac{2\pi^2}{3}(k_\mathrm{B}T)^3, \tag{3.55}$$

where $V_n = (1/\mathcal{T})\int_0^{\mathcal{T}} \mathrm{d}t V_\mathrm{b}(t) e^{in\Omega t}$. This equation for setup $\mathcal{B}$ is comparable with Eq. (3.50) for setup $\mathcal{A}$, and the difference between them has its origin in the dissimilar factors, $\left|\sum_q q S_{q-n} S_q^*\right|^2$ in setup $\mathcal{A}$ and $|eV_n|^2 = \left|\sum_q q c_{q-n} c_q^*\right|^2$ in setup $\mathcal{B}$.

Importantly, we point out that the results for the two sources are only similar at low temperatures, more specifically, when considering the constraint $k_\mathrm{B}T \ll \hbar/\sigma$ for the mesoscopic capacitor. A difference appears at higher temperatures and frequencies, when the scattering matrix of the slowly driven mesoscopic capacitor $S_\mathrm{cap}^{(0)}(t,E)$, becomes energy-dependent, see Eq. (3.9). In such a case, the shape of the emitted pulses from the mesoscopic capacitor can take a completely dissimilar shape than the pulses generated by the Lorentzian bias voltage.

Mixed-current noises

Here, we complete the transport quantities by deriving the mixed current-noise. This noise, defined as the correlator between the charge and energy currents, stems from the fact that the transported particles carry both charge and energy. Meaning that the mixed-current noise differs from the charge- and energy-current noise in the sense that it is related to the averaged energy transported by the charge of the particles.

The mixed current-noise for setup $\mathcal{A}$, using Eqs. (3.34) and (3.35), for the transport part is formulated as

$$\mathcal{P}^{IE,\mathcal{A}}_{\mathrm{tr,R}} = \frac{e}{h} D(1-D) \sum_n |S_{n,\mathrm{cap}}|^2 \int \mathrm{d}E E \times \Big\{ f_{\mathrm{R}}(E_n)[1-f_{\mathrm{L}}(E)] + f_{\mathrm{L}}(E)[1-f_{\mathrm{R}}(E_n)] \Big\}, \tag{3.56}$$

and for the interference part is given by

$$\mathcal{P}^{IE,\mathcal{A}}_{\mathrm{int,R}} = \frac{e}{h} D^2 \int \mathrm{d}E E \Big\{ f_{\mathrm{L}}(E)[1-f_{\mathrm{L}}(E)] + f_{\mathrm{R}}(E)[1-f_{\mathrm{R}}(E)] \Big\}. \tag{3.57}$$

Here, due to the absence of bias between the reservoirs, and also the energy-symmetry properties of the scattering amplitude, $|S_n|^2 = |S_{-n}|^2$, the mixed correlator vanishes,

$$\mathcal{P}^{IE,\mathcal{A}} = 0. \tag{3.58}$$

However, in setup $\mathcal{B}$, for the Lorentzian bias voltage from Ref. [23] we have

$$\mathcal{P}^{IE,\mathcal{B}}_{\mathrm{int,R}} = \frac{e}{h} D^2 e\overline{V}_{\mathrm{b}}\, k_{\mathrm{B}} T. \tag{3.59}$$

3.2.3 Transport quantities at zero temperature

In this section, we compare the transport quantities derived so far, in the zero temperature limit. In such a limit, the result is therefore only due to the driving source and the central QPC transparency D. First, we bring a summary on the charge transport properties in both setups and then, the energy transport properties is recapitulated for each case. Finally, we review all the transport properties by collecting the presented results in Tab. 3.1.

As we discussed in Sec. 3.2.1, the slowly driven mesoscopic capacitor in setup $\mathcal{A}$ injects one electron and one hole per period, resulting in a zero average charge current. On the other hand, in setup $\mathcal{B}$, the Lorentzian-shaped bias voltage give rise to the emission of only one electron with a charge $-e$ during one period, yielding a non-zero average charge current.

The charge-current noise at zero temperature is only proportional to the transport part. Information about electron-hole pair excitation, in addition to the

Table 3.1: *Comparison of the transport quantities for the two setups under consideration.*

Quantity $[1/\mathcal{T}]$	**Mesoscopic capacitor** $(\mathcal{A})$	**Lorentzian bias voltage** $(\mathcal{B})$
$\bar{I}_{\mathrm{R}}$	0	$-De$
$\mathcal{P}^{II}_{\alpha\beta} = \mathcal{P}^{II}_{tr,\alpha\beta}$	$2D(1-D)$	$D(1-D)$
$\bar{I}^{E}_{\mathrm{R}}$	$2D\mathcal{E}$	$D\mathcal{E}$
$\bar{I}^{E}_{\mathrm{L}}$	$2(1-D)\mathcal{E}$	$-D\mathcal{E}$
$\mathcal{P}^{EE}_{tr,\alpha\beta}$	$4D(1-D)\mathcal{E}^2$	$2D(1-D)\mathcal{E}^2$
$\mathcal{P}^{EE}_{in,\mathrm{RR}}$	$2D^2\mathcal{E}^2$	$D^2\mathcal{E}^2$
$\mathcal{P}^{EE}_{in,\mathrm{LL}}$	$2(1-D)^2\mathcal{E}^2$	$D^2\mathcal{E}^2$
$\mathcal{P}^{EE}_{in,\mathrm{RL}} = \mathcal{P}^{EE}_{in,\mathrm{LR}}$	$2D(1-D)\mathcal{E}^2$	$-D^2\mathcal{E}^2$

number of emitted particle, is attained by this quantity. A different factors, 1 and 2, between two setups confirm the fact that the mesoscopic capacitor emits two particles within a period, while the Lorentzian bias voltage emits only one electron in one period.

Information about the spectrum of the sources is achieved by studying the energy current and the energy-current noise which is discussed widely in the previous sections. As one can see in Tab. 3.1 the average energy current for both setups is proportional to the average energy which is carried by the emitted particles. The average energy of the injected particle is inversely proportional to the width of the temporal pulse $\mathcal{E} = \hbar/(2\sigma)$.

The differences in the energy transport quantities have two main origins: First, from the number of emitted particles, through a factor 1 and 2 for the mesoscopic capacitor and the Lorentzian bias voltage, respectively, and second, from the chirality and the dissimilar emission schemes of the two setups. More specifically, setup $\mathcal{A}$ comprises a chiral conductor and the mesoscopic capacitor is coupled to the edge state from the outside, i.e., only those particles that are injected from the left reservoir emit or absorb energy quanta. Nevertheless, this is not the case in setup $\mathcal{B}$ where the source is voltage-bias driven. It implies that both particles which are incoming to and outgoing from the left reservoir take energy quanta.

4 Analysis of single electron pulses from a mesoscopic capacitor beyond the adiabatic-response regime

In the previous chapter, we studied the slowly driven mesoscopic capacitor. In the adiabatic-response regime, through the analysis of the charge and the energy currents and their corresponding noise, we obtained information about the number of emitted particles, the temporal profile of the pulse and, consequently, its energy distribution. Moreover, we concluded that the slowly driven mesoscopic capacitor differs from the case of the Lorentzian bias voltage, driven at an arbitrary frequency, only in terms of the number of emitted particles.

Here, we modify the driving scheme of the mesoscopic capacitor by increasing the driving frequency beyond the adiabatic driving regime. Throughout this chapter, our aim is to derive the non-adiabatic transport quantities by including the next leading (first) order correction in the expansion of the scattering matrix. We investigate whether increasing the driving frequency in the mesoscopic capacitor leads to extra differences compared to the setup base on the Lorentzian bias voltage.

4.1 Emission scheme beyond the adiabatic-response regime

In this chapter, we study the same setup as in Sec. 3.1.1, but in the non-adiabatic response regime. The only difference here is that the mesoscopic capacitor is driven at a higher frequency with respect to the slow-driving regime. The scattering region is described by the general scattering matrix, given by Eq. (3.4), which we now expand up to the first order in the driving frequency. Notice that the superscript $\mathcal{A}$ is dropped henceforth, since in the present we are only dealing with the mesoscopic capacitor.

4.1.1 First-order approximation of the scattering matrix

From Sec. 2.7.1, the scattering matrix beyond the adiabatic-response regime is generally described by Eq.(2.42). To find the specific form of this scattering matrix for the mesoscopic capacitor under consideration, we start with expanding the time-dependent phase in the scattering matrix, Eq. (3.1), up to first order in $q\Omega\tau$,

$$\int_{t-q\tau}^{t} dt' U_{\rm g}(t') = U_{\rm g}(t)\, q\tau - \frac{\partial U_{\rm g}(t)}{\partial t}\frac{(q\tau)^2}{2}, \tag{4.1}$$

then, the scattering matrix in terms of the frozen scattering matrix $S^{(0)}_{cap}(t,E)$ is found to be

$$S_{\rm cap}(t,E) = S^{(0)}_{\rm cap}(t,E) + i\frac{\hbar}{2}\frac{\partial^2 S^{(0)}_{\rm cap}(t,E)}{\partial t \partial E}. \tag{4.2}$$

Importantly, in order to consistently include all the contributions of the order $(\tau\Omega)^1$, one has to approximately treat the energy dependence of the frozen scattering matrix around the Fermi level. In particular, we cannot simply take $S^{(0)}_{\rm cap}(t,E) \approx S^{(0)}_{\rm cap}(t,\mu)$, as we did in the previous chapter, but the frozen scattering matrix needs to be expanded around the Fermi level up to the first order in the energy, $S^{(0)}_{\rm cap}(t,E) \approx S^{(0)}_{\rm cap}(t,\mu) + (E-\mu)\partial S^{(0)}_{\rm cap}(t,E)/(\partial E)|_{E=\mu}$. As a result, the total scattering matrix in this regime becomes energy-dependent and it is written as

$$S_{\rm cap}(t,E) = S^{(0)}_{\rm cap}(t,\mu) + (E-\mu)\frac{\partial S^{(0)}_{\rm cap}(t,E)}{\partial E}|_{E=\mu} + i\frac{\hbar}{2}\frac{\partial^2 S^{(0)}_{\rm cap}(t,E)}{\partial t\partial E}|_{E=\mu}, \tag{4.3}$$

where $S^{(0)}_{\rm cap}(t,E)$ is the frozen scattering matrix, obtained in Eq. (3.9). The scattering matrix can also be expressed in the energy representation and written as

$$S_{\rm cap}(E_n,E) = S_n + (E-\mu)\,\frac{\partial S_{n,\rm cap}(E)}{\partial E}|_{E=\mu} + \frac{n}{2}\hbar\Omega\frac{\partial S_{n,\rm cap}(E)}{\partial E}|_{E=\mu}, \tag{4.4}$$

with $S_{n,\rm cap}(E)$ given by Eq. (3.12). The unitarity of the scattering matrix,

$$\sum_n |S_{\rm cap}(E_n,E)|^2 = 1, \tag{4.5}$$

is satisfied, when keeping terms up to order $(\Omega\sigma)^1$, consistent with the considered limit $(\Omega\sigma) \ll 1$.

By inserting $S_{\rm cap}(E_n,E)$, Eq. (4.4), into the total scattering matrix Eq. (3.4), we are now able to study the charge current, the energy current and their fluctuations up to the contribution of the first order in the driving frequency, $\Omega\sigma$.

Energy-dependent emission time and pulse width

In this subsection, we explicitly calculate the energy dependence of the emission time and the width of the temporal pulse. Previously, we have treated $t^{\rm e/h}$ and

σ as energy-independent parameters. However, when going beyond adiabatic response in the following, also their energy-derivatives will become important. The knowledge of their explicit energy dependence will be helpful to estimate the magnitude of the calculated observables.

For simplicity, we now focus on a time-dependent potential energy which is harmonic and given by $U_{\rm g}(t) = \overline{U}_{\rm g} + \delta U_{\rm g}\,\cos(\Omega t + \varphi)$. By replacing the potential energy in Eq. (3.8), we obtain

$$\phi(t, E) = 2\pi\chi(E) - 2\pi\frac{\delta U_{\rm g}}{\Delta}\cos(\Omega t + \varphi) + \pi. \tag{4.6}$$

Here, the energy-dependent phase is given by

$$\chi(E) = \frac{k_\mu L}{2\pi} + \frac{1}{\Delta}(E - \mu - \overline{U}_{\rm g}), \tag{4.7}$$

where k_μ is the wave number at the Fermi level and Δ is the level spacing in the capacitor, acting as a QD.

The emission time can be obtained when $S(t, E) \approx 1$ which, in turn, yields the resonance condition $\phi(t^{\rm res}, E) = \pi$. From that, we find

$$\cos\left(\Omega t^{e/h} + \varphi\right) = \frac{\Delta\,\chi(E)}{\delta U_{\rm g}} \;\rightarrow\; t^{e/h} = \frac{\varphi}{\Omega} \mp \frac{1}{\Omega}\arccos\left(\frac{\Delta\chi(E)}{\delta U_{\rm g}}\right). \tag{4.8}$$

We make use of this emission time to derive the half-width of the temporal pulse, σ, which is determined by Eq. (3.10),

$$\begin{aligned}\sigma &= \frac{D_{\rm s}}{4\pi\,\Omega}\;\frac{\Delta}{|\,dU_{\rm g}(t)/dt|_{t=t^{e/h}}} \\ &= \frac{D_{\rm s}}{4\pi\,\Omega}\;\frac{\Delta}{|\delta U_{\rm g}|}\;\frac{1}{\sqrt{1-[\Delta\chi(E)/(\delta U_{\rm g})]^2}}.\end{aligned} \tag{4.9}$$

Notice that $\sigma^e = -\sigma^h = \sigma$. An electron is emitted when the occupied level shifts above the Fermi level, i.e., $dU_{\rm g}(t^e)/dt > 0$. On the other hand, a hole is emitted when the occupied level moves below the Fermi level, i.e., $dU_{\rm g}(t^h)/dt < 0$.

As we pointed out in the slow-driving regime, only one level of the QD contributes to the emission processes. This can be achieved by tunning the dc component $\overline{U}_{\rm g}$ and the ac amplitude $\delta U_{\rm g}$ of the potential energy. They translate as

$$|\overline{U}_{\rm g}| < \frac{\Delta}{2} \text{ and } |\overline{U}_{\rm g}| < |\delta U_{\rm g}| < \Delta - |\overline{U}_{\rm g}|. \tag{4.10}$$

In the following, we first describe the transport quantities for a general periodically time-dependent potential energy. Then, to illustrate the main findings numerically, we consider the case of the harmonic driving potential introduced above.

4.2 Charge current

The time-dependent charge current consists of two terms: The first, representing the adiabatic-response contribution, Eq. (3.20), and the second, being the relevant correction to this adiabatic-response current. The latter term takes the form (for detailed derivations see App. D.1.2),

$$I_{\mathrm{R}}^{(1)}(t) = -\frac{e\,\hbar}{4\pi}\,D\,\frac{\partial}{\partial t}\left(\frac{\partial S_{\mathrm{cap}}^{*(0)}(t,\mu)}{\partial t}\;\;\frac{\partial S_{\mathrm{cap}}^{(0)}(t,E)}{\partial E}|_{E=\mu}\right). \tag{4.11}$$

By inserting the zeroth-order approximation of the scattering matrix, Eq. (3.9), into the equation above we end up with

$$I_{\mathrm{R}}^{(1)}(t) = -\frac{e\,\hbar}{\pi}D\left(-\frac{\partial\sigma^e}{\partial E}A^e(t) + \frac{\partial t^e}{\partial E}B^e(t) + \frac{\partial\sigma^h}{\partial E}A^h(t) + \frac{\partial t^h}{\partial E}B^h(t)\right), \tag{4.12a}$$

where we have defined the auxiliary functions

$$A^j(t) = -\frac{\sigma^3 - 3\sigma(t-t^j)^2}{\left[(t-t^j)^2+\sigma^2\right]^3}, \tag{4.12b}$$

$$B^j(t) = \frac{4(t-t^j)\sigma^2}{\left[(t-t^j)^2+\sigma^2\right]^3}, \tag{4.12c}$$

with $j = \mathrm{e,h}$ for electron and hole, respectively. Function $A^j(t)$ is an even function with respect to the emission time t^j, as depicted by the green dashed line in Fig. 4.1(b). It changes width and height of the pulse with the prefactor $\partial_E\sigma^j$. Function $B^j(t)$ is an odd function as shown by the blue dashed line in Fig. 4.1(b). It shifts the emission time with a prefactor $\partial_E t^j$. The derivative of the pulse width Eq. (4.9) and the emission time Eq. (4.8) with respect to this potential energy are found to be

$$\frac{1}{\sigma^2}\frac{\partial\sigma^{e/h}}{\partial E} = \mp\frac{4}{\hbar}\frac{\eta}{\sqrt{1-\eta^2}}\frac{\tau\Omega}{D_{\mathrm{s}}}, \tag{4.13a}$$

$$\frac{1}{\sigma^2}\frac{\partial t^{e/h}}{\partial E} = \pm\frac{8\pi}{\hbar}\frac{|\delta U_{\mathrm{g}}|}{\Delta}\sqrt{1-\eta^2}\,\frac{\tau\Omega}{D_{\mathrm{s}}^2}, \tag{4.13b}$$

where η is a dimensionless parameter defined by $\eta = \Delta\chi/\delta U_{\mathrm{g}}$. The correction term to the current, $I^{(1)}(t)$, is obtained by inserting Eqs. (4.13a) and (4.13b) into Eq. (4.12a),

$$\begin{aligned}\frac{I_{\mathrm{R}}^{(1)}(t)}{-e\,D/(\pi\,\sigma)} = &+4\frac{\eta}{\sqrt{1-\eta^2}}\frac{\tau\Omega}{D_{\mathrm{s}}}\;\sigma^3A^e + 8\pi\sqrt{1-\eta^2}\,\frac{|\delta U_{\mathrm{g}}|}{\Delta}\,\frac{\tau\Omega}{D_{\mathrm{s}}^2}\,\sigma^3B^e(t)\\ &+4\frac{\eta}{\sqrt{1-\eta^2}}\frac{\tau\Omega}{D_{\mathrm{s}}}\;\sigma^3A^h(t) - 8\pi\sqrt{1-\eta^2}\,\frac{|\delta U_{\mathrm{g}}|}{\Delta}\,\frac{\tau\Omega}{D_{\mathrm{s}}^2}\,\sigma^3B^h(t).\end{aligned} \tag{4.14}$$

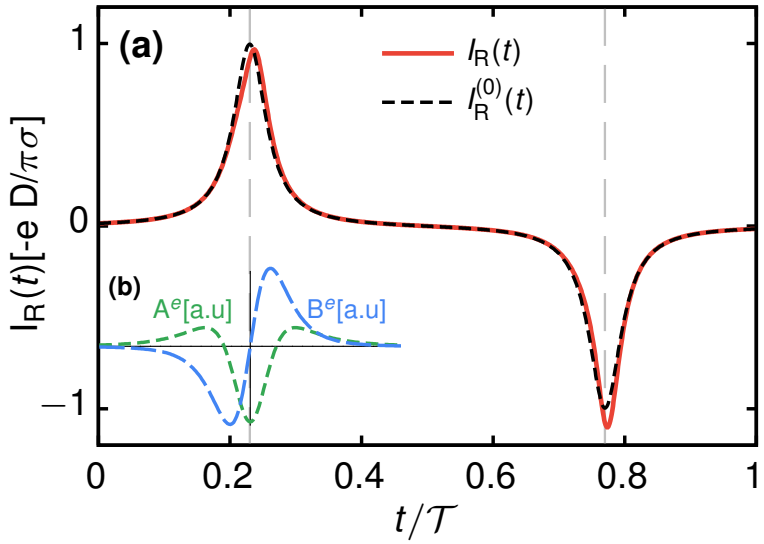

Figure 4.1: *(a) Zeroth-order component of the time-dependent current $[I_R^{(0)}(t)$, black dashed line] and the total current $[I_R(t) = I_R^{(0)}(t) + I_R^{(1)}(t)$, red solid line] are shown as a function of time in one period $\mathcal{T} = 2\pi/\Omega$. Here, $\overline{U}_g > 0$ and $\sigma\Omega = 0.03$ to make the current peaks more visible. (b) The current is corrected by two terms: Function $A^e(t)$, which is multiplied by $\partial_E\sigma$ and changes the width and the height of the pulse in time. Function $B^e(t)$ which is multiplied by $\partial_E t^e$, and shifts the pulse to the later times.*

The total time-dependent charge current beyond the adiabatic-response regime is written as $I(t) = I^{(0)}(t) + I^{(1)}(t)$, where $I^{(0)}(t)$ is given by Eq. (3.21), and is shown in Fig. 4.1(a) with the black dashed line. The correction terms, which are due to the energy dependence of both the emission times and width of the pulses, lead to a difference between the pulse of the electron and the hole.

By assuming $\overline{U}_g > 0$, i.e., the equilibrium point is located above the Fermi level, the sign of $\partial_E\sigma$ becomes positive for the electron and negative for the hole, and conversely for $\overline{U}_g < 0$. Therefore, the first term in Eq. (4.14) with $\overline{U}_g > 0$ makes the electron part of the pulse wider and thinner, and the hole part of the pulse gets higher and thinner.

The prefactor $\partial_E t^j$ is positive for electron, whereas it is negative for hole and in both cases its magnitude changes with δU_g. Hence, the second term in Eq. (4.14) causes both the electron and the hole pulses to shift to the right side, meaning that there will be a delay in the electron and the hole emission.

To find out which of the terms appearing in Eq. (4.14) dominates, we compare their order of magnitude with the help of Eqs. (4.13a) and (4.13b), and write

$$\left|\frac{\partial_E\sigma^{e/h}}{\partial_E t^{e/h}}\right| = \left|\frac{2\eta}{\sqrt{1-\eta^2}}\right| \Omega\sigma, \tag{4.15}$$

Here, we already have $\Omega\sigma \ll 1$ and from Eq. (4.10), we know that $\eta < 1$. It can be seen that if $\eta \ll 1$, i.e., the dc component of the potential energy is close to the

Fermi level, the term proportional to the width and height correction, $A^j(t)$, is much smaller than the term related to the emission-time correction, $B^j(t)$. This means the delay in the emission time is more visible than the modification of the width and the height.

The charge being carried by each pulse is obtained by integrating each of them in Fig. 4.1. The integration of each functions, $A^j(t)$ and $B^j(t)$, yields zero. Thus, every pulse still carries the same amount of charge as they did in the adiabatic-response regime, and the total average charge current remains zero.

To conclude, in the non-adiabatic response regime, like in the slow driving regime, exactly one electron and one hole are emitted per each period. It means that the charge of the emitted particles remains unchanged. However, the correction terms change the shape of the electron and hole pulses in an opposite manner, and furthermore, they lead to the shift of the emission time.

4.2.1 Spectral current

By analyzing the spectral current, we can conclude how the correction of the width and emission time affect the energetic properties of the emitted pulse. Spectral current is obtained from the energy-resolved time-integrated particle current,

$$i_R(E) = D \sum_n |S_{\mathrm{cap}}(E_n, E)|^2 \{f_L(E) - f_R(E_n)\}. \tag{4.16}$$

Here, $|S_{\mathrm{cap}}(E_n, E)|^2$ is given by Eq. (4.4) and equals

$$|S_{\mathrm{cap}}(E_n, E)|^2 = |S_{n,\mathrm{cap}}|^2 \begin{cases} 1 + \dfrac{1}{\sigma}\dfrac{\partial\sigma}{\partial E}(2E + n\hbar\Omega)(1 - n\Omega\sigma), & n > 0, \\ 1 + \dfrac{1}{\sigma}\dfrac{\partial\sigma}{\partial E}(2E + n\hbar\Omega)(1 + n\Omega\sigma), & n < 0, \\ \delta_{n,0}, & n = 0, \end{cases} \tag{4.17}$$

where $S_{n,\mathrm{cap}}$ is the frozen scattering matrix Eq. (3.3). At zero temperature, $k_{\mathrm{B}}T = 0$, where the Fermi function is taken to be $f(E) = \Theta(-E)$, the spectral current is obtained as

$$i_R(E) = De^{-2|E|\sigma/\hbar} \begin{cases} 2\Omega\sigma + \dfrac{\hbar\Omega}{2\sigma}\dfrac{\partial\sigma^e}{\partial E}\left[\dfrac{2E\sigma}{\hbar} - \dfrac{1}{2}\left(\dfrac{2E\sigma}{\hbar}\right)^2\right], & E > 0 \\ -2\Omega\sigma - \dfrac{\hbar\Omega}{2\sigma}\dfrac{\partial\sigma^h}{\partial E}\left[\dfrac{2E\sigma}{\hbar}\dfrac{1}{2}\left(\dfrac{2E\sigma}{\hbar}\right)^2\right], & E < 0 \end{cases} \tag{4.18}$$

where the electrons and holes are associated with positive and negative energies,

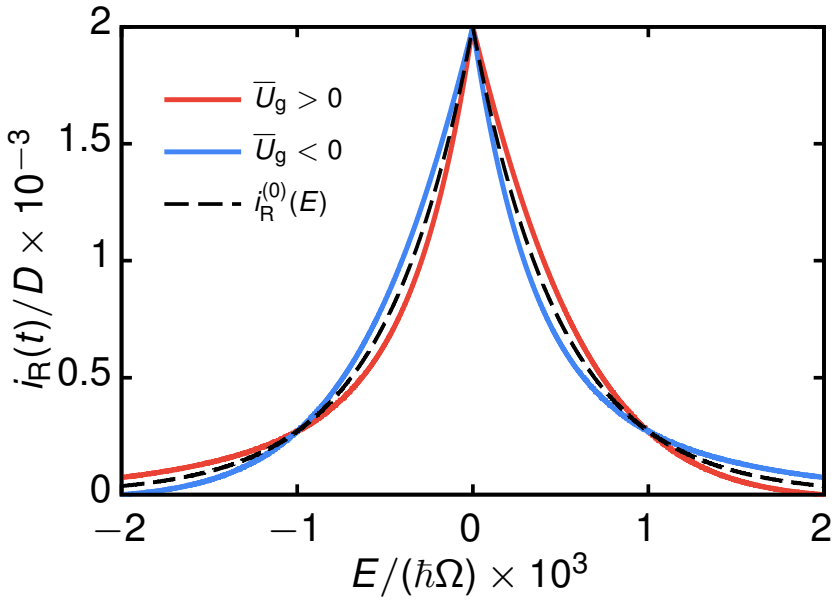

Figure 4.2: *Spectral currents for the zeroth-order component [$i_R^{(0)}(E)$, black dashed line] and the total component [$i_R(E) = i_R^{(0)}(E) + i_R^{(1)}(E)$, solid lines] are shown as a function of $E/(\hbar\Omega)$ for both positive $\overline{U}_g$ (red line) and negative $\overline{U}_g$ (blue line). Notice that, for convenience, we plot the absolute value of the electron and hole currents. We have chosen $|\hbar\Omega^2\partial_E\sigma^j| = 10^{-6}$ and $\sigma\Omega = 0.001$, different from the other plots in the present chapter to make the difference between the currents visible.*

respectively. The first terms in both lines of Eq. (4.18) are the adiabatic response spectral current, $i_R^{(0)}(E) \propto e^{-2|E|\sigma/\hbar}$ and the second and third terms describe the correction term $i_R^{(1)}(E)$. The spectral current $i_R^{(1)}(E)$, in contrast to the time-dependent charge current, is not sensitive to correction to the emission time. However, it is sensitive to $\partial_E\sigma$. The correction term causes a shift in weight to higher or lower energies, for electron or hole, depending on the sign of $\partial_E\sigma$. It can be seen from Eq. (4.13a) that this sign can be fixed by tunning the average potential energy $\overline{U}_g$. In Fig. 4.2, we plot the absolute value of the spectral current both for negative and positive values of $\overline{U}_g$. Integrating the correction term with respect to energy in Eq. (4.18), vanishes separately for positive and negative energies, which confirms that the charge of the injected particles is not modified.

4.2.2 Energy current

Studying the total time-dependent energy current at zero temperature helps us to realize how the modified driving scheme changes the energy current pulse. As derived in App. D.2.2, the correction term of the energy current can be written

as

$$I_R^{E(1)}(t) = -\frac{\hbar^2}{8\pi i} D \Bigg\{ \frac{1}{3}\frac{\partial}{\partial E}\left(\frac{\partial^3 S^{*(0)}_{\rm cap}(t,\mu)}{\partial^3 t}\, S^{(0)}_{\rm cap}(t,\mu)\right) + \frac{\partial}{\partial t}\left(\frac{\partial S^{*(0)}_{\rm cap}(t,\mu)}{\partial t}\, \frac{\partial^2 S^{(0)}_{\rm cap}(t,E)}{\partial t \partial E}|_{E=\mu}\right)\Bigg\}. \tag{4.19}$$

By inserting the frozen scattering matrix, Eq. (3.9), into the correction term of the time-dependent energy current we obtain

$$I_{\rm R}^{E(1)}(t) \;=\; \frac{\hbar^2}{2\pi}\, D\left(-\frac{\partial \sigma^e}{\partial E} A^{E,e}(t) + \frac{\partial t^e}{\partial E} B^{E,e}(t) - \frac{\partial \sigma^h}{\partial E} A^{E,h}(t) - \frac{\partial t^h}{\partial E} B^{E,h}(t)\right), \tag{4.20a}$$

where we have defined the auxiliary functions,

$$A^{E,j}(t) \;=\; -\frac{(t-t^e)^4 - 18\sigma^2(t-t^e)^2 + 5\sigma^4}{\left[(t-t^e)^2+\sigma^2\right]^4}, \tag{4.20b}$$

$$B^{E,j}(t) \;=\; -4\frac{\sigma(t-t^e)^3 - 5\sigma^3(t-t^e)}{\left[(t-t^e)^2+\sigma^2\right]^4}. \tag{4.20c}$$

Here, function $A^{E,j}(t)$ (an even function with respect to the emission time t^j) is multiplied by $\partial_E \sigma^j$. It is shown by the green dashed line in Fig. 4.3(b) and changes the width and the height of the energy current pulse. Function $B^{E,j}(t)$ (an odd function), is multiplied by $\partial_E t^j$. It shifts the emission time, as is illustrated by the blue dashed line in Fig. 4.3(b). Then, along the same lines as for the charge current, the correction term of the time-dependent energy current can be rewritten by using Eqs. (4.13a) and (4.13b),

$$\begin{aligned}\frac{I_{\rm R}^{E(1)}(t)}{\hbar D/(2\pi\,\sigma^2)} =& +4\frac{\eta}{\sqrt{1-\eta^2}}\,\frac{\tau\Omega}{D_{\rm s}}\;\sigma^4 A^{E,e}(t) + 8\pi\sqrt{1-\eta^2}\,\frac{|\delta U_{\rm g}|}{\Delta}\,\frac{\tau\Omega}{D_{\rm s}^2}\,\sigma^4 B^{E,e}(t)\\ & -4\frac{\eta}{\sqrt{1-\eta^2}}\,\frac{\tau\Omega}{D_{\rm s}}\;\sigma^4 A^{E,h}(t) + 8\pi\sqrt{1-\eta^2}\,\frac{|\delta U_{\rm g}|}{\Delta}\,\frac{\tau\Omega}{D_{\rm s}^2}\,\sigma^4 B^{E,h}(t).\end{aligned} \tag{4.21}$$

The total time-dependent energy current is $I_{\rm R}^{E}(t) = I_{\rm R}^{E(0)}(t) + I_{\rm R}^{E(1)}(t)$, where $I_{\rm R}^{E(0)}(t)$ is given by Eq. (3.28), as is shown in Fig. 4.3(a). The correction term of the energy current $I_{\rm R}^{E(1)}(t)$ changes the shape of the pulse and the emission time. When $\overline{U}_{\rm g} > 0$, the energy pulse of electrons (holes) becomes smaller (higher) and wider (thinner) with respect to their counterparts in the adiabatic driving regime, due to the presence of the first term of Eq. (4.21). In addition, the emission time is shifted to the later times due to the second term in Eq. (4.21).

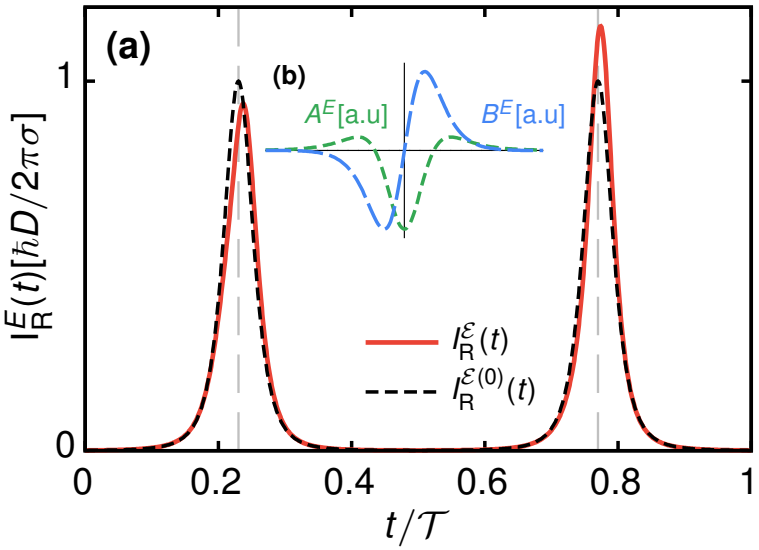

Figure 4.3: *(a) Zeroth-order component of the time-dependent energy current $[I_R^{E(0)}(t)$, dashed line] and the total energy current $[I_R^E(t) = I_R^{E(0)}(t) + I_R^{E(1)}(t)$, solid line] are shown as a function of $t/\mathcal{T}$. We have chosen $\overline{U}_g > 0$ and $\sigma\Omega = 0.03$ is assumed the same as for the charge current. (b) Energy current is corrected by: First, the correction function $A^E(t)$, multiplying $\partial_E \sigma^j$, that changes the width and height of the pulse in time. Second, the correction function $B^E(t)$, multiplying $\partial_E t^j$, that shifts the pulse to later.*

The energy which is carried by each pulse is obtained by performing the time integral for the current Eq. (4.21). The average energy carried by one pulse is obtained as

$$\frac{\bar{I}^{E,j}}{D\Omega/(2\pi)} = \frac{\hbar}{2\sigma} + \frac{1}{\hbar}\frac{\partial\sigma^j}{\partial E}\left(\frac{\hbar}{2\sigma}\right)^3. \tag{4.22}$$

In the equation above, the first term is the average energy of the particle in the slow-driving regime and appears to be the same for both electron and hole. The second term comes from the integration of function $A^{E,j}(t)$ which, in contrast to the charge pulses, generates a non-zero value. There is no trace of function $B^{E,j}(t)$. This meets our expectations, since $B^{E,j}(t)$ is only associated with shifting the emission time and does not change the average energy of the pulse.

The correction term, depending on the average potential energy $\overline{U}_g$, takes a different sign for electron and hole. When $\overline{U}_g > 0$, the average energy carried by an electron pulse is decreased and the average energy of the hole pulse is increased by the same amount. Since the correction terms of the electron pulse and hole pulse cancel each other per each period, in one full period the average energy remains the same, like in the adiabatic driving regime.

4.2.3 Current noise

So far, we have focused on the currents and their averages to study how increasing driving frequency affects the charge and the energy of the pulses. Now, we move one step further and investigate the charge-current noise and energy-current noise at zero temperature, which provide us with information about the number of emitted particles and their spectra.

To begin with, we derive the charge-current noise by substituting $S_{n,\mathrm{cap}}$ with $S_{\mathrm{cap}}(E_n, E)$ in Eq. (3.36),

$$\mathcal{P}^{II}_{\mathrm{tr,R}} = D(1-D)\frac{e^2}{h}\sum_n \int \mathrm{d}E |S_{\mathrm{cap}}(E_n, E)|^2 \times \Big\{ f_{\mathrm{L}}(E_n)\left[1 - f_{\mathrm{R}}(E)\right] + f_{\mathrm{R}}(E)\left[1 - f_{\mathrm{L}}(E_n)\right] \Big\}. \tag{4.23}$$

Here, $|S_{\mathrm{cap}}(E_n, E)|^2$ is given by Eq. (4.17). By performing the integration with respect to energy, it can be seen that the correction terms in the electron part and hole part vanish, independently. The zero correction to the charge-current noise implies that slightly increasing the driving frequency does not change the number of emitted particles.

Along the same line as for the charge-current noise, we derive the energy-current noise by substituting $S_{n,\mathrm{cap}}$ with $S_{\mathrm{cap}}(E_n, E)$ in Eqs. (3.56) and (3.49). Thereby, the transport part of the energy-current noise takes the form

$$\mathcal{P}^{EE}_{\mathrm{tr,R}} = \frac{D(1-D)}{h}\sum_n \int \mathrm{d}E E^2 \left|S_{\mathrm{cap}}(E_n, E)\right|^2 \times \Big\{ f_{\mathrm{R}}(E_n)[1 - f_{\mathrm{L}}(E)] + f_{\mathrm{L}}(E)[1 - f_{\mathrm{R}}(E_n)] \Big\}, \tag{4.24}$$

and the interference part is written as

$$\mathcal{P}^{EE}_{\mathrm{int,R}} = \frac{D^2}{h}\sum_{k,q,n} \int dE\; E_q E_k\; S_{\mathrm{cap}}(E_q, E_n) S^*_{\mathrm{cap}}(E_k, E_n) S_{\mathrm{cap}}(E_k, E) S^*_{\mathrm{cap}}(E_q, E) \times \Big\{ f_{\mathrm{L}}(E_n)[1 - f_{\mathrm{L}}(E)] + f_{\mathrm{R}}(E)[1 - f_{\mathrm{R}}(E)] \Big\}. \tag{4.25}$$

The transport part of the energy noise is obtained by inserting the scattering amplitudes from Eq. (4.17) into the equation above and performing the integral with respect to the energy. We end up with

$$\frac{\mathcal{P}^{EE}_{\mathrm{tr,\,R}}}{D(1-D)\Omega/(2\pi)} = \left(\frac{\hbar}{2\sigma}\right)^2 - \frac{12}{\hbar}\frac{\partial \sigma^e}{\partial E}\left(\frac{\hbar}{2\sigma}\right)^4 + \left(\frac{\hbar}{2\sigma}\right)^2 - \frac{12}{\hbar}\frac{\partial \sigma^h}{\partial E}\left(\frac{\hbar}{2\sigma}\right)^4, \tag{4.26}$$

The first terms in both lines are the transport part of the energy-current noise in the adiabatic response regime, discussed in Sec. 3.2.3. In contrast to the charge-current noise, the correction to the width appears in the energy-current noise in each half-period. However, the electron part (first line) and the hole part (second line) cancel each other in one period. This situation becomes even more complicated when considering the interference part of the energy-current noise, since calculating contributions of the four scattering amplitudes is a non-trivial task. Nevertheless, we find out numerically that the mixed contributions of the electron and the hole scattering amplitudes to the interference part of the energy-current noise vanish. Thus, we only need to calculate the terms corresponding to the electron part and the hole part separately. Carrying out this calculation, we find

$$\frac{\mathcal{P}^{EE}_{\mathrm{int,R}}}{D^2\Omega/h} = \left(\frac{\hbar}{2\sigma}\right)^2 + \frac{8}{\hbar}\frac{\partial\sigma^e}{\partial E}\left(\frac{\hbar}{2\sigma}\right)^4 + \left(\frac{\hbar}{2\sigma}\right)^2 + \frac{8}{\hbar}\frac{\partial\sigma^h}{\partial E}\left(\frac{\hbar}{2\sigma}\right)^4 . \tag{4.27}$$

The first terms in both lines are the interference contribution to the energy-current noise in the adiabatic-response regime. The correction terms for electrons and holes are similar to those of the transport part but with different prefactors. However, since $\partial_E\sigma^e$ and $\partial_E\sigma^h$ have always the opposite signs with respect to each other, the electron and the hole correction terms cancel each other in one period, and the total energy-current noise remains unchanged.

In this chapter, we studied the mesoscopic capacitor, introduced earlier in the thesis, when the driving frequency is beyond the adiabatic-response regime. We have presented an extensive discussion on investigating the impact of the increased driving frequency on the transport quantities. It has been shown that the charge- and energy-current pulses are modified due to the energy-dependency of the temporal-pulse width and the emission time, as depicted in Fig. 4.1 and Fig. 4.3. In addition, we have demonstrated that while the amount of the charge carried by each pulse remains the same as in the slow-driving regime, their average energy is modified by the term corresponding to $\partial_E\sigma^j$.

Moreover, in deriving the charge-current noise, the correction to the adiabatic-response regime vanishes, implying that slightly increasing the driving frequency does not change the number of emitted particles. However, this is not true for the energy-current noise, since the temporal width correction contributes to both the transport part Eq. (4.26) and the interference part Eq. (4.27) of the energy noise.

Finally we conclude that even with slightly increasing driving frequency we still inject one electron and one hole in each period. However, different driving frequency results in different charge- and energy-current pulses.

5 Detection of noise in the mesoscopic capacitor through probe fluctuations

In the previous chapters, we focused on the currents and their fluctuations, originating from the single electron sources. Now, the question arises how to experimentally access these quantities. This problem is addressed in the present chapter in which we overview the key results of the appended publication. Specifically, we propose a suitable approach to measure the charge current, the energy current and their corresponding correlations.

In this chapter, we illustrate the working principle of this method for a specific system, namely, the time-dependent driven mesoscopic capacitor, which has previously been discussed in Chap. 3. We concentrate on the investigation of charge and energy current and their fluctuations by such a system. Notice that this method is generally applicable to other on-demand single-electron sources, as explained in detail in the appended paper. First, we introduce the detection setup on which our proposed method is based on. The main component of this setup is a *small* contact acting as an electrically and thermally floating probe [53, 54]. This probe is characterized by time-dependent electrochemical potential and temperature which are subjected to fluctuations. These fluctuations originate from particles injected to the probe and also from the fact that due to the size constraint, the probe can not thermalize immediately. Next, we employ a Boltzmann-Langevin approach [46, 55] in combination with the Floquet scattering theory [40, 41] to derive how the charge current, the energy current and their correlations are related to averaged electrochemical potential, temperature and their frequency-dependent fluctuations [27, 28], respectively.

5.1 Setup

The mesoscopic conductor including the time-dependently driven mesoscopic capacitor has already been analyzed in Chap. 3. Here, we describe the setup by dividing it conceptually into two parts: the detector and the injector, as shown in Fig. 5.1. The injector part consists of the mesoscopic capacitor which is driven with frequency $\Omega = 2\pi/\mathcal{T}$ as introduced in Sec. 3.1.1, and the left electronic reservoir. This reservoir is characterized by a fixed temperature, $T_{\mathrm{L}} = T_0$, and a

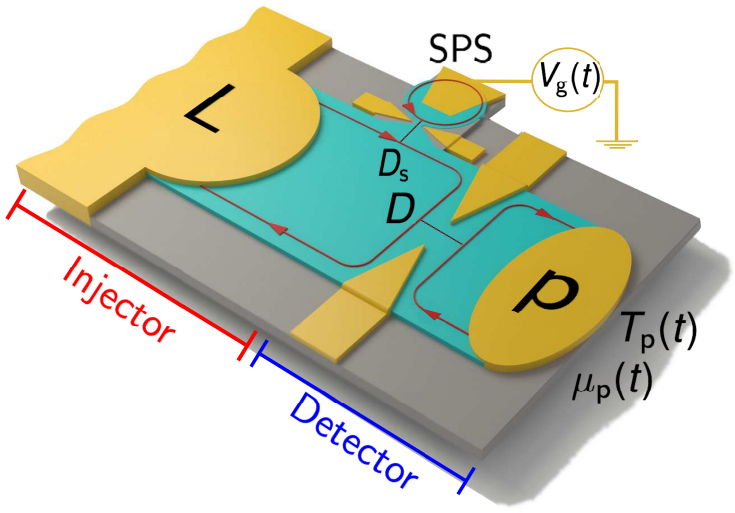

Figure 5.1: *Schematic representation of the coherent chiral mesoscopic conductor with a quantum point contact (QPC) of transparency D. The conductor is in contact with an electronic reservoir (L) on the left and with a probe (p) on the right. Reservoir L is kept at $\mu_L = 0$ and $T_L = T_0$. The floating probe has fluctuating electrochemical potential $\mu_p(t)$ and temperature $T_p(t)$ due to the emitted particles from specifically implementing time-dependently driven single-particle source (SPS). The SPS is realized here by means of a slowly driven mesoscopic capacitor at frequency Ω.*

grounded electrochemical potential, $\mu_L = 0$, meaning that particles arriving into the reservoir do not affect its temperature and electrochemical potential. However, the injector part considered here is not the most general one. On the other hand, the detector part is formed by the central QPC and the right contact. For the purpose of this chapter, we assume that the right contact is an electrically and thermally *floating* probe, since the electrochemical potential and the temperature[1] are built-up in the probe as a result of the impinging current.

5.1.1 Probe properties

Electrons in the probe rapidly relax to the local thermal equilibrium before they can escape from the probe. In other words, the relaxation time due to the electron-electron interaction in the probe, τ_{e-e}, is shorter than or of the same order of the timescale that is associated with the source driving. As a result, the probe is characterized by the Fermi distribution with well-defined temperature $T_\mathrm{p}(t)$ and electrochemical potential $\mu_\mathrm{p}(t)$ at all times.

In order to build up the electrochemical potential $\mu_\mathrm{p}(t)$ and the temperature $T_\mathrm{p}(t)$, it is crucial that the probe has a finite electrochemical capacitance C and a heat capacity C_E. The former capacitance corresponds to a geometric capacitance C_g connected in series with a quantum capacitance C_q, $C = (1/C_\mathrm{g}+1/C_\mathrm{q})^{-1}$. The

[1]Note that there is no additional, externally applied thermal bias or voltage bias in the setup.

heat capacity depends on the temperature of the probe, $C_E(T) = \nu(\pi k_B)^2 T/3$, where ν is the density of states at the Fermi level. These two capacitances determine the timescales of the fluctuations. The electrochemical potential fluctuates on a time scale set by the charge relaxation time, $\tau_{RC} = C/(Dg)$, where Dg is the electrical conductance of the QPC and $g = e^2/h$ stands for the quantum conductance per spin. The temperature fluctuates on a timescale set by the energy relaxation time $\tau_E = C_E/\kappa$. Here, κ is the thermal conductance which describes the outflow of energy from the probe and in general is assumed to consist of both electronic and phonon contributions.

Furthermore, the timescale associated with injection of particles into the conductor from the mesoscopic capacitor is much smaller than the timescales on which the electrochemical potential and the temperature fluctuate,

$$\tau_{e-e} \lesssim \mathcal{T} \ll \tau_{RC}, \tau_E. \tag{5.1}$$

This inequality implies that one deals with two different timescales: first, describing fast fluctuations of the current due to the charge injection from the source and the QPC, and second, associated with slow fluctuations of the electrochemical potential and the temperature in the probe. In consequence, it means that one can use the Boltzmann-Langevin approach to separate timescales to relate such fluctuations to each other in the probe.

5.2 Boltzmann-Langevin approach

The Boltzmann-Langevin method is a convenient tool to study current fluctuations in the probe. To begin with, the time-dependent charge and energy currents are written as a sum of the time averaged part denoted by a bar and the fluctuating time-dependent part,

$$I_p(t) = \bar{I}_p + \Delta I_p(t) \quad \text{and} \quad I_p^E(t) = \bar{I}_p^E + \Delta I_p^E(t). \tag{5.2}$$

Along the same line, the electrochemical potential and temperature take the following form,

$$\mu_p(t) = \overline{\mu}_p + \Delta\mu_p(t) \quad \text{and} \quad T_p(t) = \overline{T}_p + \Delta T_p(t). \tag{5.3}$$

The averaged currents, $\bar{I}_p$ and $\bar{I}_p^E$, are derived by means of the Floquet scattering method. The fluctuations $\Delta\mu_p(t)$ and $\Delta T_p(t)$ are induced by fluctuations in the charge and energy currents, $\Delta I_p(t)$ and $\Delta I_p^E(t)$.

The fluctuation part of the current in the probe can be further expressed as a sum of the fluctuations of the conductor and the linear fluctuations of the

temperature and electrochemical potentials,

$$\begin{pmatrix} \Delta I_{\mathrm{p}}(t) \\ \Delta I_{\mathrm{p}}^{E}(t) \end{pmatrix} = \begin{pmatrix} \delta I_{\mathrm{p}}(t) \\ \delta I_{\mathrm{p}}^{E}(t) \end{pmatrix} + \begin{pmatrix} \frac{\partial \bar{I}_{\mathrm{p}}}{\partial \overline{\mu}_{\mathrm{p}}} & \frac{\partial \bar{I}_{\mathrm{p}}}{\partial \overline{T}_{\mathrm{p}}} \\ \frac{\partial \bar{I}_{\mathrm{p}}^{E}}{\partial \overline{\mu}_{\mathrm{p}}} & \frac{\partial \bar{I}_{\mathrm{p}}^{E}}{\partial \overline{T}_{\mathrm{p}}} \end{pmatrix} \cdot \begin{pmatrix} \Delta \mu_{\mathrm{p}}(t) \\ \Delta T_{\mathrm{p}}(t) \end{pmatrix}. \tag{5.4}$$

Here, $\delta I_{\mathrm{p}}(t)$ and $\delta I_{\mathrm{p}}^{E}(t)$ are the bare fluctuations, referred to also as the so-called Langevin sources. These terms physically originate from the source, scattering at the QPC, the left reservoir temperature T_0, and the averaged temperature of the probe $\overline{T}_{\mathrm{p}}$. According to inequality (5.1), the Langevin sources are fast fluctuations whereas the electrochemical potential and temperature can be treated as slow fluctuations.

In the following, we derive a direct relation between the bare fluctuations and the electrochemical-potential and the temperature fluctuations.

5.2.1 Correlation of electrochemical-potential fluctuations

Here, we summarize the key points of the calculation for the electrochemical-potential fluctuations. We start from the continuity equation for charge, which is given by

$$\frac{\mathrm{d}Q(t)}{\mathrm{d}t} = I_{\mathrm{p}}(t). \tag{5.5}$$

Note that the time-averaged current is zero since there is no long-time accumulation of charge in the probe, meaning that $I_{\mathrm{p}}(t) = \Delta I_{\mathrm{p}}(t)$. The total charge in Eq. (5.5) is expressed classically in terms of the total electrochemical capacitance,

$$Q(t) = CV = -\frac{C}{e}\,\mu_{\mathrm{p}}(t). \tag{5.6}$$

By inserting the equation above and Eq. (5.4) into Eq. (5.5), and performing the Fourier transform, the electrochemical potential $\Delta\mu_{\mathrm{p}}(\omega)$ can be expressed in terms of the bare charge fluctuation $\delta I_{\mathrm{p}}(\omega)$,

$$\frac{\Delta\mu_{\mathrm{p}}(\omega)}{-e} = \frac{1}{Dg}\,\frac{\delta I_{\mathrm{p}}(\omega)}{1 + i\omega\tau_{RC}}, \tag{5.7}$$

where $\tau_{RC} = C/(Dg)$. This equation is valid as long as the fluctuations of the electrochemical potential remain small in order to keep the linearization performed in Eq. (5.4). This condition can be satisfied either on the timescale of the charge relaxation time in the probe, τ_{RC}, or on the timescale on which fluctuations are measured, $1/\omega$, with the effective timescale given by $\sqrt{\tau_{RC}^2 + 1/\omega^2}$.

In the next step we calculate the correlators. The frequency-dependent correlations of the electrochemical-potential fluctuations from Eq. (2.35) (by putting $X, Y = \mu$) can be found

$$\pi\delta(\omega + \omega')\mathcal{P}_{\mathrm{p}}^{\mu\mu}(\omega) = \langle \Delta\mu_{\mathrm{p}}(\omega), \Delta\mu_{\mathrm{p}}(\omega') + \Delta\mu_{\mathrm{p}}(\omega'), \Delta\mu_{\mathrm{p}}(\omega)\rangle. \tag{5.8}$$

Using the Boltzmann-Langevin approach, a large separation of timescales between fluctuations of the probe quantities and the bare fluctuations is assumed. For this reason, while the electrochemical-potential correlator is measured at relevant finite frequencies, the bare-fluctuations correlator is considered at zero frequency. Thus, we can write

$$\mathcal{P}^{\mu\mu}_{\rm p}(\omega) = \frac{e^2}{(Dg)^2} \cdot \frac{1}{1+(\omega\tau_{RC})^2}\,\mathcal{P}^{II}_{\rm p}, \tag{5.9}$$

where $\mathcal{P}^{II}_{\rm p}$ represents a charge-current noise and it can be derived using the Floquet scattering matrix. The charge-current noise for the slowly driven mesoscopic capacitor is derived in Eqs. (3.40) and (3.43), but for two contacts are kept at the same temperature. In Sec. 5.3, we explain different components of the bare fluctuations correlator, $\mathcal{P}^{II}_{\rm p}$. In order to detect the charge-current noise by reading out the electrochemical-potential correlators, we need to maximize this quantity. One way to do this task is to maximize the prefactor $e^2/\{[1+(\omega\tau_{RC})^2](Dg)^2)\}$. However, it is not as straightforward as it looks, since we have to consider the contribution of Dg to the charge-current noise. This issue is explained more precisely in the appended paper.

5.2.2 Correlation of temperature fluctuation

In the same manner as for the electrochemical potential, one can derive the temperature fluctuations. The starting point is now the continuity equation for energy

$$\frac{{\rm d}E(t)}{{\rm d}t} = I^E_{\rm p}(t) - \Sigma\mathcal{V}\left[T^5_{\rm p}(t) - T^5_0\right]. \tag{5.10}$$

The second term stems from the coupling of the probe to the phonon bath at temperature T_0 with electron-phonon coupling strength given by $\Sigma\mathcal{V}$. The energy is expressed classically in terms of the charge capacitance and heat capacity as

$$E(t) = \frac{Q^2(t)}{2C} + \frac{C_E(T_{\rm p})\,T_{\rm p}(t)}{2} = -\frac{C}{2e^2}\mu^2_{\rm p}(t) + \frac{C_E(T_{\rm p})\,T_{\rm p}(t)}{2}.$$

Note that the time-averaged energy current is zero since there is no long-time accumulation of energy in the probe, meaning that $I^E_{\rm p}(t) = \Delta I^E_{\rm p}(t)$. By inserting the equation above and Eq. (5.4) into the energy current, Eq. (5.10), in the frequency representation, we obtain then

$$(i\omega)\frac{C}{e^2}\overline{\mu}_{\rm p}\Delta\mu_{\rm p}(\omega) + (i\omega)C_E\Delta T_{\rm p}(\omega) = \delta I^E_{\rm p}(\omega) - \frac{\overline{\mu}_{\rm p}}{e^2}\Delta\mu_{\rm p}(\omega) - \kappa\Delta T_{\rm p}(\omega). \tag{5.11}$$

Here, we keep terms up to first order in $\Delta\mu_{\rm p}(t)$ and $\Delta T_{\rm p}(t)$. By substituting $\Delta\mu_{\rm p}(\omega)$ with Eq. (5.7), we get

$$\Delta T_{\rm p}(\omega) = \frac{1}{\kappa + i\omega C_E}\left[\delta I^E_{\rm p}(\omega) + \frac{\overline{\mu}_{\rm p}}{e}\delta I_{\rm p}(\omega)\right]. \tag{5.12}$$

In addition, in the equation above, one identifies the bare heat fluctuations,

$$\delta J_{\rm p}(\omega) = \delta I_{\rm p}^{E}(\omega) + \overline{\mu}_{\rm p}/e\delta I_{\rm p}(\omega), \tag{5.13}$$

which are related to the temperature fluctuations by

$$\Delta T_{\rm p}(\omega) = \frac{1}{\kappa}\frac{\delta J_{\rm p}(\omega)}{1+i\omega\tau_E}. \tag{5.14}$$

Along the same lines of what has been explained for the electrochemical-potential correlator regarding the large separation of timescales, the bare source correlator is given by the low-frequency limit while we are working in the frequency-regime relevant for temperature correlator. Therefore, we calculate the temperature correlator in terms of the energy-current noise by replacing the electrochemical potential in Eq. (5.8) with temperature, and we get:

$$\mathcal{P}_{\rm p}^{TT}(\omega) = \frac{1}{\kappa^2}\cdot\frac{1}{1+(\omega\tau_E)^2}\,\mathcal{P}_{\rm p}^{JJ}, \tag{5.15}$$

where $\mathcal{P}_{\rm p}^{JJ}$ is derived for the slowly driven mesoscopic capacitor in Eqs. (3.47) and (3.54). Experimentally, the temperature correlator needs to have a large magnitude so that the heat-current noise can be detected. It can be achieved by diminishing thermal conductance κ or tunning parameters which are related to τ_E and $\mathcal{P}_{\rm p}^{JJ}$.

Finally, the correlation between the electrochemical-potential fluctuations Eq. (5.7) and the temperature fluctuation Eq. (5.14) give direct access to the mixed-current noise through

$$\mathcal{P}_{\rm p}^{\mu T}(\omega) = \frac{-e}{Dg\kappa}\cdot\frac{1+\omega^2\tau_{RC}\tau_E}{[1+(\omega\tau_E)^2]\,[1+(\omega\tau_{RC})^2]}\,\mathcal{P}_{\rm p}^{IJ}. \tag{5.16}$$

Here, the mixed correlator is symmetrized, meaning that $\mathcal{P}_{\rm p}^{\mu T} \equiv \mathcal{P}_{\rm p}^{T\mu}$. This correlator depends on two timescales set by the charge and energy relaxation times of the probe.

5.3 Extraction of information about the source from the probe

So far, we have obtained a direct relation between the correlations of the macroscopic fluctuations of the probe variables and the correlations of the bare fluctuations of the probe. Since various parameters of the setup can be tuned, we can use these to maximize the source fluctuations while minimizing at the same time the fluctuations of the back-action in the probe. By doing that we get information about spectrum and precision of the single-electron source. Moreover, to gain further insight into the single-electron source fluctuations, in the following section we decompose the charge- and energy-current noise into two parts that originating from the source and the background fluctuations.

5.3.1 Correlator decomposition

It is instructive to write $\mathcal{P}_{\rm p}^{AB}$, where $A, B = I, J$, as a sum of terms with physically distinct origins,

$$\mathcal{P}_{\rm p}^{AB} = \mathcal{P}_{\rm s}^{AB} + \mathcal{P}_{0}^{AB}. \tag{5.17}$$

Here, $\mathcal{P}_{\rm s}^{AB}$ describes the correlations coming from the driving source. Hence, in the absence of the source, $\mathcal{P}_{\rm s}^{AB}$ is zero. The second term, $\mathcal{P}_{0}^{AB}$, represents the correlations in the absence of the source, which appear due to the non-zero and constant temperatures of the left reservoir and the probe when they are kept at the background temperature T_0. Mind that here $\overline{\mu}_{\rm p} = \mu_{\rm L} = 0$. This background noise can be written as

$$\mathcal{P}_{0}^{AB} = \frac{2}{h} D \int {\rm d}E x_A x_B \, f_0(E)[1 - f_0(E)], \tag{5.18}$$

where $x_A, x_B = -e$ for $A, B = I$, and $x_A, x_B = E$ for $A, B = J$.

Importantly, the source correlators $\mathcal{P}_{\rm s}^{AB}$ can be further divided into direct and induced correlations as

$$\mathcal{P}_{\rm s}^{AB} = \mathcal{P}_{\rm s,dir}^{AB} + \mathcal{P}_{\rm s,ind}^{AB}. \tag{5.19}$$

The direct correlator ('dir'), is obtained for the probe reservoir kept at constant temperature $\overline{T}_{\rm p} = T_0$, with the distribution function $f_0(E) = (1 + e^{E/[k_{\rm B}T_0]})^{-1}$. This correlator comes from the source driving and constant temperature of the reservoirs.

$$\begin{aligned}
\mathcal{P}_{\rm s,dir}^{AB} =& \frac{D(1-D)}{h} \sum_{n\neq 0} \int {\rm d}E \; x_A x_B |S(E_n, E)|^2 \\
&\times \Big\{ f_0(E_n) \left[1 - f_0(E)\right] + f_0(E) \left[1 - f_0(E_n)\right] \Big\} \\
&+ \frac{D^2}{h} \sum_{n\neq 0} \sum_{q,k} \int {\rm d}E \; \frac{x_{A,k} x_{B,q} + x_{A,q} x_{B,k}}{2} S^*(E_q, E) S(E_q, E_n) \\
&\times S(E_k, E) S^*(E_k, E_n) f_0(E_q)[1 - f_0(E_k)].
\end{aligned} \tag{5.20}$$

Here, $x_{A,q} = x_{B,q} = -e$ for $B = I$, and $x_{A,q} = x_{B,q} = E_q$ for $B = J$. The induced correlations ('ind') arise due to the fluctuations of the probe properties, which are affected by the source driving, constant temperature of the left reservoir and transparency of the QPC . In terms of the transport and interference contributions, we find

$$\begin{aligned}
\mathcal{P}_{\rm s,ind}^{AB} =& \frac{1}{h} D(1-D) \sum_{n\neq 0} \int {\rm d}E x_A x_B |S(E_n, E)|^2 \left[f_{\rm p}(E) - f_0(E)\right] \left[1 - 2 f_0(E_n)\right] \\
&+ \frac{1}{h} D^2 \sum_{n\neq 0} \sum_{q,k} \int {\rm d}E x_A x_B \Big\{ f_{\rm p}(E)[1 - f_{\rm p}(E)] - f_0(E)[1 - f_0(E)] \Big\}.
\end{aligned} \tag{5.21}$$

To summarize, Eqs. (5.17)-(5.21) provide us with a complete description of the correlations of the bare fluctuations in the probe. The direct part of the noise, Eq. (5.20), together with the background noise, Eq. (5.18), are calculated in Chap. 3 for a slowly driven mesoscopic capacitor. The induced noise is the new quantity and arise from the temperature gradient.

5.4 Discussion

In this chapter we have proposed a method to detect transport quantities of the mesoscopic capacitor setup, derived in Chap. 3 and 4. However, this method, based on the given argument in the appended paper, can be extended to an arbitrary time-dependently driven electron source. More specifically, we suggest that the charge-current and the energy-current fluctuations should be accessible through the detection of the macroscopic fluctuations of the temperature and the electrochemical potential of a probe contact.

Using the Boltzmann-Langevin approach, the fluctuations of the probe can be divided into fast (bare) and slow fluctuations. Temperature and electrochemical-potential fluctuations are described as slow fluctuations, while charge-current and energy-current fluctuations are defined as fast fluctuations. The correlations of the bare fluctuations are given by the low-frequency limit while the correlations of the temperature and the electrochemical-potential fluctuations are measured in the relevant frequency-regime.

Furthermore, to measure the above-mentioned macroscopic fluctuations one should optimize the detection scheme by taking into account different experimentally relevant parameters. We are concerned with two different kinds of tunable parameters: First, the main setup parameters including the QPC transparency D, the background temperature, the coupling strength $\Sigma\mathcal{V}$ and also the probe capacitances, C and C_E . Second, the source parameters, listed as the temporal width of the pulse σ and the driving frequency Ω.

Besides, we have analyzed how relevant experimental parameters enable us to detect the pure source fluctuations, Eq. (5.20), by minimizing the fluctuations due to the back-action, Eq. (5.21), from the probe. The difficulty in finding the optimum parameters is that when they are adjusted to maximize the direct part, $\mathcal{P}^{AB}_{\mathrm{s,dir}}$, the effect of the induced part, $\mathcal{P}^{AB}_{\mathrm{s,ind}}$, might be increased, both directly and indirectly. In the appended paper we have explained in more detail what is the optimal parameter range that ensures an ideal detection.

The difficulty in tunning the parameters is that while they are adjusted to maximize the direct part, $\mathcal{P}^{AB}_{\mathrm{s,dir}}$, the effect of the induced part, $\mathcal{P}^{AB}_{\mathrm{s,ind}}$, is also increased, both directly and indirectly. In the paper we explain in detail what the optimal parameter range is ensuring the ideal detection.

6 Summary

In this thesis transport quantities such as charge currents, energy currents and their corresponding noise, generated by on-demand single-electron sources have been analyzed. We have shown several examples where these transport quantities can serve as a spectroscopic tool to characterize on-demand single-electron sources. In addition, we have proposed a setup for the detection of charge and energy currents and their fluctuations *via* the fluctuations of macroscopic quantities of a probe contact. The investigations have mostly been based on the concrete example of a quantum-Hall setup with a time-dependently driven mesoscopic capacitor acting as single-electron source.

We have started by introducing two prominent examples of on-demand single-electron sources in Chap. 1: First, a time-dependently driven mesoscopic capacitor, studied as the main example system in this thesis, and second, a Lorentzian-shaped bias voltage which is used as a comparison in some cases. Then, in Chap. 2 we have described Floquet scattering theory which was used as a tool to derive the above-mentioned transport quantities.

Then, in Chap. 3, we have focused on investigating the transport quantities for a quantum-Hall setup with the slowly driven mesoscopic capacitor (setup $\mathcal{A}$). Next, we have contrasted the obtained results with those for a setup emitting single electrons by means of the Lorentzian bias voltage (setup $\mathcal{B}$), which has been previously studied in Refs. [10, 20, 21, 52]. The main difference between these two setups, in general, arises from the fact that the scattering matrix describing the mesoscopic capacitor is energy-dependent, while that of the second setup, driven with the Lorentzian bias voltage, is energy-independent. However, for the slowly driven capacitor at low temperatures ($\hbar\Omega, k_{\mathrm{B}}T \ll \hbar/\sigma$), studied here in more detail, the scattering matrix of both systems is energy-independent. Despite this, we have identified two main further differences related to the number of emitted particles and the ability of the mesoscopic capacitor to store and release charge and energy. This leads to a relative factor for the setup $\mathcal{A}$ with respect to setup $\mathcal{B}$, in the average energy current, charge-current noise and energy-current noise. Furthermore, the average charge current emitted from the mesoscopic capacitor is zero in contrast to the conductor with Lorentzian bias driving. In addition, in order to quantify the differences due to the possible charge and energy storage in the mesoscopic capacitor, we have written down continuity equations taking account of this aspect.

In Chap. 4, we have modified the driving scheme of the mesoscopic capacitor

by increasing the driving frequency beyond the adiabatic-response regime. We were thereby required to derive transport quantities including the next leading order correction in the driving frequency in an expansion of the scattering matrix. We have therefore investigated the features associated with the increased driving frequency which occur in the time-resolved charge current, the energy current, and the energy noise, while leaving the number of emitted particles intact.

Finally, in Chap. 5, which summarizes the appended paper, we have addressed the question of how one can experimentally get access to the charge current, energy current and their fluctuations. We have proposed a detection scheme exploiting frequency-dependent temperature and electrochemical-potential fluctuations in a floating probe. The important part of the setup, which is different from the devices discussed in the rest of the thesis, was that we have replaced the right reservoir with a thermally and electrically floating probe. We have employed a Boltzmann-Langevin approach to explicitly derive how the fluctuations of the source are related to the electrochemical potential and temperature fluctuations. In particular, the feasibility of our detection scheme, in presence of the slowly driven mesoscopic capacitor (previously studied in Chap. 3), has been broadly investigated in the appended paper. We have studied to what extent the back-action of the probe reduces the access to the noise of the single particle emitter. An analysis of the different, experimentally related parameters has shown how an optimization of our proposed detection scheme, indeed makes a detection of the previously investigated features in the energy-current fluctuations feasible.

Appendices

Appendix A

Current operator

In this appendix, we present a detailed derivation of the charge current operator Eq. (2.19). From the definition of the charge current operator we have

$$\hat{I}_\alpha(x,t) = -e\int d\vec{r}_\perp \hat{j}_\alpha(\vec{r},t). \tag{A.1}$$

By replacing the density operator $\hat{j}_\alpha(\vec{r},t)$ with Eq. (2.18), we get

$$\hat{I}_\alpha(x,t) = -\frac{e\hbar}{2mi}\int d\vec{r}_\perp\Big[\hat{\psi}^\dagger_\alpha(t,\vec{r})\frac{\partial\hat{\psi}_\alpha(t,\vec{r})}{\partial x} - \frac{\partial\hat{\psi}^\dagger_{t,\alpha}(\vec{r})}{\partial x}\hat{\psi}_\alpha(t,\vec{r})\Big]. \tag{A.2}$$

Inserting the field operators Eqs. (2.9) and (2.8) one obtains,

$$\begin{aligned}\hat{I}_\alpha(x,t) = &-\frac{e\hbar}{2mi}\int d\vec{r}_\perp\int \mathrm{d}E\int \mathrm{d}E'\frac{\chi_\alpha(\vec{r}_\perp)\chi_\alpha(\vec{r}_\perp)}{h\sqrt{\nu_\alpha(E)\nu_\alpha(E')}}e^{i\frac{E-E'}{\hbar}t}\\
&\Big\{\Big[\hat{a}^\dagger_\alpha(E)e^{-ik_\alpha(E)x}+\hat{b}^\dagger_\alpha(E)e^{ik_\alpha(E)x}\Big]\\
&\times\Big[ik_\alpha(E')\hat{a}_\alpha(E')e^{ik_\alpha(E')x}-ik_\alpha(E')\hat{b}_\alpha(E')e^{-ik_\alpha(E')x}\Big]\\
&-\Big[-ik_\alpha(E)\hat{a}^\dagger_\alpha(E)e^{-ik_\alpha(E)x}+ik_\alpha(E)\hat{b}^\dagger_{\alpha i}(E)e^{-ik_\alpha(E)x}\Big]\\
&\times\Big[\hat{a}_\alpha(E')e^{ik_\alpha(E')x}+\hat{b}_\alpha(E')e^{-ik_\alpha(E')x}\Big]\Big\}.\end{aligned} \tag{A.3}$$

We use the orthonormality of the transverse wave functions, $\int d\vec{r}_\perp\chi_\alpha(\vec{r}_\perp)\chi_\alpha(\vec{r}_\perp) = 1$, to find

$$\begin{aligned}\hat{I}_\alpha(x,t) = &-\frac{e\hbar}{2m}\int \mathrm{d}E\int \mathrm{d}E'\sum_i\frac{1}{\hbar\sqrt{\nu_\alpha(E)\nu_\alpha(E')}}e^{i(E-E')t/\hbar}\\
&\Big\{\hat{a}^\dagger_\alpha(E)\hat{a}_\alpha(E')e^{-i[k_\alpha(E)-k_\alpha(E')]x}\left[k_\alpha(E)+k_\alpha(E')\right]\\
&-\hat{b}^\dagger_\alpha(E)\hat{b}_\alpha(E')e^{i[k_\alpha(E)-k_\alpha(E')]x}\left[k_\alpha(E)+k_\alpha(E')\right]\\
&+\hat{a}^\dagger_\alpha(E)\hat{b}_\alpha(E')e^{-i[k_\alpha(E)+k_\alpha(E')]x}\left[k_\alpha(E)-k_\alpha(E')\right]\\
&-\hat{b}^\dagger_\alpha(E)\hat{a}_\alpha(E')e^{i[k_\alpha(E)+k_\alpha(E')]x}\left[k_\alpha(E)-k_\alpha(E')\right]\Big\}.\end{aligned} \tag{A.4}$$

If we consider E and E' to coincide or to be close to each other, then the velocities can be assumed to be approximately the same. This assumption is not always true, however, the final answer to describe the current and the current noise is obtained to be the same. Therefore, the current operator at the local lead coordinate $x = 0$ reduces to

$$\hat{I}_\alpha(t) = -\frac{e}{h} \iint \mathrm{d}E\mathrm{d}E' e^{i(E-E')t/\hbar} \left\{ \hat{a}^\dagger_\alpha(E)\hat{a}_\alpha(E') - \hat{b}^\dagger_\alpha(E)\hat{b}_{\alpha i}(E') \right\}. \tag{A.5}$$

Appendix B

Energy current density

Here, we do some algebra to show that how one can get the second term of Eq. (2.26) from the second term of Eq. (2.25),

$$\begin{aligned}
&-\frac{\hbar^2}{2m}\left[\partial_t\psi^*\vec{\nabla}^2\psi+\psi^*\vec{\nabla}^2\partial_t\psi+\partial_t\psi\vec{\nabla}^2\psi^*+\psi\vec{\nabla}^2\partial_t\psi^*\right]\\
&\stackrel{?}{=}-\frac{\hbar^2}{2m}\vec{\nabla}\left[-\partial_t\psi^*\vec{\nabla}\psi+\psi^*\vec{\nabla}\partial_t\psi-\partial_t\psi\vec{\nabla}\psi^*+\psi\vec{\nabla}\partial_t\psi^*-\frac{4m}{\hbar^2}U(t)j(\vec{r},t)\right]
\end{aligned} \tag{B.1}$$

Notice that, the first term in Eqs. (2.25) and (2.26) are the source term due to the time-dependent driving potential.

We start with the first line of Eq. (B.1):

$$\begin{aligned}
&-\frac{\hbar^2}{2m}\left(\partial_t\psi^*\vec{\nabla}^2\psi+\psi^*\vec{\nabla}^2\partial_t\psi+\partial_t\psi\vec{\nabla}^2\psi^*+\psi\vec{\nabla}^2\partial_t\psi^*\right)\\
=&-\frac{\hbar^2}{2m}\vec{\nabla}\left(\partial_t\psi^*\vec{\nabla}\psi+\psi^*\vec{\nabla}\partial_t\psi+\partial_t\psi\vec{\nabla}\psi^*+\psi\vec{\nabla}\partial_t\psi^*\right)\\
&+\frac{\hbar^2}{2m}\left(\partial_t\vec{\nabla}\psi^*\vec{\nabla}\psi+\vec{\nabla}\psi^*\vec{\nabla}\partial_t\psi+\partial_t\vec{\nabla}\psi\vec{\nabla}\psi^*+\vec{\nabla}\psi\vec{\nabla}\partial_t\psi^*\right)\\
=&-\frac{\hbar^2}{2m}\vec{\nabla}\left(\partial_t\psi^*\vec{\nabla}\psi+\psi^*\vec{\nabla}\partial_t\psi+\partial_t\psi\vec{\nabla}\psi^*+\psi\vec{\nabla}\partial_t\psi^*\right)\\
&+\frac{\hbar^2}{m}\left(\vec{\nabla}\partial_t\psi^*\vec{\nabla}\psi+\vec{\nabla}\partial_t\psi\vec{\nabla}\psi^*\right)\\
=&-\frac{\hbar^2}{2m}\vec{\nabla}\left(-\partial_t\psi^*\vec{\nabla}\psi+\psi^*\vec{\nabla}\partial_t\psi-\partial_t\psi\vec{\nabla}\psi^*+\psi\vec{\nabla}\partial_t\psi^*\right)\\
&+\frac{\hbar^2}{m}\left(\partial_t\psi^*\vec{\nabla}^2\psi+\partial_t\psi\vec{\nabla}^2\psi^*\right)
\end{aligned} \tag{B.2}$$

From Schrödinger equation, we have $i\hbar\partial_t\hat{\psi}_\alpha(t,\vec{r})=\mathcal{H}\hat{\psi}_\alpha(t,\vec{r})$ and $-i\hbar\partial_t\hat{\psi}^\dagger_\alpha(t,\vec{r})=\mathcal{H}\hat{\psi}^\dagger_\alpha(t,\vec{r})$, where $\mathcal{H}(t,\vec{r})=-\vec{\nabla}^2\hbar^2/2m+U(t)$. We can write the last line of

Eq. (B.2) as

$$
\begin{aligned}
&-\frac{\hbar^2}{m}\left(\partial_t\psi^*\vec{\nabla}^2\psi+\partial_t\psi\vec{\nabla}^2\psi^*\right)\\
&=-\frac{\hbar}{im}\left(\frac{\hbar^2}{2m}\vec{\nabla}^2\psi^*\,\vec{\nabla}^2\psi-U(\vec{r},t)\psi^*\,\vec{\nabla}^2\psi\right)\\
&\quad+\frac{\hbar}{im}\left(\frac{\hbar^2}{2m}\vec{\nabla}^2\psi\,\vec{\nabla}^2\psi^*+U(\vec{r},t)\psi\,\vec{\nabla}^2\psi^*\right)\\
&=-\frac{\hbar}{im}\vec{\nabla}\left(-U(\vec{r},t)\psi^*\,\vec{\nabla}\psi+U(\vec{r},t)\psi\,\vec{\nabla}\psi^*\right)\\
&\quad+\frac{\hbar}{im}\left(\vec{\nabla}U(\vec{r},t)\right)\left(-\psi^*\,\vec{\nabla}\psi+\psi\,\vec{\nabla}\psi^*\right)\\
&=2\vec{\nabla}\left(U(\vec{r},t)j(\vec{r},t)\right)-2\,\left(\vec{\nabla}U(\vec{r},t)\right)j(\vec{r},t).
\end{aligned}
\tag{B.3}
$$

The second term vanishes, since no potential energy gradient is assumed to be present in the reservoirs while the current is measured. Therefore, Eq. (B.2) is found to be

$$
\begin{aligned}
&-\frac{\hbar^2}{2m}\left(\partial_t\psi^*\vec{\nabla}^2\psi+\psi^*\vec{\nabla}^2\partial_t\psi+\partial_t\psi\vec{\nabla}^2\psi^*+\psi\vec{\nabla}^2\partial_t\psi^*\right)\\
&=-\frac{\hbar^2}{2m}\vec{\nabla}\left(-\partial_t\psi^*\vec{\nabla}\psi+\psi^*\vec{\nabla}\partial_t\psi-\partial_t\psi\vec{\nabla}\psi^*+\psi\vec{\nabla}\partial_t\psi^*\right)\\
&\quad+2\vec{\nabla}\left(U(\vec{r},t)j(\vec{r},t)\right),
\end{aligned}
\tag{B.4}
$$

Appendix C

Scattering matrix of the mesoscopic capacitor

In this appendix, we first describe the general scattering matrix of the mesoscopic capacitor, Eq. (3.1), and then derive the scattering matrix when the capacitor is driven slowly.

The capacitor is connected to the conductor through a QPC. The scattering matrix describing the relation between amplitudes of the impinging and the scattered particles is given by

$$\begin{pmatrix} o \\ o_{\mathrm{c}} \end{pmatrix} = \begin{pmatrix} r & t^* \\ t & -r^* \end{pmatrix} \cdot \begin{pmatrix} i \\ i_{\mathrm{c}} \end{pmatrix}, \tag{C.1}$$

A particle propagating from left, along the edge state, can be reflected from the source QPC with the probability amplitude r and continue propagation in the conductor or, it can be transmitted to the capacitor with the probability amplitude t. The particle after q times turning around the capacitor and taking time- and energy-dependent phase is transmitted to the edge state of the conductor with probability amplitude t. Now, we can construct the scattering matrix of the

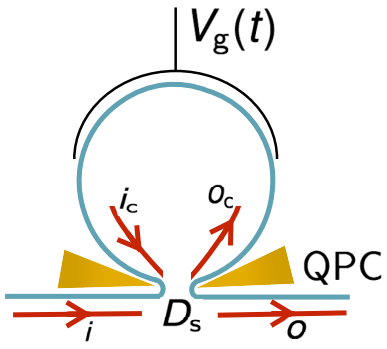

Figure C.1: *The impinging amplitudes to the QPC, i and i_c are scattered to amplitudes o and o_c, while the transparency of the QPC is defind as $D_s = |t^2|$.*

capacitor and write

$$S(t,E) = r + |t^2| \sum_{q=1}^{\infty} (-r^*)^{q-1}\, e^{iqkL}\, e^{-\frac{i}{\hbar}\int_{t-q\tau}^{t} \mathrm{d}t' U_{\mathrm{g}}(t')}, \tag{C.2}$$

where k is the wave number of the particle which makes one turn around the capacitor with length L in time $\tau = m_e L/\hbar k$). For simplicity, we remove the subscript "cap" for the notation $S_{\mathrm{cap}}(t,E) = S(t,E)$. In the following, we obtain the modified scattering matrix for the slow driving regime.

C.1 Scattering matrix in slow driving regime

In the slow driving regime, $\int_{t-q\tau}^{t} \mathrm{d}t' U_{\mathrm{g}}(t') \approx U_{\mathrm{g}}(t)\, q\tau$, the scattering matrix is obtained as

$$\begin{aligned} S^{(0)}(t,E) &= r + |t^2|(-r^*)^{-1} \sum_{q=1}^{\infty} (-r^*)^q\, e^{iq(kL - \frac{\tau}{\hbar}U_{\mathrm{g}}(t))} \\ &= \frac{r + e^{iq(kL-\frac{\tau}{\hbar}U_{\mathrm{g}}(t))}}{1 + r^* e^{iq(kL-\frac{\tau}{\hbar}U_{\mathrm{g}}(t))}}. \end{aligned} \tag{C.3}$$

We replace $r = e^{i\theta}\sqrt{1-D_{\mathrm{s}}}$ by assuming $\theta = 0$ or π,

$$S^{(0)}(t,E) = \frac{\sqrt{1-D_{\mathrm{s}}} + e^{\phi(t,E)}}{1 + \sqrt{1-D_{\mathrm{s}}} e^{\phi(t,E)}}. \tag{C.4}$$

With

$$\phi(t,E) = kL - 2\pi\Delta^{-1}\overline{U}_{\mathrm{g}} - 2\pi\Delta^{-1}\delta U_{\mathrm{g}}(t) - \theta. \tag{C.5}$$

One can expand the wave number k around the Fermi wave number, meaning that $kL = k_\mu L + (E-\mu)L/(\hbar v)$. Therefore, Eq. (C.5) is reduced to

$$\phi(t,E) = k_\mu L + 2\pi\Delta^{-1}(E - \mu - \overline{U}_{\mathrm{g}}) - 2\pi\Delta^{-1}\delta U_{\mathrm{g}}(t) - \theta. \tag{C.6}$$

The ratio L/v is found to be the time τ during which, the electron with the Fermi velocity v turns around the capacitor of length L.

Here, we are interested to have well-separated injection of electrons and holes. For this reason, we are concerned with the weak-coupling limit, i.e., $D_{\mathrm{s}} \ll 1$. Thereby, we can write $\sqrt{1-D_{\mathrm{s}}} = 1 - D_{\mathrm{s}}/2$ in Eq. (C.4). On the other hand, the time of crossing, t^{res}, is when the scattering amplitude is maximized and defined by $S^{(0)}(t,E) = 1$. That corresponds to $\phi(t^{\mathrm{res}},E) = \pi$. If the deviation from the resonance is considered to be $\delta\phi(t,E) = \phi(t,E) - \phi(t^{\mathrm{res}},E)$, then expanding the exponential component of the phase gives,

$$e^{i\phi(t,E)} = e^{i\phi(t^{\mathrm{res}},E)} e^{i\delta\phi(t,E)} = -1 - i\delta\phi(t,E) - h.o. \tag{C.7}$$

In consequence, taking into account all of the discussed simplifications, the scattering matrix can be expressed as

$$\begin{aligned} S^{(0)}(t,E) &= e^{i\theta}\frac{1-D_\mathrm{s}/2+(-1-i\delta\phi(t))}{1+(1-D_\mathrm{s}/2)(-1-i\delta\phi(t))} \\ &= e^{i\theta}\frac{\delta\phi(t)-iD_\mathrm{s}/2}{\delta\phi(t)+iD_\mathrm{s}/2} \end{aligned} \tag{C.8}$$

Furthermore, by expanding $\delta\phi(t,E) = (t-t^\mathrm{res})\frac{\mathrm{d}\phi(t,E)}{\mathrm{d}t}|_{t^\mathrm{res}}$, it becomes

$$S^{(0)}(t,E) = \frac{t-t^\mathrm{res}-i\sigma^\mathrm{res}}{t-t^\mathrm{res}+i\sigma^\mathrm{res}}, \tag{C.9}$$

where

$$\sigma^\mathrm{res} = \frac{D_\mathrm{s}}{2\frac{d\phi(t,E)}{\mathrm{d}t}|_{t^\mathrm{res}}} = \frac{D_\mathrm{s}}{-4\pi\frac{d\delta U_\mathrm{g}(t)}{\mathrm{d}t}|_{t^\mathrm{res}}}. \tag{C.10}$$

The equation above can be expressed for electrons and holes, separately by considering the following argument: An electron is emitted when the occupied level shifts above the Fermi level by increasing the potential energy, i.e. $\mathrm{d}\delta U_\mathrm{g}(t)/\mathrm{d}t > 0$ and as a result, $\sigma^e = -\sigma$. On the other hand, a hole is emitted when the empty level of the capacitor moves below the Fermi level by decreasing the potential, i.e. $\mathrm{d}\delta U_\mathrm{g}(t)/\mathrm{d}t < 0$ and thus, $\sigma^h = +\sigma$. Here, σ is defined by

$$\sigma = \left|\frac{D_\mathrm{s}}{2\frac{\mathrm{d}\phi(t,E)}{\mathrm{d}t}|_{t^{e/h}}}\right|. \tag{C.11}$$

Then, the scattering matrix for the electron part and the hole part can be defined separately as

$$S^{(0)}_\mathrm{cap}(t,E) = \begin{cases} \dfrac{t-t^h_\mathrm{cap}-i\sigma_\mathrm{cap}}{t-t^h_\mathrm{cap}+i\sigma_\mathrm{cap}}, & 0 \le t < \mathcal{T}/2 \\ \dfrac{t-t^e_\mathrm{cap}+i\sigma_\mathrm{cap}}{t-t^e_\mathrm{cap}-i\sigma_\mathrm{cap}}, & \mathcal{T}/2 \le t < \mathcal{T}, \end{cases} \tag{C.12}$$

Appendix D

Currents with the mixed-representation scattering matrix

D.1 Time-dependent charge current

In this appendix, we derive the general time-dependent charge current in terms of the mixed-representation of the scattering matrix Eq. (2.13). To begin with, we start with Eq. (2.20),

$$\begin{aligned} I_\alpha(t) &= -\frac{e}{h}\sum_\beta\sum_{n,l}\int \mathrm{d}E e^{-i(l)\Omega t}\, S^*_{\alpha\beta}(E,E_n)S_{\alpha\beta}(E_l,E_n)\{f_\beta(E_n)-f_\alpha(E)\} \\ &= -\frac{e}{h}\sum_\beta\sum_{n,l}\int \mathrm{d}E e^{-i(l-n)\Omega t}\, S^*_{\alpha\beta}(E_n,E)S_{\alpha\beta}(E_l,E)\,\{f_\beta(E)-f_\alpha(E_n)\}. \end{aligned} \tag{D.1}$$

By employing the partial Fourier transform of the scattering matrix Eq. (2.14), the current can be written as

$$\begin{aligned} I_\alpha(t) &= -\frac{e}{h}\sum_\beta\sum_{n,l}\int \mathrm{d}E\,\{f_\beta(E)-f_\alpha(E_n)\}e^{-i(l-n)\Omega t} \\ &\qquad\times\iint\frac{\mathrm{d}t'}{\mathcal{T}}\frac{\mathrm{d}t''}{\mathcal{T}}e^{-in\Omega t'}\, e^{il\Omega t''}\, S^*_{\alpha\beta}(t',E)\, S_{\alpha\beta}(t'',E) \\ &= -\frac{e}{h}\sum_\beta\sum_{n}\int \mathrm{d}E\,\{f_\beta(E)-f_\alpha(E_n)\}\int\frac{\mathrm{d}t'}{\mathcal{T}}e^{in\Omega(t-t')}\, S^*_{\alpha\beta}(t',E)\, S_{\alpha\beta}(t,E). \end{aligned} \tag{D.2}$$

In the next section, we derive the adiabatic-response current Eq. (3.20) and the correction term to adiabatic-response regime Eq. (4.11) by expanding the scattering matrix in terms of the driving frequency that for the case of the mesoscopic capacitor is described by Eq. (3.4).

D.1.1 Adiabatic-response regime

The expression for the charge current in the adiabatic-response regime is obtained by inserting the energy-independent frozen scattering matrix $S^{(0)}_{\alpha\beta}(t,\mu)$ into Eq. (D.2). We find

$$\begin{aligned} I^{(0)}_{\alpha}(t) &= -\frac{e}{h}\sum_{\beta}\sum_{n}\int\frac{\mathrm{d}t'}{\mathcal{T}}\,(n\hbar\Omega)\,e^{in\Omega(t-t')}\;\;S^{*(0)}_{\alpha\beta}(t',\mu)\,S^{(0)}_{\alpha\beta}(t,\mu) \\ &= -\frac{e}{h}\sum_{\beta}\sum_{n}\int\frac{\mathrm{d}t'}{\mathcal{T}}\,e^{in\Omega(t-t')}\;\;\frac{\partial S^{*(0)}_{\alpha\beta}(t',\mu)}{\partial t'}\,S^{(0)}_{\alpha\beta}(t,\mu)\,(\frac{\hbar}{i}) \\ &= -\frac{e}{i2\pi}\sum_{\beta}\frac{\partial S^{*(0)}_{\alpha\beta}(t,\mu)}{\partial t}\,S^{(0)}_{\alpha\beta}(t,\mu), \end{aligned} \tag{D.3}$$

where, we additionally assume $\mu_{\mathrm{L}}-\mu_{\mathrm{R}}=0$.

D.1.2 Correction to the adiabatic-response regime

Charge current beyond the adiabatic-response regime is describe by considering the next leading order correction in the expansion of the scattering matrix. Using the scattering matrix Eq. (4.3), the correction to the current is found to be

$$\begin{aligned} I^{(1)}_{\alpha}(t) = &-\frac{e}{h}\sum_{\beta}\sum_{n}\int\mathrm{d}E\,\{f_{\beta}(E)-f_{\alpha}(E_n)\}\int\frac{\mathrm{d}t'}{\tau}e^{in\Omega(t-t')} \\ &\times\Bigg\{E\left[S^{*(0)}_{\alpha\beta}(t,\mu)\frac{\partial S^{(0)}_{\alpha\beta}(t,E)}{\partial E}|_{E=\mu}+\frac{\partial S^{*(0)}_{\alpha\beta}(t',E)}{\partial E}|_{E=\mu}\,S^{(0)}_{\alpha\beta}(t,E)\right] \\ &+i\frac{\hbar}{2}\left[-\frac{\partial^2 S^{*(0)}_{\alpha\beta}(t',E)}{\partial t'\partial E}|_{E=\mu}\,S^{(0)}_{\alpha\beta}(t,\mu)+S^{*(0)}_{\alpha\beta}(t,\mu)\,\frac{\partial^2 S^{*(0)}_{\alpha\beta}(t,E)}{\partial t\partial E}|_{E=\mu}\right]\Bigg\}. \end{aligned} \tag{D.4}$$

By assuming $\mu_{\mathrm{L}}-\mu_{\mathrm{R}}=0$ and performing the integrals, we obtain

$$\begin{aligned} I^{(1)}_{\alpha}(t) = &-\frac{e}{h}\sum_{\beta}\Bigg\{-\frac{\hbar^2}{2}\left[\frac{\partial^2 S^{*}_{\alpha\beta}(t,\mu)}{\partial^2 t}\frac{\partial S^{(0)}_{\alpha\beta}(t,E)}{\partial E}|_{E=\mu}+\frac{\partial^3 S^{*(0)}_{\alpha\beta}(t,E)}{\partial^2 t\partial E}|_{E=\mu}\,S(t,\mu)\right] \\ &+\frac{\hbar^2}{2}(\frac{\hbar}{i})\left[-\frac{\partial^3 S^{*(0)}_{\alpha\beta}(t,E)}{\partial^2 t\partial E}|_{E=\mu}\,S(t,\mu)+\frac{\partial S^{*}_{\alpha\beta}(t,\mu)}{\partial t}\,\frac{\partial^2 S^{*(0)}_{\alpha\beta}(t,E)}{\partial t\partial E}|_{E=\mu}\right]\Bigg\}, \end{aligned} \tag{D.5}$$

Carrying out the remaining algebra in the equation above, the correction to the current is simplified to

$$I_\alpha^{(1)}(t) = -\frac{e\,\hbar}{4\pi}\frac{\partial}{\partial t}\left(\frac{\partial S^{*(0)}_{\alpha\beta}(t,\mu)}{\partial t}\quad \frac{\partial S^{(0)}_{\alpha\beta}(t,E)}{\partial E}|_{E=\mu}\right). \tag{D.6}$$

D.2 Time-dependent energy current

Along the same lines of the charge current, we express the time-dependent energy current in terms of the mixed-representation of the scattering matrix Eq. (2.13). As an starting point, we rewrite Eq. (2.30),

$$\begin{aligned} I_\alpha^E(t) = \frac{1}{h}\sum_\beta\sum_{n,l}\int \mathrm{d}E\,(E+\frac{l\hbar\Omega}{2})\,e^{-i(l)\Omega t}S^*_{\alpha\beta}(E,E_n)S_{\alpha\beta}(E_l,E_n) \\ \times\{f_\beta(E_n)-f_\alpha(E)\}, \end{aligned} \tag{D.7}$$

Using $l\to l+n$, we have

$$\begin{aligned} I_\alpha^E(t) = \frac{1}{h}\sum_\beta\sum_{n,l}\int \mathrm{d}E\,(E+\frac{l+n}{2}\hbar\Omega)\,e^{-i(l-n)\Omega t}\;S^*_{\alpha\beta}(E_n,E)S_{\alpha\beta}(E_l,E) \\ \times\{f_\beta(E)-f_\alpha(E_n)\}. \end{aligned} \tag{D.8}$$

By employing the partial Fourier transform of the scattering matrix Eq. (**??**), the current can be written as

$$\begin{aligned} I_\alpha^E(t) &= \frac{1}{h}\sum_\beta\sum_{n,l}\int \mathrm{d}E\,(E+\frac{l+n}{2}\hbar\Omega)\,e^{-i(l-n)\Omega t}\iint\frac{\mathrm{d}t'}{\tau}\frac{\mathrm{d}t''}{\tau}e^{-in\Omega t'}\;e^{il\Omega t''} \\ &\quad\times S^*_{\alpha\beta}(t',E)\,S_{\alpha\beta}(t'',E)\,\{f_\beta(E)-f_\alpha(E_n)\}, \\ &= \frac{1}{h}\sum_\beta\sum_{n}\int dE\,\{f_\beta(E)-f_\alpha(E_n)\}\int\frac{\mathrm{d}t'}{\tau}e^{in\Omega(t-t')} \\ &\quad\times\{(E+\frac{n\hbar\Omega}{2})S^*_{\alpha\beta}(t',E)\,S_{\alpha\beta}(t,E)-\frac{\hbar}{2i}S^*_{\alpha\beta}(t',E)\,\frac{\partial S_{\alpha\beta}(t,E)}{\partial t}\}. \end{aligned} \tag{D.9}$$

Now, we can derive the adiabatic-response energy current Eq. (3.27), and the correction term to it Eq. (4.19) by using the scattering matrix Eq. (4.3), which describes the driven mesoscopic capacitor setup.

D.2.1 Adiabatic-response regime

The time-dependent energy current in the adiabatic-response regime is described in terms of the frozen scattering matrix. By considering $\mu_\mathrm{L}-\mu_\mathrm{R}=0$, the energy

current is given by

$$I_{\alpha}^{E(0)}(t)=\frac{1}{h}\sum_{\beta}\sum_{n}\int\frac{\mathrm{d}t'}{\tau}(n\hbar\Omega)e^{in\Omega(t-t')}(-\frac{\hbar}{2i})S_{\alpha\beta}^{*(0)}(t',\mu)\,\frac{\partial S_{\alpha\beta}^{(0)}(t,\mu)}{\partial t}, \tag{D.10}$$

Performing the integrals, the energy current is derived to be

$$I_{\alpha}^{E(0)}(t)=\frac{\hbar}{4\pi}\sum_{\beta}\frac{\partial S_{\alpha\beta}^{*(0)}(t,\mu)}{\partial t,\mu}\,\frac{\partial S_{\alpha\beta}^{(0)}(t)}{\partial t}. \tag{D.11}$$

D.2.2 Correction to the adiabatic-response regime

The correction to the adiabatic-response energy current is obtained as

$$\begin{aligned}
I_{\alpha}^{E(1)}(t)=\frac{1}{h}\sum_{\beta}\sum_{n}\int\mathrm{d}E\{f_{\beta}(E)-f_{\alpha}(E_n)\}\int\frac{\mathrm{d}t'}{\tau}e^{in\Omega(t-t')}\\
\times\Bigg\{(E+\frac{n\hbar\Omega}{2})\\
\times\Bigg(E\left[S_{\alpha\beta}^{*(0)}(t',\mu)\frac{\partial S_{\alpha\beta}^{(0)}(t,E)}{\partial E}|_{E=\mu}+\frac{\partial S_{\alpha\beta}^{*(0)}(t',E)}{\partial E}|_{E=\mu}S_{\alpha\beta}^{(0)}(t,\mu)\right]\\
-i\frac{\hbar}{2}\left[S_{\alpha\beta}^{*(0)}(t',\mu)\;\frac{\partial^2 S_{\alpha\beta}^{(0)}(t,E)}{\partial t\partial E}|_{E=\mu}+\frac{\partial^2 S_{\alpha\beta}^{*(0)}(t',E)}{\partial t'\partial E}|_{E=\mu}\;S_{\alpha\beta}^{(0)}(t,\mu)\right]\Bigg)\\
-\frac{\hbar}{2i}\\
\times\Bigg(E\left[S_{\alpha\beta}^{*(0)}(t',\mu)\frac{\partial^2 S_{\alpha\beta}^{(0)}(t,E)}{\partial t\partial E}|_{E=\mu}+\frac{\partial S_{\alpha\beta}^{*(0)}(t',E)}{\partial E}|_{E=\mu}\frac{\partial S^{(0)}(t,\mu)}{\partial t}\right]\\
-i\frac{\hbar}{2}\left[S_{\alpha\beta}^{*(0)}(t',\mu)\;\frac{\partial^3 S_{\alpha\beta}^{(0)}(t,E)}{\partial^2 t\partial E}|_{E=\mu}+\frac{\partial^2 S_{\alpha\beta}^{*(0)}(t',E)}{\partial t'\partial E}|_{E=\mu}\;\frac{\partial S^{(0)}(t,\mu)}{\partial t}\right]\Bigg)\Bigg\}
\end{aligned} \tag{D.12}$$

By considering $\mu_{\mathrm{L}}-\mu_{\mathrm{R}}=0$ and performing the integral, we have

$$I_{\alpha}^{E(1)}(t)=\frac{-\hbar^2}{8\pi i}\left\{\frac{1}{3}\frac{\partial}{\partial E}\left(\frac{\partial^3 S_{\alpha\beta}^{*(0)}(t,\mu)}{\partial^3 t}\,S_{\alpha\beta}^{(0)}(t,\mu)\right)+\frac{\partial}{\partial t}\left(\frac{\partial S_{\alpha\beta}^{*(0)}(t,\mu)}{\partial t}\,\frac{\partial^2 S_{\alpha\beta}^{(0)}(t,E)}{\partial t\partial E}|_{E=\mu}\right)\right\} \tag{D.13}$$

Appendix E

Average energy current for the mesoscopic capacitor setup

The average energy current in the mesoscopic capacitor setup $\mathcal{A}$ which is given in Eq. (3.29) is derived in the present appendix.

We start by inserting the energy-independent frozen scattering matrix, $S(E_n, E) = S_n$, in Eq. (2.31). We obtain

$$\bar{I}_{\mathrm{R}}^{E,\mathcal{A}(0)} = \frac{D}{h}\sum_n |S_n|^2 \int \mathrm{d}E E\left[f_{\mathrm{L}}(E_n) - f_{\mathrm{R}}(E)\right]. \tag{E.1}$$

Recalling that, there is no bias voltage ($\mu_{\mathrm{L}} - \mu_{\mathrm{R}} = 0$), and solving the integral with respect to energy, followed by inserting the expression for S_n in Eq. (3.12), we find

$$\bar{I}_{\mathrm{R}}^{E,\mathcal{A}(0)} = \frac{D}{h}\sum_{n>0}(2\sigma\Omega)^2 e^{-2n\sigma\Omega}(n\hbar\Omega)^2 = \frac{\hbar\Omega^2}{2\pi}\frac{(2\sigma\Omega)^2 e^{2\sigma\Omega}(1+e^{2\sigma\Omega})}{(e^{2\sigma\Omega}-1)^3}. \tag{E.2}$$

Finally, making use of the condition $\sigma\Omega \ll 1$ to the leading order in $\sigma\Omega$, we get

$$\bar{I}_{\mathrm{R}}^{E,\mathcal{A}(0)} = 2D\frac{\mathcal{E}}{\mathcal{T}}. \tag{E.3}$$

Appendix F

Interference part of the energy-current noise

Here, we present a detailed calculations of the interference part of the energy-current noise in the case when the source is the slowly driven mesoscopic capacitor Eq. (3.50).

The interference part of the energy-current noise is proportional to D^2, and equals

$$\mathcal{P}_{\mathrm{int,R}}^{EE,\mathcal{A}(0)} = \frac{D^2}{h}\int \mathrm{d}E \Big\{ \sum_{k,q,n} E_q E_k \; S_{q-n}S^*_{k-n}S_kS^*_q f_{\mathrm{L}}(E_n)[1-f_{\mathrm{L}}(E)] + E^2 \, f_{\mathrm{R}}(E)[1-f_{\mathrm{R}}(E)]\Big\}$$

We start by writing the first integral as a sum of three terms

$$\int \mathrm{d}E \sum_{k,q,n} E_q E_k \; S_{q-n}S^*_{k-n}S_kS^*_q \; f_{\mathrm{L}}(E_n)[1-f_{\mathrm{L}}(E)] = p_1 + p_2 + p_3 \tag{F.1}$$

where

$$\begin{aligned}
p_1 &= \int \mathrm{d}E E^2 \sum_{k,q,n} E_q E_k \; S_{q-n}S^*_{k-n}S_kS^*_q \; f_{\mathrm{L}}(E_n)[1-f_{\mathrm{L}}(E)] \\
p_2 &= (\hbar\Omega)\int \mathrm{d}E E \sum_{q,k,n} (k+q) \; S_{q-n}S^*_{k-n}S_kS^*_q \; f_{\mathrm{L}}(E_n)[1-f_{\mathrm{L}}(E)] \\
p_3 &= (\hbar\Omega)^2\int \mathrm{d}E \sum_{q,k,n} kq \; S_{q-n}S^*_{k-n}S_kS^*_q \; f_{\mathrm{L}}(E_n)[1-f_{\mathrm{L}}(E)].
\end{aligned}$$

Using the unitarity of S_n, we have directly

$$\begin{aligned}
p_1 &= \int \mathrm{d}E E^2 f(E)[1-f(E)] = \frac{\pi^2}{3}(k_{\mathrm{B}}T)^3, \\
p_2 &= 2(\hbar\Omega)\int \mathrm{d}E E f(E)[1-f(E)] \sum_q q|S_q|^2 = 0.
\end{aligned} \tag{F.2}$$

For the third term, p_3, we first reformulate it as

$$\begin{aligned} p_3 &= (\hbar\Omega)^2 \int \mathrm{d}E \sum_n f(E_n)[1-f(E)] \left| \sum_q q S_{q-n} S_q^* \right|^2 \\ &= (\hbar\Omega)^2 \sum_{n>0} \left| \sum_q q S_{q-n} S_q^* \right|^2 (n\hbar\Omega) \coth\left(\frac{n\hbar\Omega}{2k_\mathrm{B}T}\right). \end{aligned} \tag{F.3}$$

As a result, the total interference part is obtained by

$$\begin{aligned} \mathcal{P}_{\mathrm{int,R}}^{EE,\mathcal{A}(0)} &= \frac{D^2}{h}(2p_1 + p_2 + p_3) \\ &= \frac{D^2}{h}\frac{2\pi^2}{3}(k_\mathrm{B}T)^3 + \frac{D^2}{h}\,(\hbar\Omega)^2 \sum_{n>0} \left| \sum_q q S_{q-n} S_q^* \right|^2 (n\hbar\Omega) \coth\left(\frac{n\hbar\Omega}{2k_\mathrm{B}T}\right) \end{aligned} \tag{F.4}$$

References

[1] J. P. Pekola, O.-P. Saira, V. F. Maisi, A. Kemppinen, M. Möttönen, Y. A. Pashkin, and D. V. Averin, "Single-electron current sources: Toward a refined definition of the ampere", Rev. Mod. Phys. **85**, 1421–1472 (2013) (cit. on p. 1).

[2] Y. Sherkunov, N. d'Ambrumenil, P. Samuelsson, and M. Büttiker, "Optimal pumping of orbital entanglement with single-particle emitters", Phys. Rev. B **85**, 081108 (2012) (cit. on p. 1).

[3] E. Bocquillon, V. Freulon, F. D. Parmentier, J.-M. Berroir, B. Plaçais, C. Wahl, J. Rech, T. Jonckheere, T. Martin, C. Grenier, D. Ferraro, P. Degiovanni, and G. Fève, "Electron quantum optics in ballistic chiral conductors", Ann. Phys. **526**, 1–30 (2014) (cit. on p. 1).

[4] J. Dubois, T. Jullien, F. Portier, P. Roche, A. Cavanna, Y. Jin, W. Wegscheider, P. Roulleau, and D. C. Glattli, "Minimal-excitation states for electron quantum optics using levitons", Nature **502**, 659–663 (2013) (cit. on pp. 1–4, 17).

[5] Y. Ji, Y. Chung, D. Sprinzak, M. Heiblum, D. Mahalu, and H. Shtrikman, "An electronic Mach–Zehnder interferometer", Nature **422**, 415–418 (2003) (cit. on p. 1).

[6] G. Fève, A. Mahé, J.-M. Berroir, T. Kontos, B. Plaçais, D. C. Glattli, A. Cavanna, B. Etienne, and Y. Jin, "An On-Demand Coherent Single-Electron Source", Science **316**, 1169–1172 (2007) (cit. on pp. 1–3, 17, 18).

[7] M. Vanević, Y. V. Nazarov, and W. Belzig, "Elementary Events of Electron Transfer in a Voltage-Driven Quantum Point Contact", Phys. Rev. Lett. **99**, 076601 (2007) (cit. on p. 1).

[8] M. Vanević, Y. V. Nazarov, and W. Belzig, "Elementary charge-transfer processes in mesoscopic conductors", Phys. Rev. B **78**, 245308 (2008) (cit. on p. 1).

[9] J. Gabelli and B. Reulet, "Shaping a time-dependent excitation to minimize the shot noise in a tunnel junction", Phys. Rev. B **87**, 075403 (2013) (cit. on p. 1).

[10] M. Moskalets and M. Büttiker, "Heat production and current noise for single- and double-cavity quantum capacitors", Phys. Rev. B **80**, 081302 (2009) (cit. on pp. 1, 23, 26, 53).

[11] G. Rosselló, F. Battista, M. Moskalets, and J. Splettstoesser, "Interference and multiparticle effects in a Mach-Zehnder interferometer with single-particle sources", Phys. Rev. B **91**, 115438 (2015) (cit. on p. 1).

[12] F. Ronetti, M. Carrega, D. Ferraro, J. Rech, T. Jonckheere, T. Martin, and M. Sassetti, "Polarized heat current generated by quantum pumping in two-dimensional topological insulators", Phys. Rev. B **95**, 115412 (2017) (cit. on p. 1).

[13] M. F. Ludovico, J. S. Lim, M. Moskalets, L. Arrachea, and D. Sánchez, "Dynamical energy transfer in ac-driven quantum systems", Phys. Rev. B **89**, 161306 (2014) (cit. on p. 1).

[14] F. Zhan, S. Denisov, and P. Hänggi, "Electronic heat transport across a molecular wire: Power spectrum of heat fluctuations", Phys. Rev. B **84**, 195117 (2011) (cit. on p. 1).

[15] A. Crépieux and F. Michelini, "Mixed, charge and heat noises in thermoelectric nanosystems", J. Phys.: Condens. Matter **27**, 015302 (2015) (cit. on p. 1).

[16] P. Eyméoud and A. Crépieux, "Mixed electrical-heat noise spectrum in a quantum dot", Phys. Rev. B **94**, 205416 (2016) (cit. on p. 1).

[17] R. Sánchez and M. Büttiker, "Detection of single-electron heat transfer statistics", EPL **100**, 47008 (2012) (cit. on p. 1).

[18] R. Sánchez and M. Büttiker, "Erratum: Detection of single-electron heat transfer statistics", EPL **104**, 49901 (2013) (cit. on p. 1).

[19] R. Sánchez, B. Sothmann, A. N. Jordan, and M. Büttiker, "Correlations of heat and charge currents in quantum-dot thermoelectric engines", New J. Phys. **15**, 125001 (2013) (cit. on p. 1).

[20] M. Moskalets, "Floquet Scattering Matrix Theory of Heat Fluctuations in Dynamical Quantum Conductors", Phys. Rev. Lett. **112**, 206801 (2014) (cit. on pp. 1, 23, 26, 28, 29, 53).

[21] M. Moskalets, "Erratum: Floquet Scattering Matrix Theory of Heat Fluctuations in Dynamical Quantum Conductors [Phys. Rev. Lett. 112, 206801 (2014)]", Phys. Rev. Lett. **113**, 069902 (2014) (cit. on pp. 1, 23, 26, 28, 29, 53).

[22] F. Battista, F. Haupt, and J. Splettstoesser, "Energy and power fluctuations in ac-driven coherent conductors", Phys. Rev. B **90**, 085418 (2014) (cit. on pp. 1, 2, 21, 27–29).

[23] F. Battista, F. Haupt, and J. Splettstoesser, "Correlations between charge and energy current in ac-driven coherent conductors", J. Phys. Conf. Ser. **568**, 052008 (2014) (cit. on pp. 1, 31).

[24] L. Vannucci, F. Ronetti, J. Rech, D. Ferraro, T. Jonckheere, T. Martin, and M. Sassetti, "Minimal excitation states for heat transport in driven quantum Hall systems", Phys. Rev. B **95**, 245415 (2017) (cit. on p. 1).

[25] A. Mahé, F. D. Parmentier, E. Bocquillon, J.-M. Berroir, D. C. Glattli, T. Kontos, B. Plaçais, G. Fève, A. Cavanna, and Y. Jin, "Current correlations of an on-demand single-electron emitter", Phys. Rev. B **82**, 201309 (2010) (cit. on p. 1).

[26] F. D. Parmentier, E. Bocquillon, J.-M. Berroir, D. C. Glattli, B. Plaçais, G. Fève, M. Albert, C. Flindt, and M. Büttiker, "Current noise spectrum of a single-particle emitter: Theory and experiment", Phys. Rev. B **85**, 165438 (2012) (cit. on p. 1).

[27] F. Battista, M. Moskalets, M. Albert, and P. Samuelsson, "Quantum Heat Fluctuations of Single-Particle Sources", Phys. Rev. Lett. **110**, 126602 (2013) (cit. on pp. 2, 45).

[28] T. L. van den Berg, F. Brange, and P. Samuelsson, "Energy and temperature fluctuations in the single electron box", New J. Phys. **17**, 075012 (2015) (cit. on pp. 2, 45).

[29] J. S. Lim, R. López, and D. Sánchez, "Dynamic thermoelectric and heat transport in mesoscopic capacitors", Phys. Rev. B **88**, 201304 (2013) (cit. on p. 2).

[30] L. S. Levitov, H. Lee, and G. B. Lesovik, "Electron counting statistics and coherent states of electric current", Journal of Mathematical Physics **37**, 4845 (1998) (cit. on pp. 2, 3, 17, 21).

[31] D. A. Ivanov, H. W. Lee, and L. S. Levitov, "Coherent states of alternating current", Phys. Rev. B **56**, 6839 (1997) (cit. on pp. 2, 3, 21).

[32] J. Keeling, I. Klich, and L. S. Levitov, "Minimal Excitation States of Electrons in One-Dimensional Wires", Phys. Rev. Lett. **97**, 116403 (2006) (cit. on pp. 2, 3, 21).

[33] K. Flensberg, A. A. Odintsov, F. Liefrink, and P. Teunissen, "TOWARDS SINGLE-ELECTRON METROLOGY", Int. J. Mod. Phys. B **13**, 2651 (2012) (cit. on p. 2).

[34] R. P. G. McNeil, M. Kataoka, C. J. B. Ford, C. H. W. Barnes, D. Anderson, G. A. C. Jones, I. Farrer, and D. A. Ritchie, "On-demand single-electron transfer between distant quantum dots", Nature **477**, 439–442 (2011) (cit. on p. 2).

[35] S. Hermelin, S. Takada, M. Yamamoto, S. Tarucha, A. D. Wieck, L. Saminadayar, C. Bauerle, and T. Meunier, "Electrons surfing on a sound wave as a platform for quantum optics with flying electrons", Nature **477**, 435–438 (2011) (cit. on p. 2).

[36] J. P. Pekola, J. J. Vartiainen, M. Möttönen, O.-P. Saira, M. Meschke, and D. V. Averin, "Hybrid single-electron transistor as a source of quantized electric current", Nat. Phys. **4**, 120–124 (2008) (cit. on p. 2).

[37] D. A. Ryndyk, "Landauer-Büttiker Method", SpringerLink, 17–54 (2016) (cit. on p. 5).

[38] Y. M Blanter and M Büttiker, "Shot noise in mesoscopic conductors", Physics reports **336**, 1–166 (2000) (cit. on pp. 5, 14).

[39] W. Li and L. E. Reichl, "Floquet scattering through a time-periodic potential", Phys. Rev. B **60**, 15732–15741 (1999) (cit. on p. 5).

[40] M. Moskalets and M. Büttiker, "Floquet scattering theory of quantum pumps", Phys. Rev. B **66**, 205320 (2002) (cit. on pp. 5, 6, 15, 45).

[41] M. Moskalets and M. Büttiker, "Adiabatic quantum pump in the presence of external ac voltages", Phys. Rev. B **69**, 205316 (2004) (cit. on pp. 6, 45).

[42] M. Grifoni and P. Hänggi, "Driven quantum tunneling", Phys. Rep. **304**, 229–354 (1998) (cit. on p. 6).

[43] J. H. Shirley, "Solution of the Schrödinger Equation with a Hamiltonian Periodic in Time", Phys. Rev. **138**, B979 (1965) (cit. on p. 6).

[44] W. Li and L. E. Reichl, "Floquet scattering through a time-periodic potential", Phys. Rev. B **60**, 15732 (1999) (cit. on p. 6).

[45] W. Li and L. E. Reichl, "Floquet scattering through a time-periodic potential", Phys. Rev. B **60**, 15732–15741 (1999) (cit. on p. 7).

[46] M Büttiker, "Scattering theory of current and intensity noise correlations in conductors and wave guides", Phys. Rev. B **46**, 12485 (1992) (cit. on pp. 8, 13, 14, 45).

[47] M. V Moskalets, *Scattering matrix approach to non-stationary quantum transport* (World Scientific, 2011) (cit. on pp. 14, 16, 20).

[48] M. Moskalets, P. Samuelsson, and M. Büttiker, "Quantized Dynamics of a Coherent Capacitor", Phys. Rev. Lett. **100**, 086601 (2008) (cit. on p. 18).

[49] M. Misiorny, G. Fève, and J. Splettstoesser, "Shaping charge excitations in chiral edge states with a time-dependent gate voltage", arXiv (2017), eprint: 1711.00119 (cit. on p. 20).

[50] M. Büttiker, A. Prêtre, and H. Thomas, "Dynamic conductance and the scattering matrix of small conductors", Phys. Rev. Lett. **70**, 4114–4117 (1993) (cit. on p. 20).

[51] A. Prêtre, H. Thomas, and M. Büttiker, "Dynamic admittance of mesoscopic conductors: Discrete-potential model", Phys. Rev. B **54**, 8130–8143 (1996) (cit. on p. 20).

[52] J. Splettstoesser, S. Ol'khovskaya, M. Moskalets, and M. Büttiker, "Electron counting with a two-particle emitter", Phys. Rev. B **78**, 205110 (2008) (cit. on pp. 20, 23, 26, 53).

[53] M. Büttiker, "Coherent and sequential tunneling in series barriers", IBM Journal of Research and Development **32**, 63–75 (1988) (cit. on p. 45).

[54] M. Büttiker, "Four-Terminal Phase-Coherent Conductance", Phys. Rev. Lett. **57**, 1761 (1986) (cit. on p. 45).

[55] T. T. Heikkilä, *The Physics of Nanoelectronics* (Oxford University Press, 2013) (cit. on p. 45).